2012

An experimental investigation on the spray flow exhausted from a co-swirling air-blast nozzle

Daniel Dean Dvorak
Iowa State University

An experimental investigation on the spray flow exhausted from a co-swirling air-blast nozzle

by

Daniel Dean Dvorak

A thesis submitted to the graduate faculty

in partial fulfillment of the requirements for the degree of

MASTER OF SCIENCE

Major: Aerospace Engineering

Program of Study Committee:

Hui Hu, Major Professor

Richard Wlezien

Terry Meyer

Iowa State University

Ames, Iowa

2012

TABLE OF CONTENTS

LIST OF TABLES iv

LIST OF FIGURES v

ACKNOWLEDGEMENTS xii

ABSTRACT xiii

CHAPTER 1. INTRODUCTION AND MOTIVATION 1

1.1 Introduction 1

1.2 Motivation 3

CHAPTER 2. REVIEW OF LITERATURE 8

2.1 Variation of Input Parameters Experiments 8

2.2 PIV Measurement Based Experiments 9

CHAPTER 3. EXPERIMENTAL SETUP AND PROCEDURES 13

3.1 General Setup 13

3.2 Water and Air Measurements 19

3.3 Air Only Measurements 20

3.4 Fuel Substitute and Air Measurements 21

3.5 Stereoscopic PIV 22

3.6 LDV Comparison 23

CHAPTER 4. 2D PIV RESULTS 25

4.1 Water and Air Measurements 25

4.2 Air Only Measurements 31

4.3 Fuel Substitute and Air Measurements 33

CHAPTER 5. STEREOSCOPIC PIV RESULTS 39

CHAPTER 6. VELOCITY PROFILE COMPARISONS 50

6.1 Velocity Profile Comparisons 50

6.2 Comparison Between PIV and LDV 61

6.3 Error Discussion 64

CHAPTER 7. CONCLUSION 67

APPENDIX A. CALCULATIONS 69

APPENDIX B. ADDITIONAL RESULTS 71

APPENDIX C. FUEL SUBSTITUTE TECHNICAL SPECIFICATIONS . . 90

BIBLIOGRAPHY 106

LIST OF TABLES

Table 3.1 Water and Air Flow Combinations and Corresponding Air to Liquid Mass Flow Ratios 18

Table 3.2 Fuel Substitute and Air Flow Combinations and Corresponding Air to Liquid Mass Flow Ratios 18

Table 6.1 Physical Parameters for the Fuel Substitute and Water at 60° F 50

LIST OF FIGURES

Figure 1.1 United States Petroleum Production and Consumption: All Sectors, 1973 - 2035 5

Figure 1.2 United States Petroleum Production and Transportation Consumption, 1973 - 2035 6

Figure 1.3 Total National Emissions of the Criteria Air Pollutants by Sector, 2008 (millions of short tons / percentage) 6

Figure 3.1 Atomizer Schematic 15

Figure 3.2 Experimental Test Setup, Flow Meters and Pressure Gauges 16

Figure 3.3 Experimental Test Setup 17

Figure 3.4 Stereoscopic PIV Experimental Test Setup 17

Figure 3.5 Water and Air Experimental Setup Schematic 20

Figure 3.6 Air Only Experimental Setup Schematic 21

Figure 3.7 Fuel Substitute and Air Experimental Setup Schematic 22

Figure 3.8 SPIV Fuel Substitute and Air Experimental Setup Schematic 23

Figure 4.1 Average Velocity Profile for Water Flow of 3.33×10^{-3} kg/s and Air Flow of 2.47×10^{-3} kg/s 26

Figure 4.2 Average Velocity Profile for Water Flow of 6.66×10^{-3} kg/s and Air Flow of 2.47×10^{-3} kg/s 27

Figure 4.3 Average Velocity Profile for Water Flow of 9.99×10^{-3} kg/s and Air Flow of 2.47×10^{-3} kg/s 27

Figure 4.4 Average Velocity Profile for Water Flow of 3.33×10^{-3} kg/s and Air Flow of 4.93×10^{-3} kg/s 28

Figure 4.5 Average Velocity Profile for Water Flow of 6.66×10^{-3} kg/s and Air Flow of 4.93×10^{-3} kg/s 28
Figure 4.6 Average Velocity Profile for Water Flow of 9.99×10^{-3} kg/s and Air Flow of 4.93×10^{-3} kg/s 29
Figure 4.7 Average Velocity Profile for Water Flow of 3.33×10^{-3} kg/s and Air Flow of 7.40×10^{-3} kg/s 29
Figure 4.8 Average Velocity Profile for Water Flow of 6.66×10^{-3} kg/s and Air Flow of 7.40×10^{-3} kg/s 30
Figure 4.9 Average Velocity Profile for Water Flow of 9.99×10^{-3} kg/s and Air Flow of 7.40×10^{-3} kg/s 30
Figure 4.10 Average Velocity Profile for Air Only Flow of 2.47×10^{-3} kg/s 32
Figure 4.11 Average Velocity Profile for Air Only Flow of 4.93×10^{-3} kg/s 32
Figure 4.12 Average Velocity Profile for Air Only Flow of 7.40×10^{-3} kg/s 33
Figure 4.13 Average Velocity Profile for Fuel Substitute Flow of 2.57×10^{-3} kg/s and Air Flow of 2.47×10^{-3} kg/s 34
Figure 4.14 Average Velocity Profile for Fuel Substitute Flow of 2.57×10^{-3} kg/s and Air Flow of 4.93×10^{-3} kg/s 35
Figure 4.15 Average Velocity Profile for Fuel Substitute Flow of 2.57×10^{-3} kg/s and Air Flow of 7.40×10^{-3} kg/s 35
Figure 4.16 Average Velocity Profile for Fuel Substitute Flow of 5.13×10^{-3} kg/s and Air Flow of 2.47×10^{-3} kg/s 36
Figure 4.17 Average Velocity Profile for Fuel Substitute Flow of 5.13×10^{-3} kg/s and Air Flow of 4.93×10^{-3} kg/s 36
Figure 4.18 Average Velocity Profile for Fuel Substitute Flow of 5.13×10^{-3} kg/s and Air Flow of 7.40×10^{-3} kg/s 37
Figure 4.19 Average Velocity Profile for Fuel Substitute Flow of 7.70×10^{-3} kg/s and Air Flow of 2.47×10^{-3} kg/s 37
Figure 4.20 Average Velocity Profile for Fuel Substitute Flow of 7.70×10^{-3} kg/s and Air Flow of 4.93×10^{-3} kg/s 38

Figure 4.21 Average Velocity Profile for Fuel Substitute Flow of 7.70×10^{-3} kg/s and Air Flow of 7.40×10^{-3} kg/s 38

Figure 5.1 3D Average Velocity Profile for Fuel Substitute Mass Flow Rate of 2.57×10^{-3} kg/s and Air Mass Flow Rate of 2.47×10^{-3} kg/s 39

Figure 5.2 2D Average Velocity Projection for Fuel Substitute Mass Flow Rate of 2.57×10^{-3} kg/s and Air Mass Flow Rate of 2.47×10^{-3} kg/s 40

Figure 5.3 3D Average Velocity Profile for Fuel Substitute Mass Flow Rate of 2.57×10^{-3} kg/s and Air Mass Flow Rate of 4.93×10^{-3} kg/s 40

Figure 5.4 2D Average Velocity Projection for Fuel Substitute Mass Flow Rate of 2.57×10^{-3} kg/s and Air Mass Flow Rate of 4.93×10^{-3} kg/s 41

Figure 5.5 3D Average Velocity Profile for Fuel Substitute Mass Flow Rate of 2.57×10^{-3} kg/s and Air Mass Flow Rate of 7.40×10^{-3} kg/s 41

Figure 5.6 2D Average Velocity Projection for Fuel Substitute Mass Flow Rate of 2.57×10^{-3} kg/s and Air Mass Flow Rate of 7.40×10^{-3} kg/s 42

Figure 5.7 3D Average Velocity Profile for Fuel Substitute Mass Flow Rate of 5.13×10^{-3} kg/s and Air Mass Flow Rate of 2.47×10^{-3} kg/s 42

Figure 5.8 2D Average Velocity Projection for Fuel Substitute Mass Flow Rate of 5.13×10^{-3} kg/s and Air Mass Flow Rate of 2.47×10^{-3} kg/s 43

Figure 5.9 3D Average Velocity Profile for Fuel Substitute Mass Flow Rate of 5.13×10^{-3} kg/s and Air Mass Flow Rate of 4.93×10^{-3} kg/s 43

Figure 5.10 2D Average Velocity Projection for Fuel Substitute Mass Flow Rate of 5.13×10^{-3} kg/s and Air Mass Flow Rate of 4.93×10^{-3} kg/s 44

Figure 5.11 3D Average Velocity Profile for Fuel Substitute Mass Flow Rate of 5.13×10^{-3} kg/s and Air Mass Flow Rate of 7.40×10^{-3} kg/s 44

Figure 5.12 2D Average Velocity Projection for Fuel Substitute Mass Flow Rate of 5.13×10^{-3} kg/s and Air Mass Flow Rate of 7.40×10^{-3} kg/s 45

Figure 5.13 3D Average Velocity Profile for Fuel Substitute Mass Flow Rate of 7.70×10^{-3} kg/s and Air Mass Flow Rate of 2.47×10^{-3} kg/s 45

Figure 5.14 2D Average Velocity Projection for Fuel Substitute Mass Flow Rate of 7.70×10^{-3} kg/s and Air Mass Flow Rate of 2.47×10^{-3} kg/s 46

Figure 5.15 3D Average Velocity Profile for Fuel Substitute Mass Flow Rate of 7.70×10^{-3} kg/s and Air Mass Flow Rate of 4.93×10^{-3} kg/s 46

Figure 5.16 2D Average Velocity Projection for Fuel Substitute Mass Flow Rate of 7.70×10^{-3} kg/s and Air Mass Flow Rate of 4.93×10^{-3} kg/s 47

Figure 5.17 3D Average Velocity Profile for Fuel Substitute Mass Flow Rate of 7.70×10^{-3} kg/s and Air Mass Flow Rate of 7.40×10^{-3} kg/s 47

Figure 5.18 2D Average Velocity Projection for Fuel Substitute Mass Flow Rate of 7.70×10^{-3} kg/s and Air Mass Flow Rate of 7.40×10^{-3} kg/s 48

Figure 6.1 Velocity Component Profiles for Water Flow Rate of 3.33×10^{-3} kg/s, Fuel Substitute Flow Rate of 2.57×10^{-3} kg/s, and Air Flow Rate of 2.47×10^{-3} kg/s. 52

Figure 6.2 Velocity Component Profiles for Water Flow Rate of 3.33×10^{-3} kg/s, Fuel Substitute Flow Rate of 2.57×10^{-3} kg/s, and Air Flow Rate of 4.93×10^{-3} kg/s. 53

Figure 6.3 Velocity Component Profiles for Water Flow Rate of 3.33×10^{-3} kg/s, Fuel Substitute Flow Rate of 2.57×10^{-3} kg/s, and Air Flow Rate of 7.40×10^{-3} kg/s. 54

Figure 6.4 Velocity Component Profiles for Water Flow Rate of 6.66×10^{-3} kg/s, Fuel Substitute Flow Rate of 5.13×10^{-3} kg/s, and Air Flow Rate of 2.47×10^{-3} kg/s. 55

Figure 6.5 Velocity Component Profiles for Water Flow Rate of 6.66×10^{-3} kg/s, Fuel Substitute Flow Rate of 5.13×10^{-3} kg/s, and Air Flow Rate of 4.93×10^{-3} kg/s. 56

Figure 6.6 Velocity Component Profiles for Water Flow Rate of 6.66×10^{-3} kg/s, Fuel Substitute Flow Rate of 5.13×10^{-3} kg/s, and Air Flow Rate of 7.40×10^{-3} kg/s. 57

Figure 6.7 Velocity Component Profiles for Water Flow Rate of 9.99×10^{-3} kg/s, Fuel Substitute Flow Rate of 7.70×10^{-3} kg/s, and Air Flow Rate of 2.47×10^{-3} kg/s. 58

Figure 6.8 Velocity Component Profiles for Water Flow Rate of 9.99×10^{-3} kg/s, Fuel Substitute Flow Rate of 7.70×10^{-3} kg/s, and Air Flow Rate of 4.93×10^{-3} kg/s. 59

Figure 6.9 Velocity Component Profiles for Water Flow Rate of 9.99×10^{-3} kg/s, Fuel Substitute Flow Rate of 7.70×10^{-3} kg/s, and Air Flow Rate of 7.40×10^{-3} kg/s. 60

Figure 6.10 Comparison of Radial Velocity for LDV and PIV Measurements for Liquid Flow of 2.52×10^{-3} kg/s and Air Flow of 3.46×10^{-3} kg/s 62

Figure 6.11 Comparison of Axial Velocity for LDV and PIV Measurements for Liquid Flow of 2.52×10^{-3} kg/s and Air Flow of 3.46×10^{-3} kg/s 63

Figure 6.12 Comparison of Radial Velocity for LDV and PIV Measurements for Liquid Flow of 7.36×10^{-3} kg/s and Air Flow of 6.93×10^{-3} kg/s 63

Figure 6.13 Comparison of Axial Velocity for LDV and PIV Measurements for Liquid Flow of 7.36×10^{-3} kg/s and Air Flow of 6.93×10^{-3} kg/s 64

Figure 6.14 Raw Image for Fuel Substitute Flow of 5.13×10^{-3} kg/s and Air Flow of 4.93×10^{-3} kg/s. 65

Figure B.1 Average Velocity Profile for Water Flow of 5.00×10^{-3} kg/s and Air Flow of 2.47×10^{-3} kg/s 71

Figure B.2 Average Velocity Profile for Water Flow of 8.33×10^{-3} kg/s and Air Flow of 2.47×10^{-3} kg/s 72

Figure B.3 Average Velocity Profile for Water Flow of 3.33×10^{-3} kg/s and Air Flow of 3.70×10^{-3} kg/s 72

Figure B.4 Average Velocity Profile for Water Flow of 5.00×10^{-3} kg/s and Air Flow of 3.70×10^{-3} kg/s 73

Figure B.5 Average Velocity Profile for Water Flow of 6.66×10^{-3} kg/s and Air Flow of 3.70×10^{-3} kg/s 73
Figure B.6 Average Velocity Profile for Water Flow of 8.33×10^{-3} kg/s and Air Flow of 3.70×10^{-3} kg/s 74
Figure B.7 Average Velocity Profile for Water Flow of 9.99×10^{-3} kg/s and Air Flow of 3.70×10^{-3} kg/s 74
Figure B.8 Average Velocity Profile for Water Flow of 5.00×10^{-3} kg/s and Air Flow of 4.93×10^{-3} kg/s 75
Figure B.9 Average Velocity Profile for Water Flow of 8.33×10^{-3} kg/s and Air Flow of 4.93×10^{-3} kg/s 75
Figure B.10 Average Velocity Profile for Water Flow of 3.33×10^{-3} kg/s and Air Flow of 6.17×10^{-3} kg/s 76
Figure B.11 Average Velocity Profile for Water Flow of 5.00×10^{-3} kg/s and Air Flow of 6.17×10^{-3} kg/s 76
Figure B.12 Average Velocity Profile for Water Flow of 6.66×10^{-3} kg/s and Air Flow of 6.17×10^{-3} kg/s 77
Figure B.13 Average Velocity Profile for Water Flow of 8.33×10^{-3} kg/s and Air Flow of 6.17×10^{-3} kg/s 77
Figure B.14 Average Velocity Profile for Water Flow of 9.99×10^{-3} kg/s and Air Flow of 6.17×10^{-3} kg/s 78
Figure B.15 Average Velocity Profile for Water Flow of 5.00×10^{-3} kg/s and Air Flow of 7.40×10^{-3} kg/s 78
Figure B.16 Average Velocity Profile for Water Flow of 8.33×10^{-3} kg/s and Air Flow of 7.40×10^{-3} kg/s 79
Figure B.17 Average Velocity Profiles for Water Flow Rates of 5.00×10^{-3} kg/s and 8.33×10^{-3} kg/s and Air Flow of 2.47×10^{-3} kg/s 80
Figure B.18 Average Velocity Profiles for Water Flow Rates of 3.33×10^{-3}, 5.00×10^{-3}, 6.66×10^{-3}, 8.33×10^{-3}, and 9.99×10^{-3} kg/s and Air Flow of 3.70×10^{-3} kg/s 81

Figure B.19 Average Velocity Profiles for Water Flow Rates of 5.00×10^{-3} kg/s and 8.33×10^{-3} kg/s and Air Flow of 4.93×10^{-3} kg/s 82

Figure B.20 Average Velocity Profiles for Water Flow Rates of 3.33×10^{-3}, 5.00×10^{-3}, 6.66×10^{-3}, 8.33×10^{-3}, and 9.99×10^{-3} kg/s and Air Flow of 6.17×10^{-3} kg/s 83

Figure B.21 Average Velocity Profiles for Water Flow Rates of 5.00×10^{-3} kg/s and 8.33×10^{-3} kg/s and Air Flow of 7.40×10^{-3} kg/s 84

Figure B.22 Average Velocity Profile for Water Flow of 3.33×10^{-3} kg/s and Air Flow of 3.22×10^{-3} kg/s 85

Figure B.23 Average Velocity Profile for Fuel Substitute Flow of 2.52×10^{-3} kg/s and Air Flow of 3.22×10^{-3} kg/s 86

Figure B.24 3D Average Velocity Profile for Fuel Substitute Mass Flow Rate of 2.52×10^{-3} kg/s and Air Mass Flow Rate of 3.46×10^{-3} kg/s 86

Figure B.25 2D Average Velocity Projection for Fuel Substitute Mass Flow Rate of 2.52×10^{-3} kg/s and Air Mass Flow Rate of 3.46×10^{-3} kg/s 87

Figure B.26 Average Velocity Profile for Water Flow of 9.48×10^{-3} kg/s and Air Flow of 6.69×10^{-3} kg/s 87

Figure B.27 Average Velocity Profile for Fuel Substitute Flow of 7.36×10^{-3} kg/s and Air Flow of 6.69×10^{-3} kg/s 88

Figure B.28 3D Average Velocity Profile for Fuel Substitute Mass Flow Rate of 7.36×10^{-3} kg/s and Air Mass Flow Rate of 6.93×10^{-3} kg/s 88

Figure B.29 2D Average Velocity Projection for Fuel Substitute Mass Flow Rate of 7.36×10^{-3} kg/s and Air Mass Flow Rate of 6.93×10^{-3} kg/s 89

ACKNOWLEDGEMENTS

I would like to acknowledge and say thank you to everyone who has helped me on conducting this research and writing this thesis. First, I would like to thank my major professor, Dr. Hui Hu, for the opportunity of working with him in his research group, and for his patience and guidance on this project. Also, I would like to thank the other members of my committee, Dr. Richard Wlezien and Dr. Terry Meyer, for their effort and input on this thesis. I would like to thank all of my colleagues in the research group for their help and camaraderie. In addition, I would like to thank Spencer Pack and Goodrich Engine Components for their cooperation, help, support, and funding of this project. Finally, I would especially like to thank all of my friends and family for their love and support. Thank you all very much.

ABSTRACT

The velocity field for a spray produced by an air-blast atomizer is measured using Particle Image Velocimetry (PIV). These measurements are conducted at a variety of input liquid and air mass flow rates producing many different air to liquid mass flow ratios (ALR). The experiment is repeated with two different liquids, water and a hydrocarbon based fuel substitute. It is found that the velocity field depends heavily on the type of fluid used as opposed to the ALR. The experiments are repeated using a Stereoscopic Particle Image Velocimetry (SPIV) measurement technique. These results are compared to the 2D PIV results, and the differences are discussed. Finally, the 2D PIV and SPIV results are compared to existing Laser Doppler Velocimetry (LDV) results. It is seen that the results from the two different techniques are not well correlated.

CHAPTER 1. INTRODUCTION AND MOTIVATION

The following is an experimental investigation into the phenomenon of spray flow produced by a co-swirling air-blast atomizer. In this experiment the major method of investigation is measuring the flow field velocity with particle image velocimetry. The air to liquid mass flow ratio is systematically changed while the nozzle geometry is held constant. Two different liquids are investigated. Finally, the results are compared to laser doppler velocimetry results to validate the method. In this chapter, an introduction is given into spray flows and motivation for conducting this experimental investigation.

1.1 Introduction

Spray flows are an important class of flow in today's world. Spray flow is created when a liquid is delivered through a nozzle, injector, or atomizer into a gaseous medium. Spray flows are used in a wide variety of applications, a few being: painting, drying, industrial manufacturing, and combustion. This paper will focus on combustion, primarily within a gas turbine engine. Spray flow is a complicated multiphase process, and this is especially true in gas turbine combustion. Along with multiple phases, the flow is unsteady, reacting, and at high temperature and pressure. The mechanisms that govern this process are not fully understood, and it is often difficult to make measurements in such a flow. Because of this, there is interest in using laser based measurement techniques, such as Particle Image Velocimetry (PIV), to measure spray flows. Using PIV and other similar techniques, it is possible to measure the velocity and other characteristics of the spray flow instantaneously and non-intrusively. From this insight, we can better understand the physical mechanisms that govern spray flows. In turn, we can design nozzles that better control the spray flow. In gas turbines, this can lead

to lower pollution emissions, and improved combustion efficiency and performance.

There are many types of sprayers and atomizers. A common type of atomizer used in gas turbine engines is an airblast atomizer. In an airblast atomizer, liquid fuel with relatively low momentum is mixed with a high momentum air stream. This causes a large amount of shear between the liquid and the air that results in the atomization of the liquid. In addition to atomizing the fuel, an airblast atomizer can help create a desired flow field downstream of the atomizer, e.g., in the combustor. The air flow and fluid flow are usually coaxial. Swirl can be added to either the liquid, the air, or both. In combustion, the swirl helps the atomization and evaporation process, and helps to stabilize the flame.

In addition to the geometry of the nozzle, other factors effect the spray flow characteristics. The incoming flow conditions of the liquid and the air greatly effect the spray flow. The main incoming flow conditions are the temperature and pressure of both the air and the liquid, and the relative momentum and mass flow rates of the liquid to the air. In addition, the ambient condition in which the spray flow is created has a large role in forming the spray flow characteristics. The ambient conditions that affect the flow are the temperature and pressure of the ambient air. The spray flow characteristics that can be measured are: the liquid and air velocity, the droplet size, the droplet temperature, the spray cone angle and solidity, and the liquid core breakup distance. Some characteristics are relatively easy to measure and have direct known correlations to specific input conditions. For example, as the ambient pressure increases the spray cone angle decreases. Rottenkolber, G. et al. (2002)

Ideally, to help understand the unsteady nature of spray flows, time resolved measurements are desired for all of the measurable characteristics; however, this is very difficult, especially when a wide range of input conditions are considered. In this paper, both standard 2-D PIV and stereoscopic PIV are applied to measure the instantaneous and average velocity field produced by the spray flow at a variety of input conditions, specifically the air to liquid mass flow ratio (ALR). It can be seen in the work of Karnawat, J. and Kushari, A. (2006) that the variation of the ALR can make large changes in the spray cone angle, solidity, break up distance, and Sauter Mean Diameter (SMD). Thus, it can be assumed that changing the ALR will change the velocity profile of the spray flow. This change in the velocity profile would be

critical in changing the chemical processes that are present in the combustion of the fuel. Spray flow from an airblast atomizer with swirl is a complex three dimensional flow. This is made evident by the works of Midgley, K. et al. (2005) and Spencer, A. et al. (2008). Therefore, stereoscopic PIV is conducted along with and compared to standard 2-D PIV for the same conditions for several values of ALR. Another investigation made in this paper studies the effect of using different liquids as the atomization medium. Most of the literature uses water as the atomization liquid because of its convenience. This study investigates whether this causes errors in the velocity measurement. This is accomplished by conducting PIV measurements for both water and a hydrocarbon based jet fuel substitute for the same ALR and comparing the results. Finally, both the standard 2-D PIV and stereoscopic PIV for both water and fuel substitute are compared to Laser Doppler Velocimetry (LDV) measurements at two specific flow conditions.

1.2 Motivation

There are many reasons to study fuel atomizer spray flows. One is to better understand the atomization process. The experimental data can be used to validate or lead to the formulation of models for the atomization process. With better models and understanding, fuel injector performance can be improved. Improved performance can lead to increased fuel economy and decreased pollution emissions. An increased understanding in the basic underlying physics can lead to improvements of other processes that use spray flows.

In the particular case of a gas turbine fuel atomizer, there is strong interest in increasing the fuel economy and decreasing pollution emissions. Figures 1.1 and 1.2 help illustrate the desire for increased fuel economy. Figure 1.1 shows the United States petroleum production and consumption for all sectors from 1973 to 2035. The solid line on this figure represents the projected petroleum production using current production techniques, laws, and sources. The dotted line is the projected petroleum production using non-petroleum sources, i.e. ethanol. It can be seen that in the last thirty years the overall United States petroleum consumption has increased by about 23%, while the production has decreased by 38%. Currently, the consumption is 144% greater than production. In the next thirty years consumption is predicted to raise

another 18%. Gas turbine engines are mainly used in two sectors shown on Figure 1.1, transportation and electrical power generation. The consumption for electrical power generation is actually decreasing; however, the consumption for transportation has increased by 33% over the last thirty years and is projected to increase by another 33% over the next thirty years. To investigate this further, Figure 1.2 shows the United States total petroleum production and the transportation consumption from 1973 to 2035. Figure 1.2 clearly shows that the petroleum consumption for the transportation sector alone is larger than the total petroleum production. Within the transportation sector, gas turbine engines mainly are placed in the aircraft category. This category makes up 8% of the total transportation petroleum consumption. Over the last thirty years, aircraft consumption has increased in proportion with the total transportation at 33%. This is significant, because as consumption continues to outpace production, the price of petroleum will continue to increase. Therefore, the price of operating an aircraft will increase as well. An improvement to fuel injectors that increases the fuel economy would help offset this price of operation. In addition, sizable decreases in aircraft petroleum consumption would have a measureable effect on total petroleum consumption. Besides a decrease in cost of operation by increasing the fuel economy, aircraft performance characteristics would also improve. Both range and payload would increase with increased fuel economy.

Better control of the atomization process could lead to decreased pollution emissions. Figure 1.3 shows the United States air pollution emissions by sector. Aircraft is included in the off-highway transportation sub-sector. This sub-sector alone makes up one-fourth of all carbon monoxide and nitrous oxide emissions. With more stringent emission laws coming into effect, especially in Europe, there is great interest in reducing the amount of emissions of gas turbine engines.

Besides improvements to fuel injector performance, there are other benefits for a better understanding of the atomization process. Atomizing sprayers are used in various applications, and a better understanding of the process would improve these applications, too. For example, atomizing sprayers are heavily used in the painting industry. With an improved sprayer, the paint would be more even with less over-spray, thus producing a higher quality finish with less product. Similar examples can be found throughout industry.

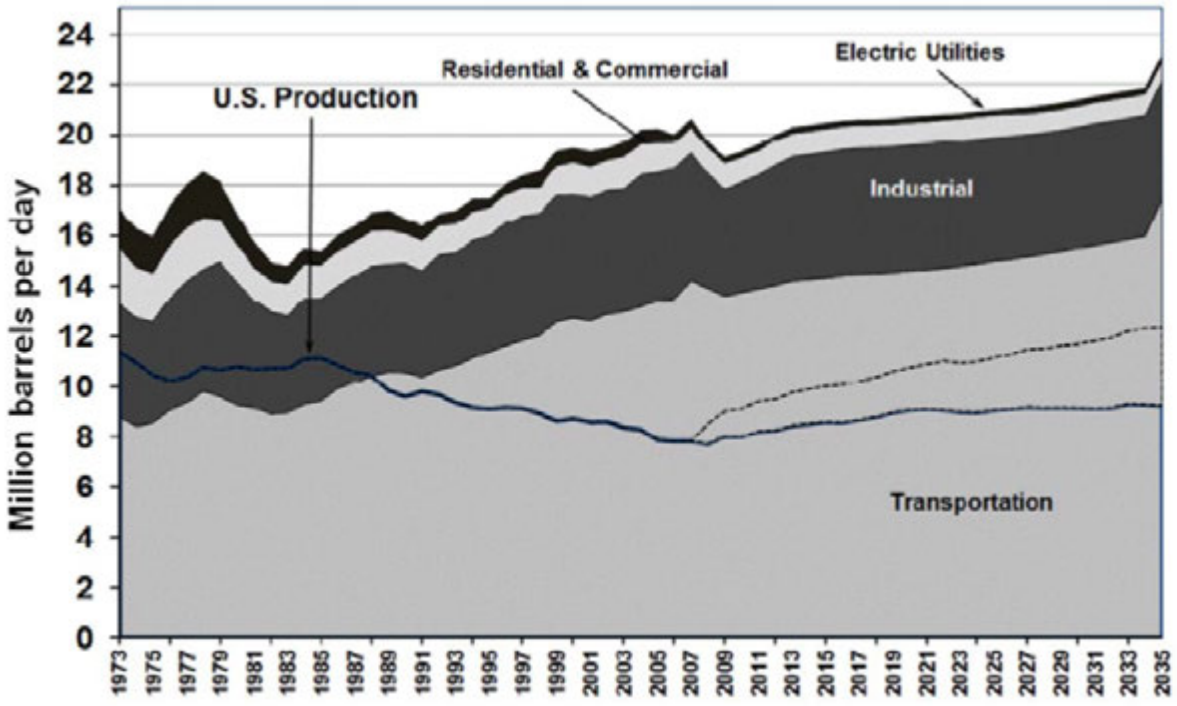

Figure 1.1 United States Petroleum Production and Consumption: All Sectors, 1973 - 2035

Davis, S. C. et al. (2011)

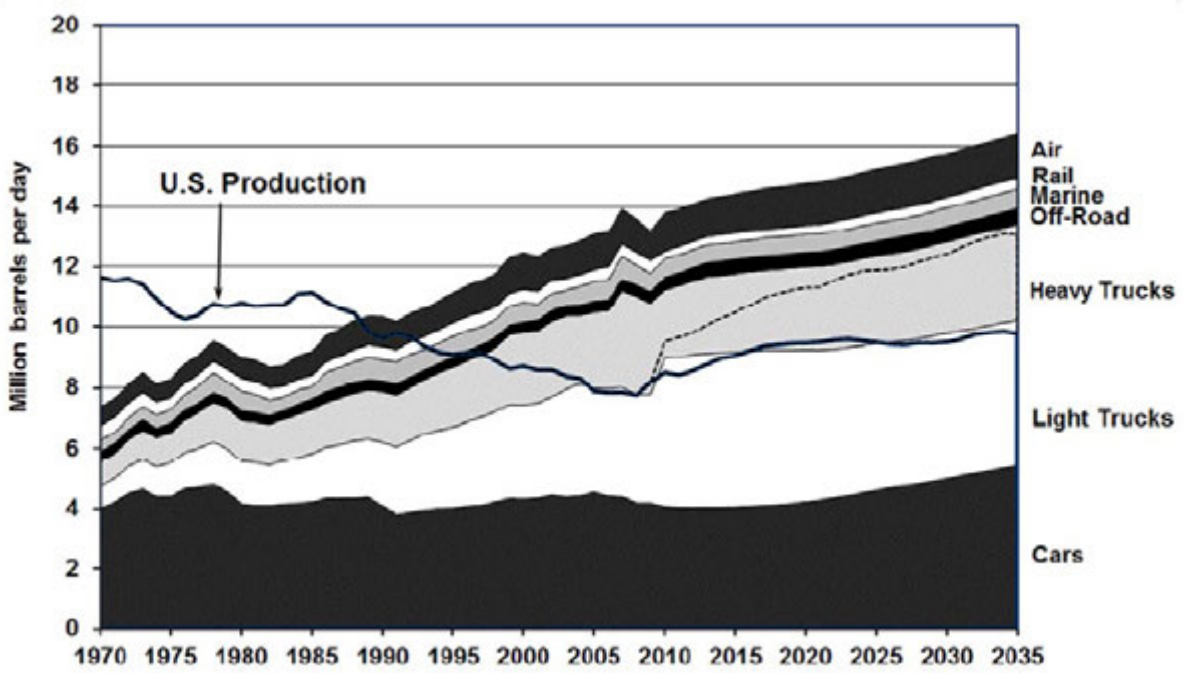

Figure 1.2 United States Petroleum Production and Transportation Consumption, 1973 - 2035

Davis, S. C. et al. (2011)

Sector	CO	NOx	VOC	PM-10	PM-2.5	SO_2
Highway vehicles	**38.87**	**5.21**	**3.42**	**0.17**	**0.11**	**0.06**
	50.0%	*31.9%*	*21.5%*	*1.2%*	*0.1%*	*0.6%*
Other off-highway	**18.04**	**4.26**	**2.59**	**0.30**	**0.28**	**0.46**
	23.2%	*26.0%*	*16.2%*	*2.1%*	*5.1%*	*4.0%*
Transportation total	**56.90**	**9.46**	**6.00**	**0.48**	**0.39**	**0.52**
	73.2%	*57.9%*	*37.7%*	*3.2%*	*7.2%*	*4.5%*
Stationary source fuel combustion	**5.28**	**5.57**	**1.45**	**1.33**	**1.03**	**9.80**
	6.8%	*34.1%*	*9.1%*	*9.0%*	*19.0%*	*85.7%*
Industrial processes	**2.18**	**0.93**	**6.77**	**1.17**	**0.48**	**1.00**
	2.8%	*5.7%*	*42.5%*	*7.9%*	*8.8%*	*8.7%*
Waste disposal and recycling total	**1.58**	**0.12**	**0.37**	**0.29**	**0.27**	**0.03**
	2.0%	*0.7%*	*2.3%*	*1.9%*	*4.9%*	*0.2%*
Miscellaneous	**11.73**	**0.26**	**1.33**	**11.54**	**3.28**	**0.09**
	15.1%	*1.6%*	*8.4%*	*77.9%*	*60.2%*	*0.7%*
Total of all sources	**77.69**	**16.34**	**15.93**	**14.81**	**5.45**	**11.43**
	100.0%	100.0%	100.0%	100.0%	100.0%	100.0%

Figure 1.3 Total National Emissions of the Criteria Air Pollutants by Sector, 2008 (millions of short tons / percentage)

Davis, S. C. et al. (2011)

Another possible benefit of this research is the improvement of measurement techniques. This is accomplished by applying different measurement techniques to a spray flow. The benefits and limitations of each technique can then be determined for this application. With this knowledge, future experiments can be planned using the appropriate measurement technique.

CHAPTER 2. REVIEW OF LITERATURE

Since spray flows from fuel injectors are a major part of modern society, there has been a significant amount of research done on this topic. The studies range in scope from experimental work to computational simulations, and phases from the liquid core to combustion. The works reviewed in this chapter focus on experimental works studying the atomization process. Two main types of investigations have been done in the past, variation of input parameters and PIV measurements. However, there is little research that uses PIV to investigate the variation of input parameters. Also lacking in the current publications is a study using different liquids in the experiment.

2.1 Variation of Input Parameters Experiments

Many experimental investigations studying the effects of varying the input parameters of mass flow rates, pressure, and temperature on spray flow from an airblast atomizer have been done. Karnawat, J. and Kushari, A. (2006) studied the spray cone angle, solidity, breakup distance, and droplet size produced by a twin-fluid internally mixed swirl atomizer by varying the liquid supply pressure and the ALR. In this atomizer, the liquid (water) was mixed with air inside of the atomizer. It was then passed through a swirling chamber before being force through a small orifice. The spray was illuminated by a laser sheet passing through the centerline of the flow and recorded with a Charge-Coupled Device (CCD) camera. A finding of this work was that ALR is the main parameter that controls spray flow properties, especially spray cone angle, solidity, and breakup distance. The researchers also noted that the SMD becomes more dependent on ALR as ALR increases.

In work done by Hadef, R. and Lenze, B. (2005), phase-Doppler anemometry (PDA) was

used to measure droplet size, velocity, and turbulent kinetic energy (TKE). They also investigated the effects of temperature via preheating the air. The atomizer reportedly used by Hadef and Lenze is similar to the one used in this thesis research, where the liquid is sandwiched between two co-swirling air streams. The liquid used by Hadef, R. and Lenze, B. (2005) was kerosene, and all of the input parameters were held constant except for the temperature in the temperature investigation. The kerosene was injected into a ten centimeter combustion chamber at atmospheric pressure and burned. Their results showed that there exists both center and corner recirculation zones. Most of the liquid is located in the shear layer between the two recirculation zones with the largest droplets biased towards the center. One important observation is that all three components of velocity of the flow — axial, radial, and tangential — are of the same order of magnitude. Finally, in the temperature investigation the incoming stream of air was preheated prior to meeting the liquid. The results show that when the air was preheated, the droplets were smaller, the velocity was higher, and the penetration distance was shorter.

The frequency of spray flow fluctuations produced by an air-blast atomizer was investigated by Batarseh, F. Z. et al. (2009). They used a LDV/PDA system to measure the flow varying the liquid and air flow rates as well as the chamber pressure. They proposed that a Strouhal number could be found for a particular nozzle geometry, and it could be used to predict the flow fluctuations. They found that the frequency of fluctuations was the same for all of the spray characteristics, e.g., velocity, SMD, and cone angle.

Sivakumar, D. and Kulkarni, V. (2011) studied the breakup process from a gas-centered swirl coaxial atomizer at various gas and liquid flow rates using a high speed camera and strobe light. The liquid used was water and was sprayed into ambient conditions. It was determined that there were four major types of breakups: wave-assisted sheet, perforated sheet, segmented sheet, and pulsation spray. The type of breakup seen depended upon the ALR of the flow.

2.2 PIV Measurement Based Experiments

PIV is gaining popularity as a way to study spray flows. It has the advantage of providing a non-intrusive whole field velocity measurement. This can be used to study different aspects

of spray flow. Spencer, A. et al. (2008) studied vortex breakdown in swirling flows from a fuel injector. The main emphasis of the investigation compared the flow field properties for the cases of a swirling flow with and without a central non-swirling jet. They also compared the flow field for different nozzle geometries that produced different swirl numbers both with and without the jet. This experiment was conducted with single phase flow in water. They found that the presence of a central jet greatly stabilized the vortex breakdown. Without the jet, many flow characteristics began to fluctuate and the central recirculation zone turned into a processing vortex core (PVC). When the swirl number was changed the frequency and intensity of these fluctuations also changed.

Rottenkolber, G. et al. (2002) used PIV to investigate a direct-injection spark-ignition engine. In this investigation, the air in a chamber was seeded with a fluorescent tracer particle and the gasoline was injected through a high-pressure swirl injector. PIV measurements were first taken of the gasoline flow and then of the entrained air flow. The injection pressure was held constant at 5 MPa while the chamber pressure was varied from 0.1 to 1.1 MPa. The measurements were taken from start of injection to 2.5 ms after the start of injection. It was found that the spray cone angle decreased greatly as the chamber pressure increased. This was due to a change in the relative strength of the inner and outer entrained vortexes. Then single camera, two-phase PIV measurements were made on the same flow using two different techniques with mild success. The first technique was to separate the two phases by their relative intensities and contributions to the gray scale histogram. The second technique was using double correlation peaks to obtain two velocity vectors in areas of mixed flow.

In a study by Ghaemi, S. et al. (2008), droplet centricity and velocity were measured from an effervescent atomizer. The geometry for this particular atomizer mixed the air and water together in the nozzle, and then the mixture exited the nozzle through a small orifice. Only one set of input conditions were tested with an ALR of 0.085. The spray was then measured by shadowgraphy and Stereo PIV. The droplet size, centricity, and velocity were calculated using the shadowgraphy. Shadowgraphy velocity was then compared to the Stereo PIV velocity. The results showed that the two velocities differed in the near field but agreed in the far field. It was determined that the Stereo PIV velocity was biased towards the velocity of droplets of

the size that is most present in that particular region of the flow. Near the exit of the nozzle, there are droplets of different sizes that are traveling at different velocities. The researchers also postulated that Stereo PIV might have light sheet problems in very dense regions of the spray near the nozzle exit. Therefore, SPIV has larger error in the region near the nozzle exit and under predicts the velocity.

Providakis, T. et al. (2010) studied a dodecane-air mixture in a two-staged multi-injection nozzle using a high speed PIV system. This nozzle geometry consisted of a central fuel nozzle surrounded with an air swirler. Further downstream was a second fuel injection location. This location had ten evenly spaced injection ports around the incoming flow. Around these second injection ports was a second air swirler. The two swirlers were co-swirling and had a swirl value of one. Twenty percent of the air went through the first swirler and the remaining eighty percent went through the second. In the experiment, the ratio of fuel that went through the two fuel injectors varied from all of the fuel being injected in the first nozzle to only forty percent through the first nozzle and the remainder through the second nozzle. This study concluded that air is the major factor in determining flow properties. When the fuel ratio was changed, the velocity field of the spray did not change. However, the droplet distribution changed slightly. From the time resolved PIV analysis, a PVC was detected and its frequency computed. Neither the frequency of the PVC nor the phase shifts of velocity as a function of radial position changed when the fuel ratio was changed.

Unsteady flow structures in a radial swirler fuel injector were investigated by Midgley, K. et al. (2005) using a standard PIV system. The fuel injector had a single central jet surrounded by a swirling stream. The experiment was conducted in a water tank with water being used for both the central jet and swirler stream fluids. Time averaged velocity profiles were computed and used to calculate the turbulent length scales. Using these length scales to appropriately resolve the flow field, the turbulent properties of the flow were computed. A PVC was found and its characteristic frequency was calculated. Finally, the double helixial axial vortices were analyzed in detail. This investigation showed that to correctly capture the unsteady and turbulent nature of the flow, the multiple turbulent length scales of the flow must be accounted for.

The selected works cited in this literature review are not an exhaustive list of spray flow research. However, they are pertinent and helpful to the present investigation.

CHAPTER 3. EXPERIMENTAL SETUP AND PROCEDURES

In this experiment, two different laser based measurement techniques – standard 2-D PIV and Stereoscopic PIV – were applied to three different spray flows produced from a co-swirling airblast atomizer. The flows are water and air, fuel substitute and air, and air only. For each of these flows, different flow conditions, ALR's, were tested. The following sections provide the experimental setup and procedures for each of these individual tests.

3.1 General Setup

An experimental test atomizer from Goodrich Engine Components was used. The particular configuration of the test nozzle had a 30° inner swirler and a 30° outer swirler surrounding the fuel circuit. The Goodrich test injector had the capability to vary the inner and outer air swirlers while maintaining the same fuel circuit. The different swirlers produce various amounts of swirl in different directions; however, in this experiment the configuration of the nozzle was fixed at 30° for both. The atomizer geometry was such that it produced three coaxial, axially symmetric flows. The swirling liquid flow, swirling in the same direction as the air, was located in-between two co-swirling air flows. The atomizer was contained within a metal chamber pressurized with air. A pressurized liquid line fed directly into the atomizer. A schematic drawing of the atomizer is shown in Figure 3.1. The spray was created inside a clear test chamber at ambient conditions of room temperature and pressure. Pictures of the test set up for the 2-D PIV are shown in Figures 3.2 and 3.3; the Stereoscopic PIV setup is displayed in Figure 3.4. The incoming flow rates were varied, and the pressure and temperature of the supply air and liquid were measured. The equipment used for the flow measurements were:

- Omega FMA-1612A Gas Flow Meter (Water and Air, and Air Only)

- Omega FMA-2612A Gas Flow Controller (Fuel Substitute and Air, and Stereoscopic PIV)
- Omega FLR-1605A Water Flow Meter
- Datarate Series 200 Flow Computer (Fuel Substitute and Air, and Stereoscopic PIV)
- Omega DPG1001B-100G Digital Pressure Gage
- Omega DPG1001B-05G Digital Pressure Gage

The PIV system used to take the measurements included a 532 nm double-pulsed Nd:YAG laser, New Wave Solo PIV laser (500 mJ / 5 ns), with optics to produce a one millimeter thick light sheet on the central axis of the flow. The delay between the two laser pulses depended on the flow conditions being tested. As the incoming flow conditions changed, the velocity of the spray flow changed. Ergo, the time delay, Δt, needed to be changed to maintain the accuracy of the PIV measurements. The timing of the system was controlled by a delay generator, BNC555. A CCD camera — Cooke Corporation SensiCam^{QE} with a Nikon AF Nikkor 35-70 mm lens — with a double shutter feature was used to capture the two images. The f-number was set at 2.8 and the focus length was held constant at 70 mm. The images were then saved on a computer. A standard PIV tracking algorithm, Insight v2.0, was used to construct the liquid velocity vector field. The interrogation window was 32 x 32 pixels with a 50% overlap. The velocity vectors were analyzed by a post-processing program that detects and deletes erroneous vectors; masks shadow regions; computes the vorticity, turbulent kinetic energy, and Reynold's stresses; and computes the ensemble averages. The representitive sample of the ensemble averaged velocity vector field was 750 instantaneous velocity vector fields. The experiments were conducted at various ALR and flow combinations, which are noted in Tables 3.1 and 3.2.

In all of the experiments, a consistent axis is kept. The origin is located at the center of the nozzle. The x axis is horizontal and is positive on the right side of the image. The y axis is vertical and is positive going up. The z axis completes a right-handed coordinate system and is horizontal and positive coming out of the plane. The laser location is always constant coming from the left (negative x axis).

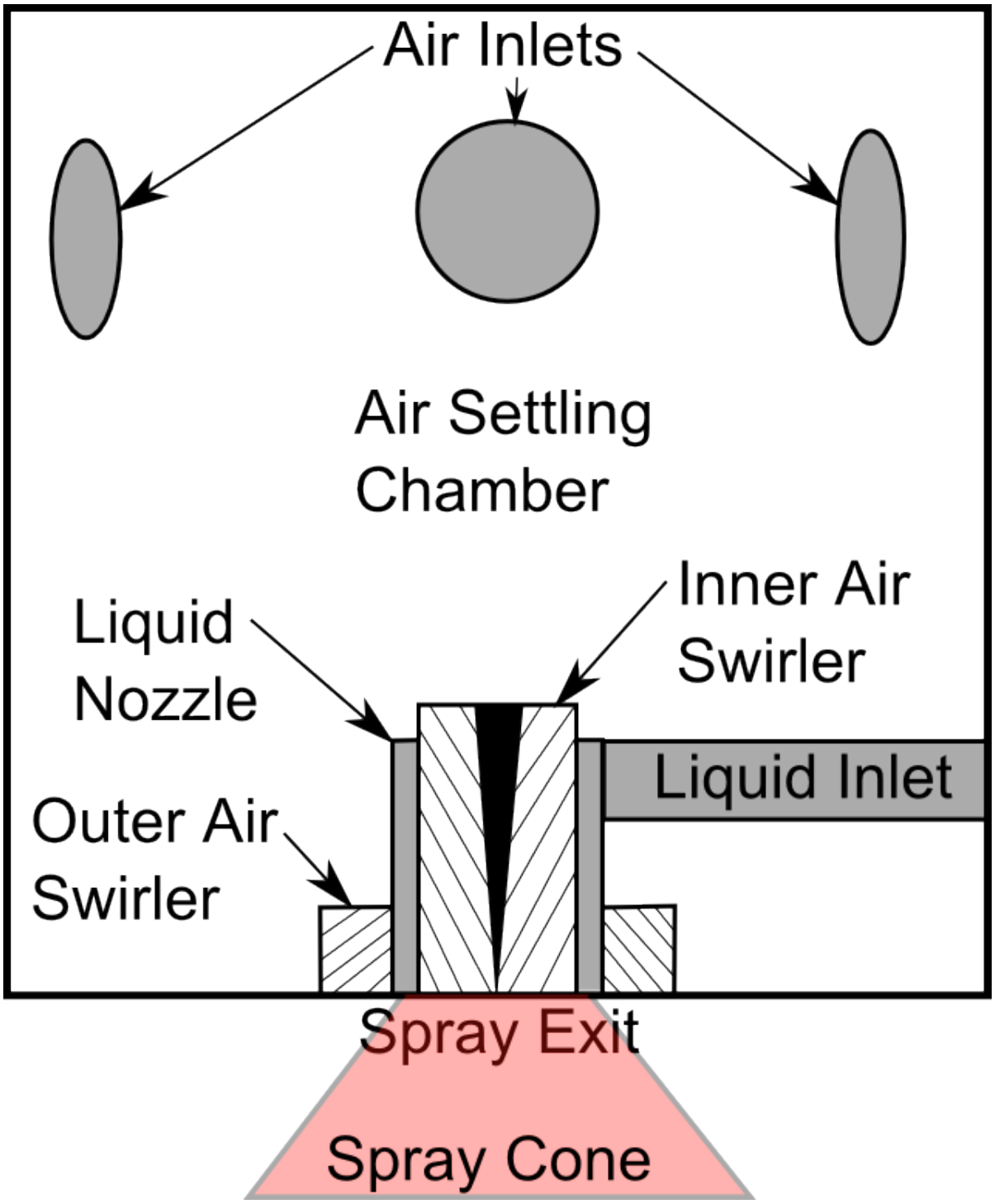

Figure 3.1 Atomizer Schematic

Figure 3.2 Experimental Test Setup, Flow Meters and Pressure Gauges

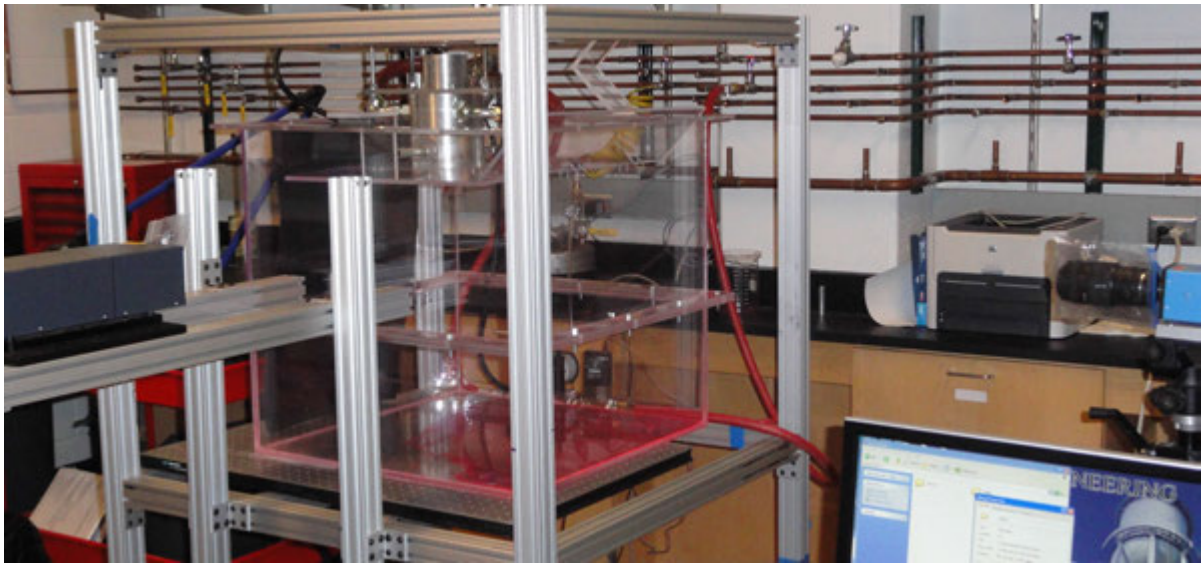

Figure 3.3 Experimental Test Setup

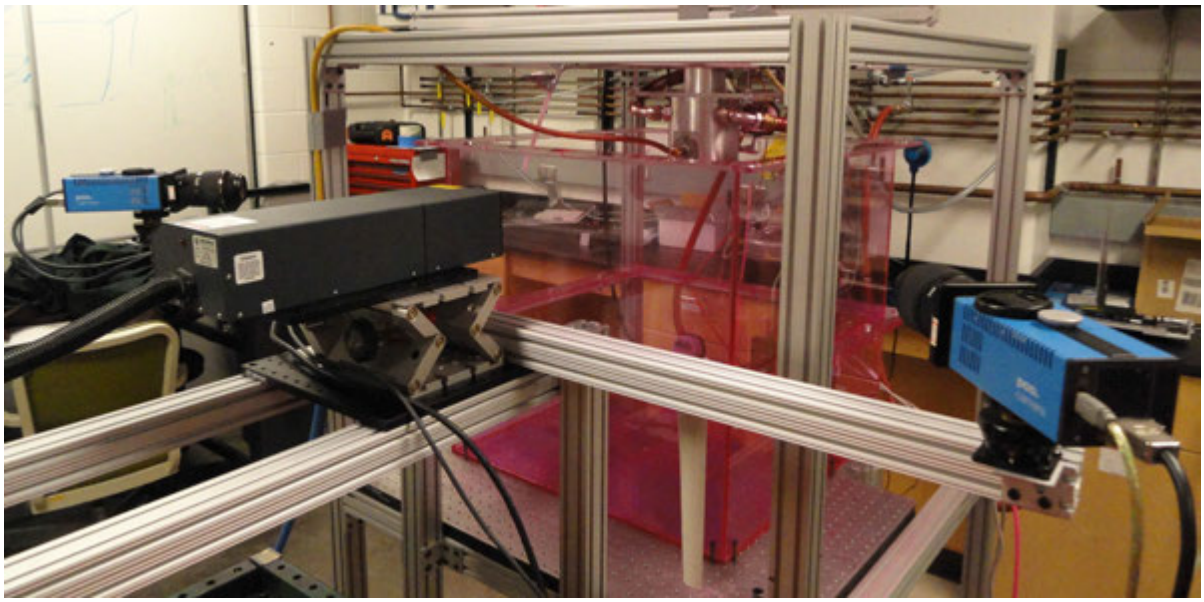

Figure 3.4 Stereoscopic PIV Experimental Test Setup

		Water (kg/s)				
		3.33×10^{-3}	5.00×10^{-3}	6.66×10^{-3}	8.33×10^{-3}	9.99×10^{-3}
Air (kg/s)	2.47×10^{-3}	0.741	0.494	0.370	0.296	0.247
	3.70×10^{-3}	1.11	0.741	0.556	0.444	0.370
	4.93×10^{-3}	1.48	0.988	0.741	0.593	0.494
	6.17×10^{-3}	1.85	1.23	0.926	0.741	0.617
	7.40×10^{-3}	2.22	1.48	1.11	0.889	0.741

Table 3.1 Water and Air Flow Combinations and Corresponding Air to Liquid Mass Flow Ratios

		Fuel Substitute (kg/s)		
		2.57×10^{-3}	5.13×10^{-3}	7.70×10^{-3}
Air (kg/s)	2.47×10^{-3}	0.960	0.481	0.320
	4.93×10^{-3}	1.92	0.962	0.641
	7.40×10^{-3}	2.88	1.44	0.961

Table 3.2 Fuel Substitute and Air Flow Combinations and Corresponding Air to Liquid Mass Flow Ratios

3.2 Water and Air Measurements

The first experiment used a 2-D PIV technique to measure the spray flow of water, seeded with Rhodamine B, and air at several different ALR as shown in Table 3.1. The initial concentration of the Rhodamine B solution was 5×10^{-4} M; however, due to evaporation during the experiment, it was unknown what the exact concentration of the solution was during any particular test. In this technique, only the velocity of the liquid was measured as the liquid droplets form the "seeding" particles that are tracked in the PIV algorithm. The laser pulse excites the Rhodamine B in the water, and it begins to fluoresce. The CCD camera was filtered with a long pass filter of 550 nm to capture Rhodamine B's fluorescent frequency, 585 nm, and was placed perpendicular to the laser sheet. The position of the droplets were more accurately determined by recording only the fluorescent light since the Mie scattering of the laser light was filtered out. The time delay varied with the air flow rate and were, from high flow rate to low flow rate: 90, 120, 150, 225, and 300 μs. With these time delays, the in-plane pixel displacement ranged between ten to twenty pixels per image pair. During this experiment the camera was placed at two different locations. For the tests with an ALR of 0.741, as listed in Table 3.1, the camera was located 2.6 m away from the nozzle. This gave a magnification factor of 0.235 mm/pixel. For all other tests in Table 3.1, the camera was located 1.5 m away from the nozzle resulting in a magnification factor of 0.132 mm/pixel. Figure 3.5 shows a schematic of the water and air experiment setup.

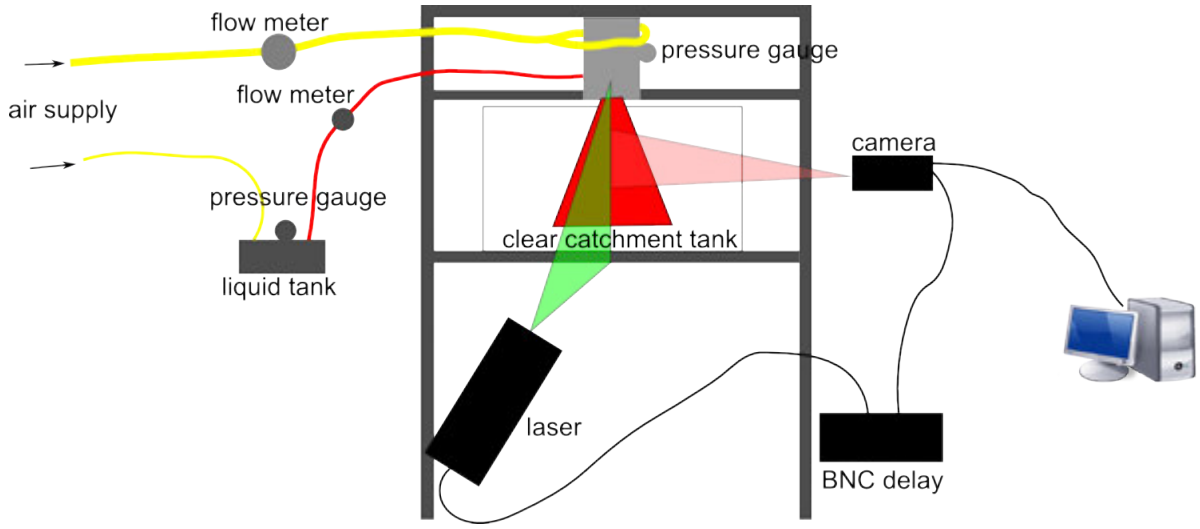

Figure 3.5 Water and Air Experimental Setup Schematic

3.3 Air Only Measurements

In the air only measurements, only the gas flow from the nozzle was measured by a standard 2D PIV technique. The liquid circuit was turned off, so there were no liquid droplets in the flow. The compressed air supplied to the nozzle was seeded with oil droplets using a Topas Aerosolgenerator ATM 210 seeding generator. The seeded oil droplets were less than one micron in size. The same PIV setup and equipment was used; however, the CCD camera was no longer filtered, and the scattered laser light was collected. Air only measurements were conducted at three different gas mass flow rates: 2.47×10^{-3}, 4.93×10^{-3}, and 7.40×10^{-3} kg/s. The time delays were 300, 150, and 90 μs respectively. The in-plane pixel displacement was similar to the water and air measurements. In all tests, the camera location was 1.0 m from the nozzle and the magnification factor was 0.087 mm/pixel. Figure 3.6 shows a schematic for the air only experimental setup.

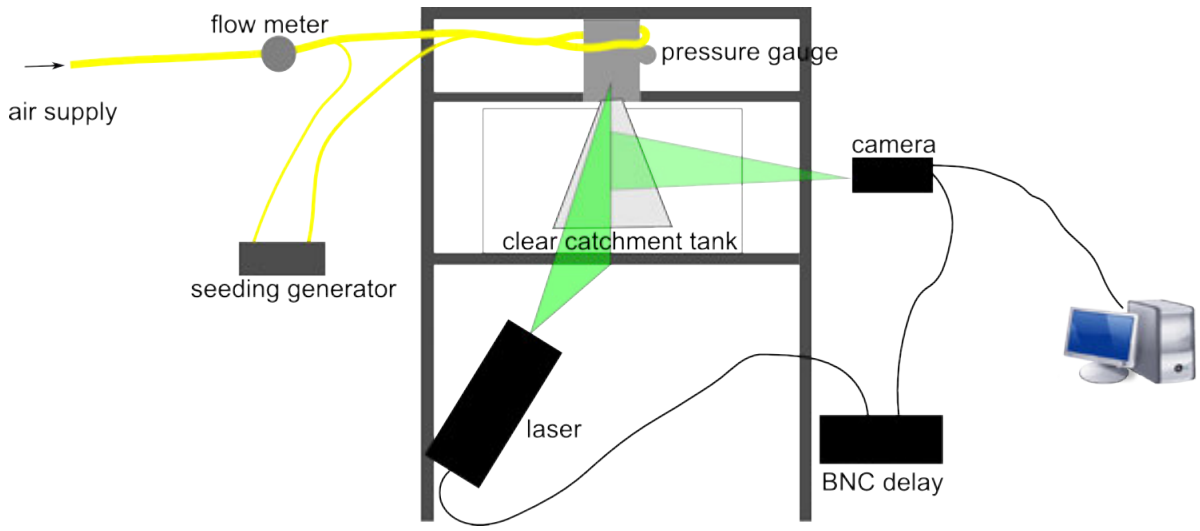

Figure 3.6 Air Only Experimental Setup Schematic

3.4 Fuel Substitute and Air Measurements

The fuel substitute and air measurements were conducted similarly to the water and air measurements. The main difference was that instead of water, a hydrocarbon based jet fuel simulation liquid was used, and a reduced number of ALR cases were tested (Table 3.2). The fuel substitute is defined in MIL-PRF-7024 Type II (Appendix C). The liquid was seeded with Rhodamine B. In order to accomplish that, the Rhodamine B was first dissolved in ethyl alcohol and then in the fuel substitute. This method was presented in a paper by Saeki and Hart. Saeki, S. and Hart, D. P. (2001) The total solution concentration initially was 5×10^{-4} M. The camera was filtered with a 550 nm long pass filter so only the fluorescence was recorded. With the exception of liquid and gas flow meters, all other equipment and setup remained the same. The flow meter used to measure the fuel substitute was a Datarate Series 200 Flow Computer, and the gas flow meter was an Omega FMA-2612A Gas Flow Controller. From the high flow rate to the low flow rate the time delays were: 50, 80, and 150 μs. With these smaller time delays, the in-plane pixel displacement range was reduced to six to twelve pixels per image pair. For all tests listed in Table 3.2, the magnification factor was 0.104 mm/pixel and the camera was located 1.2 m from the nozzle. In Figure 3.7, a schematic of the experimental setup for the fuel

substitute and air is shown.

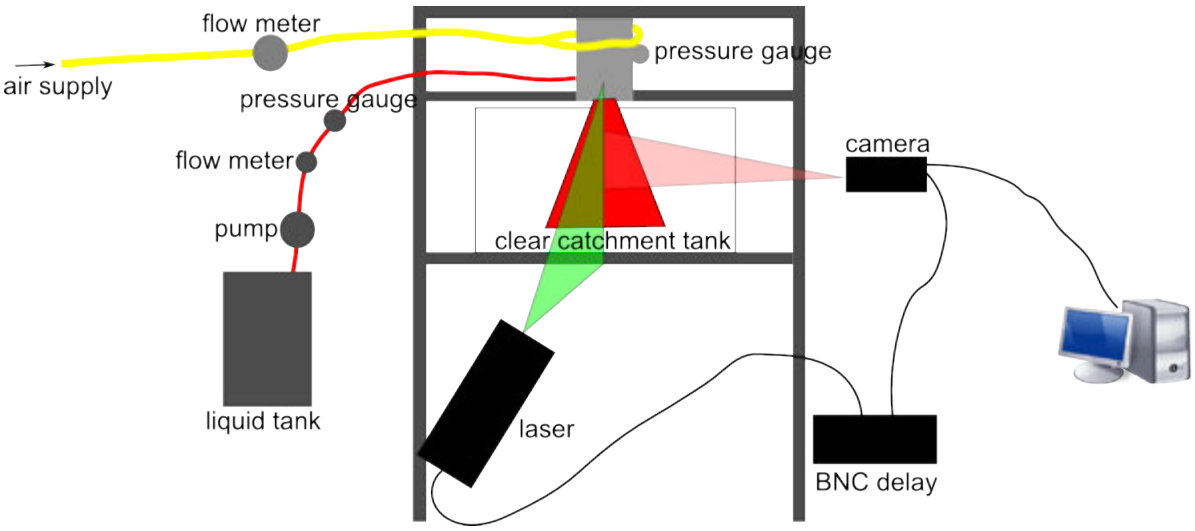

Figure 3.7 Fuel Substitute and Air Experimental Setup Schematic

3.5 Stereoscopic PIV

Stereoscope PIV measurements were conducted. The flow conditions used for the stereoscopic PIV measurements were the same as with the 2D PIV for the fuel substitute and air, and are outlined in Table 3.2. The fluid used for the stereoscopic PIV was the fuel substitute, seeded with Rhodamine B at an initial concentration of 5×10^{-4} M. In order to take the stereoscopic PIV measurements, the setup had to be changed. The difference in the setup was the use of two identical filtered Cooke Corporation pco.1600 cameras with Sigma DG macro 105 lenses connected with Scheimpflug mounts. The cameras were placed at the same angle, approximately 45°, on opposite sides of the laser sheet in a back scatter arrangement. A picture of the setup is provided in Figure 3.4. Both of the cameras focus on the center plane of the spray as the laser sheet location has not moved. This allowed for a direct comparison of the 2D standard PIV results and the 3D stereoscopic PIV results since the axes have not moved. Both cameras were located 1.11 m from the nozzle. In stereoscopic PIV the magnification factor is not constant for the whole image; however, an average value can be estimated from the reconstructed field of view of 0.0878 mm/pixel. The cameras were optically filtered to capture only the Rhodamine

B fluorescence, using 550 nm and 570 nm long pass filters. Each camera only had one filter. The sensitivity of the cameras was adjusted so that the images had the same intensity values. The f-number for the lens with the 570 nm filter was 2.8 while the f-number for the lens with the 550 nm filter was 4. The SPIV system was calibrated by moving a clear plate with a known grid of dots and Fiducial mark through the laser sheet location. These calibration images were processed by Insight v3.0 to obtain the calibration equations that related the pixel locations to the physical locations. The raw images were processed by Insight v3.0 to calculate the velocity vector field. The velocity vector fields were post-processed by a modified version of the 2D post-processing code. For SPIV, the ensemble averages were computed from more than one thousand instantaneous image pairs. The rest of the setup and experimental procedure was the same as the 2D fuel substitute and air measurements. A schematic for this SPIV experiment can be viewed in Figure 3.8.

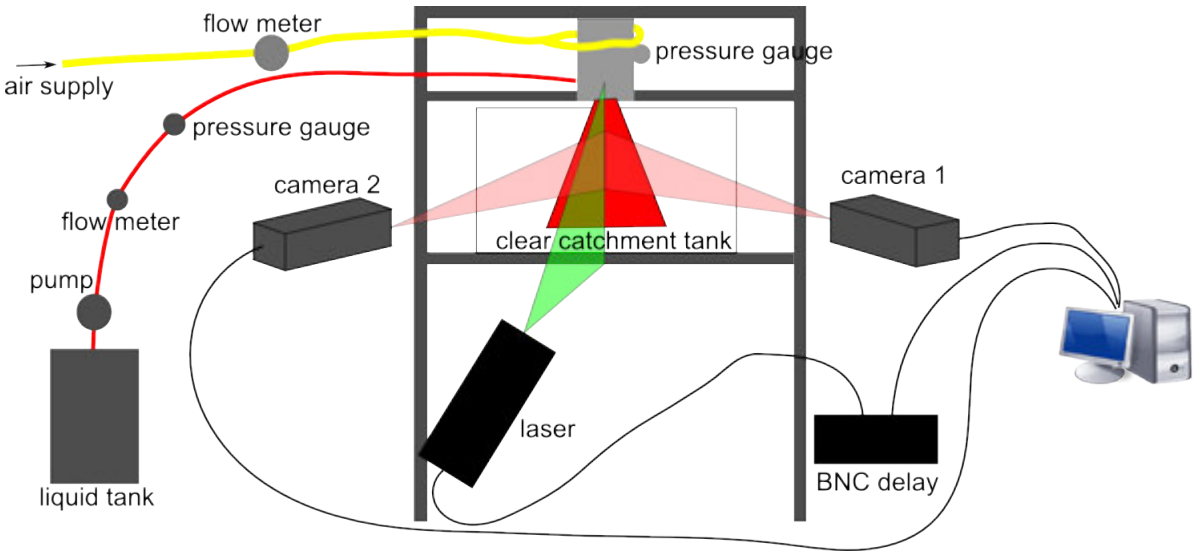

Figure 3.8 SPIV Fuel Substitute and Air Experimental Setup Schematic

3.6 LDV Comparison

LDV measurements have been previously performed on this nozzle for two specific flow conditions by Goodrich Engine Components. These two conditions define two control experiments

that were used to compare the LDV measurements to the PIV measurements. In this way, the validity of our method could be tested. In the first control, the pressurized air supplied to the atomizer was at room temperature and a flow rate of 3.46×10^{-3} kg/s. The liquid, seeded with Rhodamine B, was at room temperature and a flow rate of 2.52×10^{-3} kg/s. In the second control, flow rate of the supply air was 6.93×10^{-3} kg/s and the liquid was 7.36×10^{-3} kg/s. This produced an ALR of 1.37 and 0.942 respectively. The control conditions were tested for both water and the fuel substitute using the standard 2D PIV and again for the fuel substitute using SPIV. However, due to an error in calculating the liquid mass flow rate, the water flow rate was actually 3.33×10^{-3} kg/s for the first control case and 9.48×10^{-3} kg/s for the second control case. Therefore, the ALR's of the water and air control cases were 1.04 and 0.731. The error was made converting the units that Goodrich Engine Components used in their LDV measurements into the units used to make our PIV measurements. In addition, each measurement device recorded mass flow rates, pressures, and temperatures in different units. These measurements were all converted to SI units in this paper for clarity and comparison. For more information on what units were recorded and the conversion to SI units, see Appendix A. The time delays used for the high flow rate case were 90 μs for water and 50 μs for the fuel substitute. For the low flow rate case, the time delays were 300 μs for water and 100 μs for the fuel substitute. These time delays gave similar in-plane pixel displacements as the other experiments. The two control conditions were measured along with the other conditions for that particular experiment. Therefore, the setups were identical to the ones given for that experiment. For example, in the water and air experiment, the conditions given in Table 3.1 were tested. Then without changing the setup, the two control conditions were tested. In the water and air experiment only, the camera was located at two locations during the experiment. The location of the camera for the water and air experiment control cases was 2.6 m.

CHAPTER 4. 2D PIV RESULTS

The results for all of the standard 2D PIV measurements are reported in this chapter. These results include the velocity vector fields for the water and air, the air only, and the fuel substitute and air experiments. In all of these plots, the velocity vectors are the arrows and the contours are the magnitude of velocity. All of the axes are shown in millimeters and the velocities are meters per second. The scales are not necessarily the same for all plots. Additionally, velocity profiles comparing all of the cases taken at specific locations in the flow, are located in in Chapter 6. All of the standard 2D PIV average velocities are calculated from over 750 image pairs.

4.1 Water and Air Measurements

The PIV measurements of the average velocity field of the water and air combined flow are shown in Figures 4.1 – 4.9. The intermediate combinations are not presented in the main text, as they are similar to the rest of the results, and the trends and differences are easier to see with the larger change of parameters. The intermediate combinations are located in Appendix B. All of the velocity fields show similar results, especially in the far field. All show a tri-lobed velocity profile with the highest velocity located at the outside of the spray. Near the nozzle exit, the flow fields deviate more. At low air flow rates, the regions of high flow velocity are located at the edge of the flow and relatively slow flow velocity is located at the center. As the gas flow rate increases, the velocity of the spray in the center increases greatly, and is more than the velocity at the edge of the flow. In addition, the spray flow penetration depth decreases as the air flow rate increases. Little change is noted from changing the liquid flow rate. Thus, it is evident that the major driving force for producing the flow velocity is the air flow rate. It

is also noted that the shape of the different velocity profiles remains similar for constant ALR, but the magnitude increases as the flow rates increase. Because there is little change between the different cases, the remaining tests are done with a reduced number of input combinations.

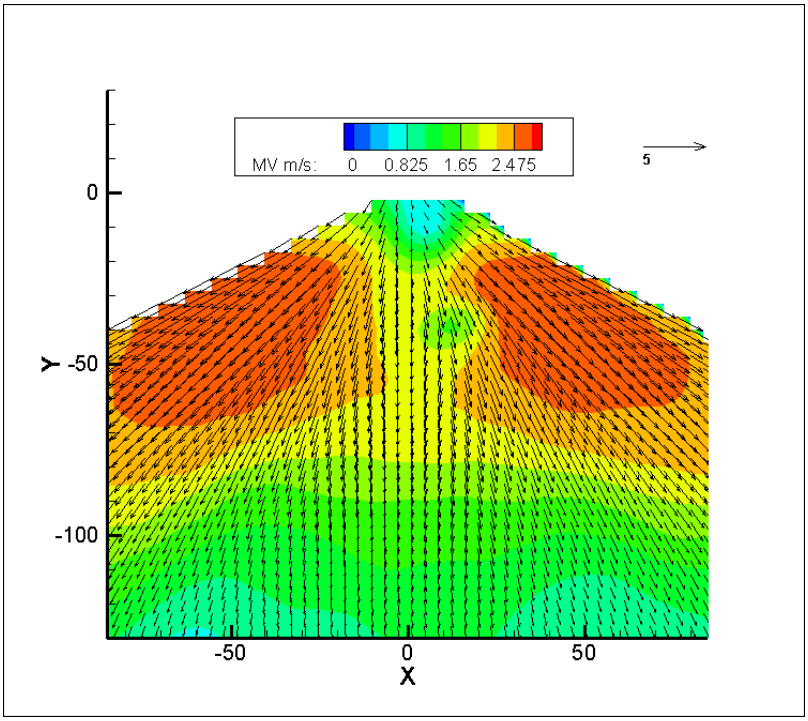

Figure 4.1 Average Velocity Profile for Water Flow of 3.33×10^{-3} kg/s and Air Flow of 2.47×10^{-3} kg/s

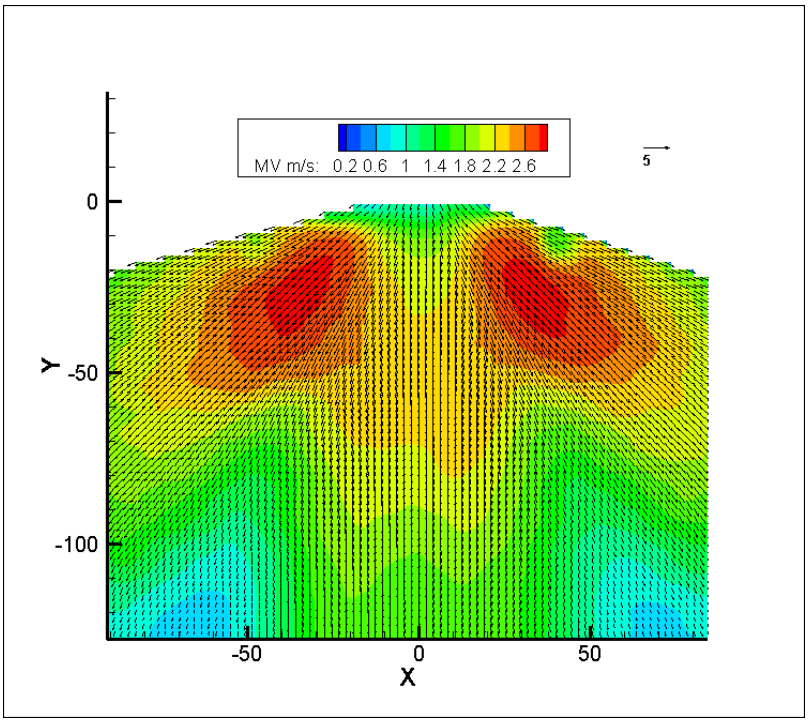

Figure 4.2 Average Velocity Profile for Water Flow of 6.66×10^{-3} kg/s and Air Flow of 2.47×10^{-3} kg/s

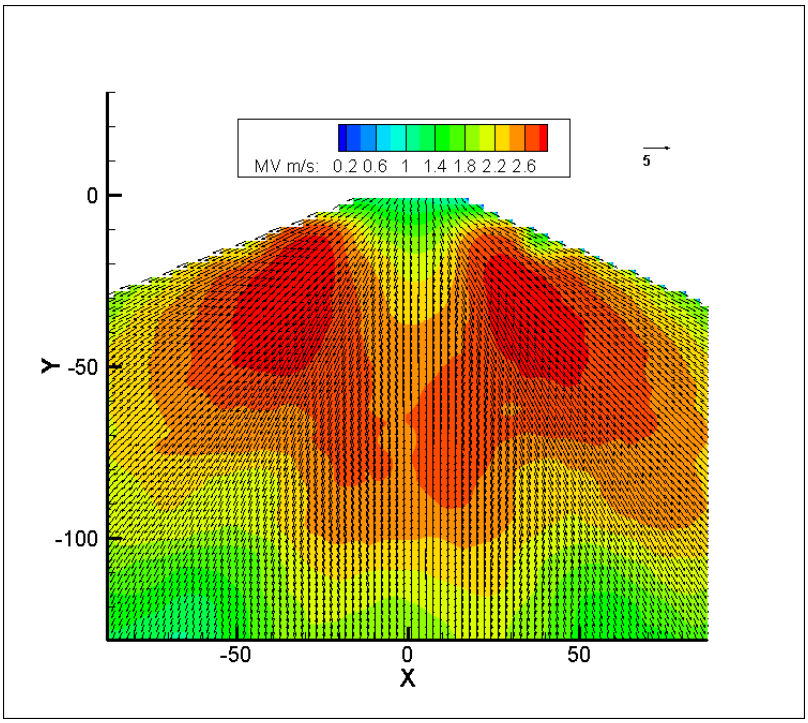

Figure 4.3 Average Velocity Profile for Water Flow of 9.99×10^{-3} kg/s and Air Flow of 2.47×10^{-3} kg/s

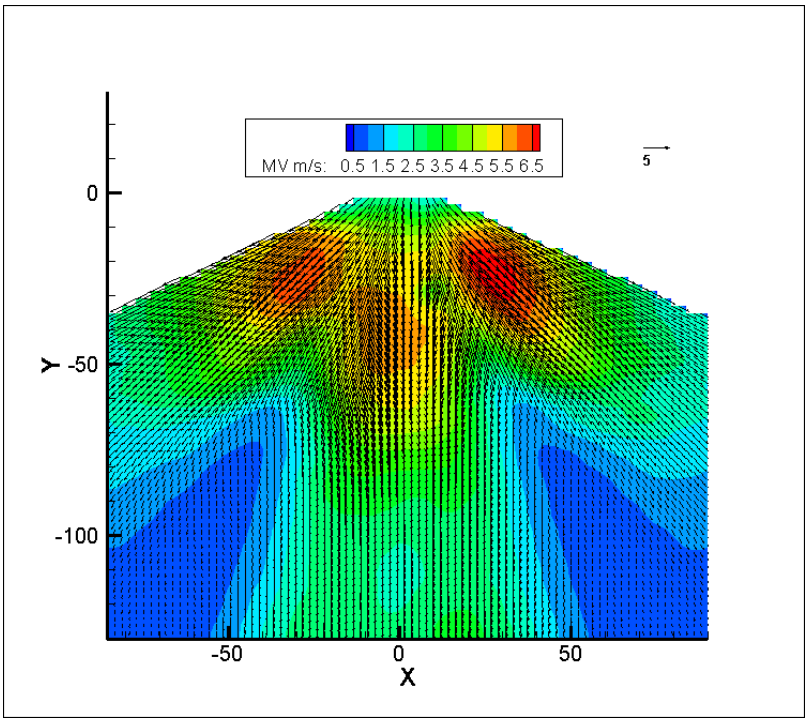

Figure 4.4 Average Velocity Profile for Water Flow of 3.33×10^{-3} kg/s and Air Flow of 4.93×10^{-3} kg/s

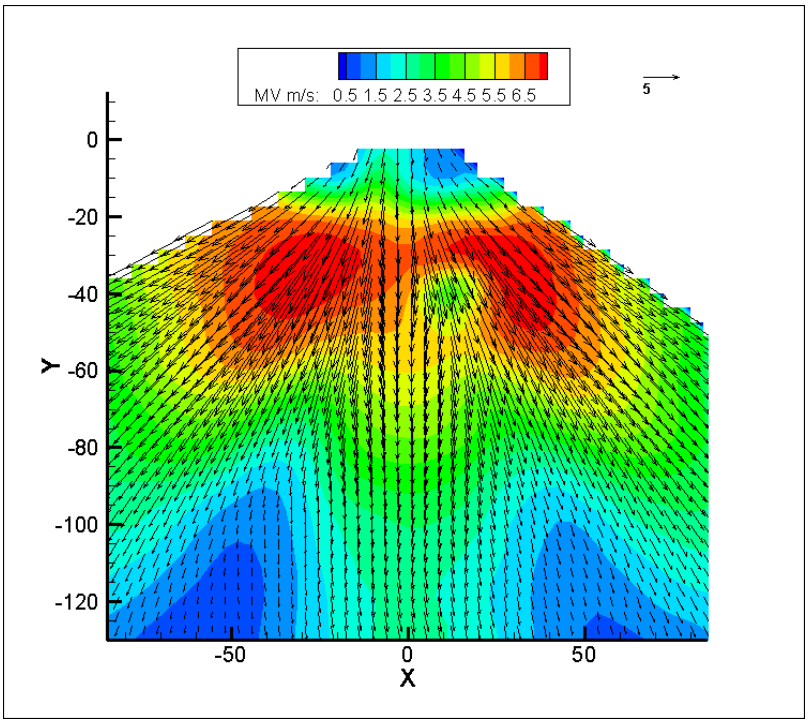

Figure 4.5 Average Velocity Profile for Water Flow of 6.66×10^{-3} kg/s and Air Flow of 4.93×10^{-3} kg/s

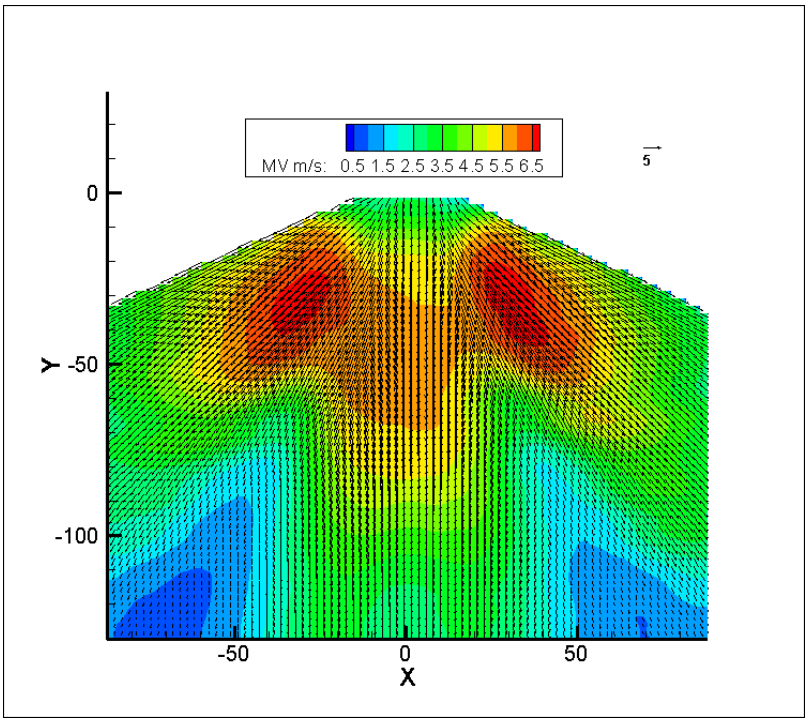

Figure 4.6 Average Velocity Profile for Water Flow of 9.99×10^{-3} kg/s and Air Flow of 4.93×10^{-3} kg/s

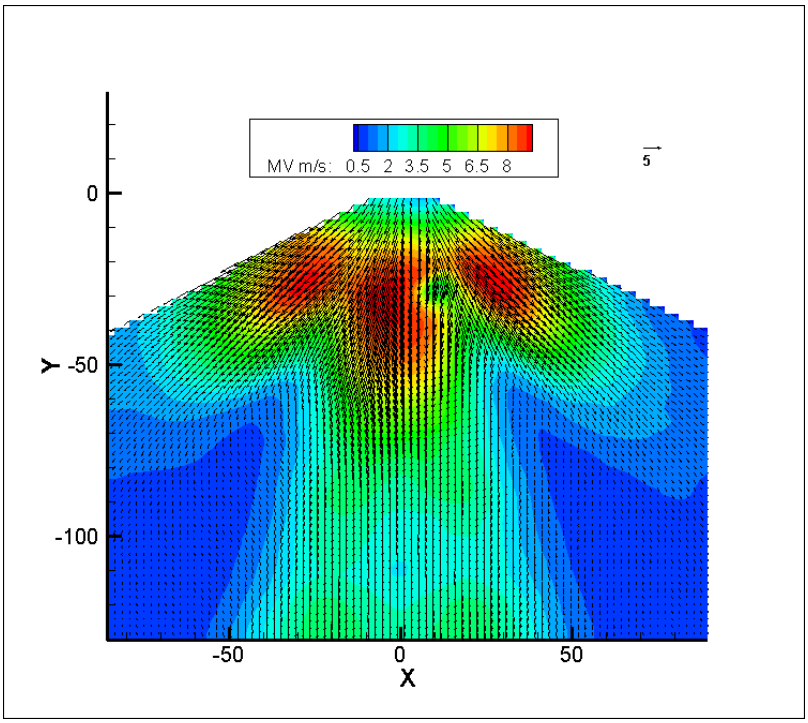

Figure 4.7 Average Velocity Profile for Water Flow of 3.33×10^{-3} kg/s and Air Flow of 7.40×10^{-3} kg/s

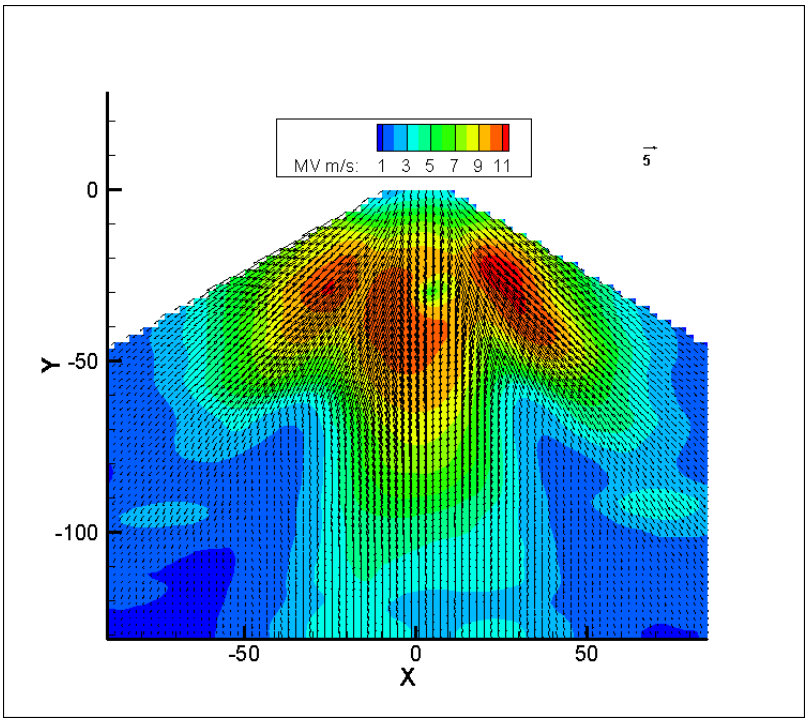

Figure 4.8 Average Velocity Profile for Water Flow of 6.66×10^{-3} kg/s and Air Flow of 7.40×10^{-3} kg/s

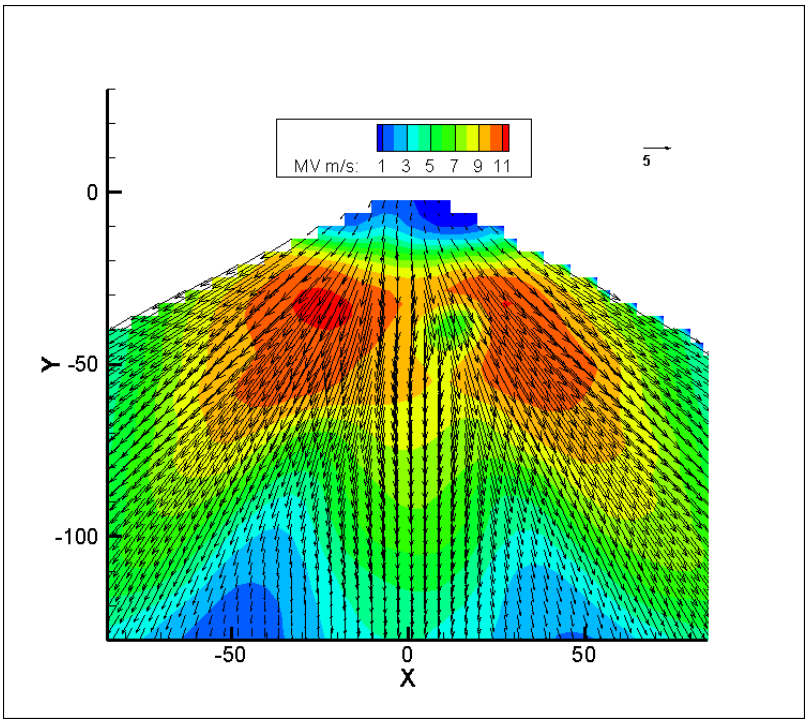

Figure 4.9 Average Velocity Profile for Water Flow of 9.99×10^{-3} kg/s and Air Flow of 7.40×10^{-3} kg/s

4.2 Air Only Measurements

The results for the air only PIV measurements are shown in Figures 4.10 – 4.12. These velocity profiles are quite different than the water and air combined flow profiles. The air only profiles show only two regions of high flow velocity at the edges of the flow. In the center of the flow is a region of very low velocity. The center of the flow is a reverse flow region. This phenomenon is expected, and it has been reported by many researchers. Hadef and Lenze called it a central toroidal recirculation zone (CTRZ). Hadef, R. and Lenze, B. (2005) The CTRZ becomes larger for the higher gas flow rates. The total velocity and the size of the spray cone increase for the larger flow rates, too. One possibility for the difference in the shape of the air only flow verses the water and air combined flow is that the flow in the center of the combined flow comes primarily from the liquid. The method used to calculate the combined flow actually measures the liquid flow that is under the influence of the air flow. The air flow then can only be inferred. This observation was also made by Hadef and Lenze when they measured the droplet size distribution. They noted that the center of the flow contained mainly larger droplets that seemed to overpower the CTRZ. Hadef, R. and Lenze, B. (2005) This hypothesis is constant with the data presented here. In general the spray cone angle is smaller for the air only flow than the water and air combined, and the air only flow is highly asymmetric. This asymmetry probably comes from the swirling nature of the flow. This effect is more pronounced in the air only results, since there is no liquid to absorb some of the air momentum. Finally, the magnitude of the velocity is much lower than expected. These anomalies cannot be explained, and are recommended as topics for further investigation.

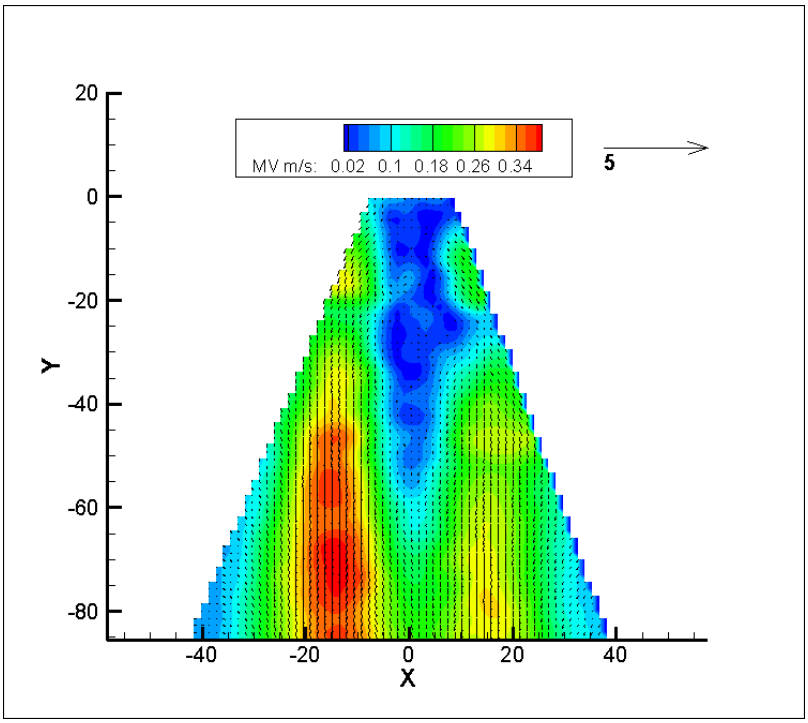

Figure 4.10 Average Velocity Profile for Air Only Flow of 2.47×10^{-3} kg/s

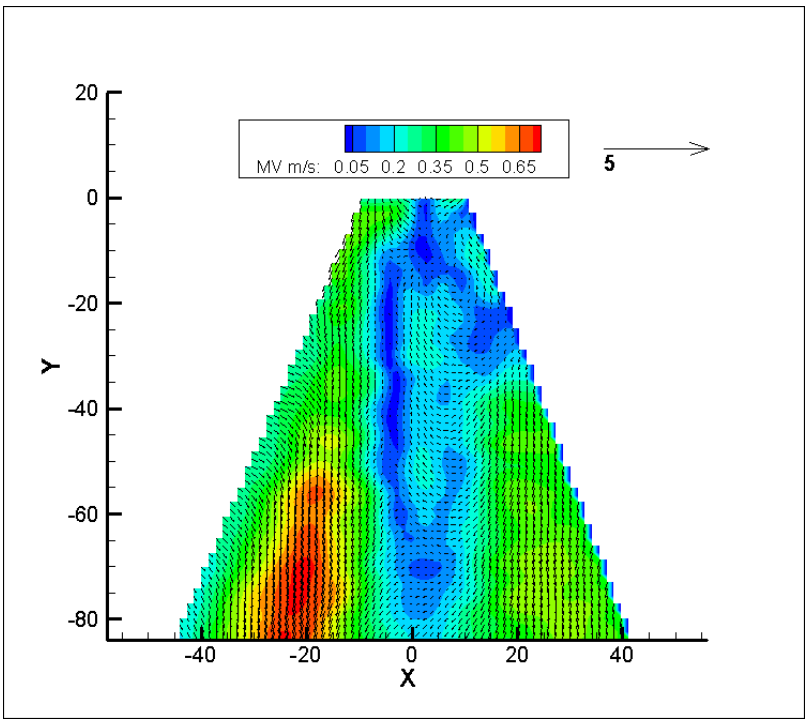

Figure 4.11 Average Velocity Profile for Air Only Flow of 4.93×10^{-3} kg/s

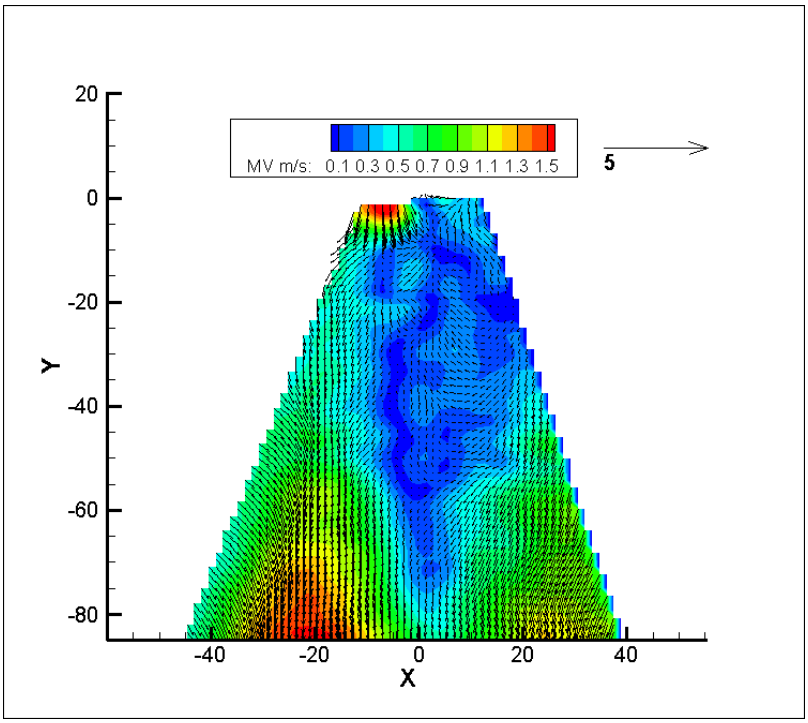

Figure 4.12 Average Velocity Profile for Air Only Flow of 7.40×10^{-3} kg/s

4.3 Fuel Substitute and Air Measurements

The results of the average velocity field for the fuel substitute and air combination flow are given in Figures 4.13 – 4.21. These velocity profiles are interesting, as they are a combination of the water and air flow and the air only profiles. At a low air flow rate of 2.47×10^{-3} kg/s the velocity profile closely resembles the water and air combined flow profile. It has clear tri-lobed high velocity regions. However in the far field, the center lobe starts to grow and split into two lobes. In the center of the middle lobe, a region of slow velocity flow develops. Although it is not reverse flow, it points to evidence that there is a CTRZ airflow that is opposing the liquid flow. As the air flow rate increases, the flow becomes less like the water and air combined flow and more like the air only flow. The outside two lobes become smaller and the inner lobe becomes larger. The central low velocity region also becomes larger. This leads to an overall shrinking of the spray cone angle. The transition from a flow velocity profile that is similar to the water and air profile to one that is like the air only profile happens slower at higher liquid flow rates. This suggests that there is some ALR at which this transition starts to occur for

this particular liquid. The transition value of ALR is around one, with values greater than one looking like the air only flow and values less than one that is similar to the water and air combined flow. Although the water and air measurements and the fuel substitute and air measurements are at different ALR's, the range of ALR's where this transition takes place for the fuel substitute and air is inside the range tested for the water and air measurements. This transition noted in the fuel substitute and air measurements is not noted in the water and air measurements. Therefore, it can be inferred that this transition ALR is dependent on the type of liquid used. Hence, the liquid physical properties, like viscosity and specific gravity, are important to the atomization process. This is also apparent because the fuel substitute is affected by the air much more than the water, especially at high ALR's. Finally, care must be taken when planning experiments to study spray flows. The liquid chosen to be studied should be very similar to the one used in the actual flow.

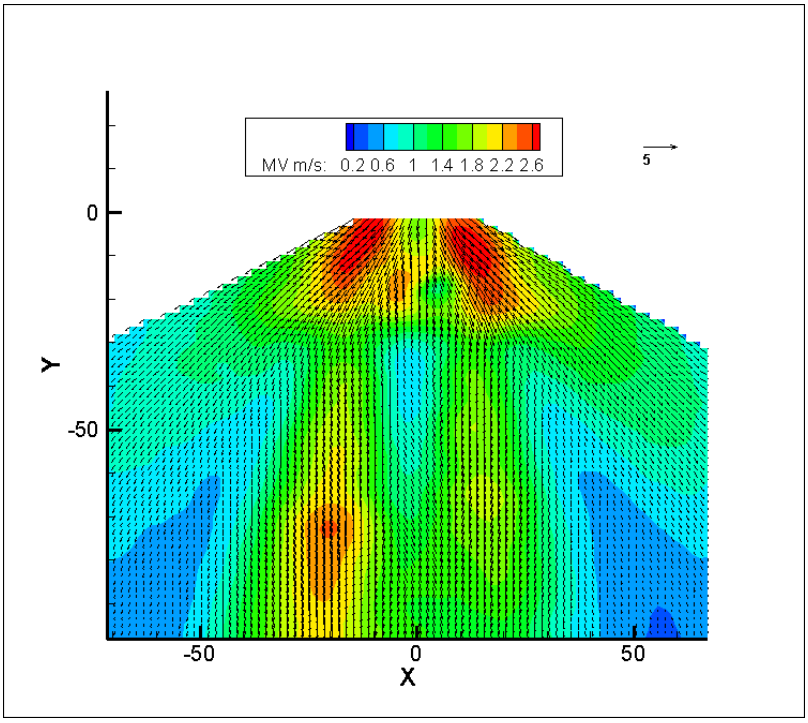

Figure 4.13 Average Velocity Profile for Fuel Substitute Flow of 2.57×10^{-3} kg/s and Air Flow of 2.47×10^{-3} kg/s

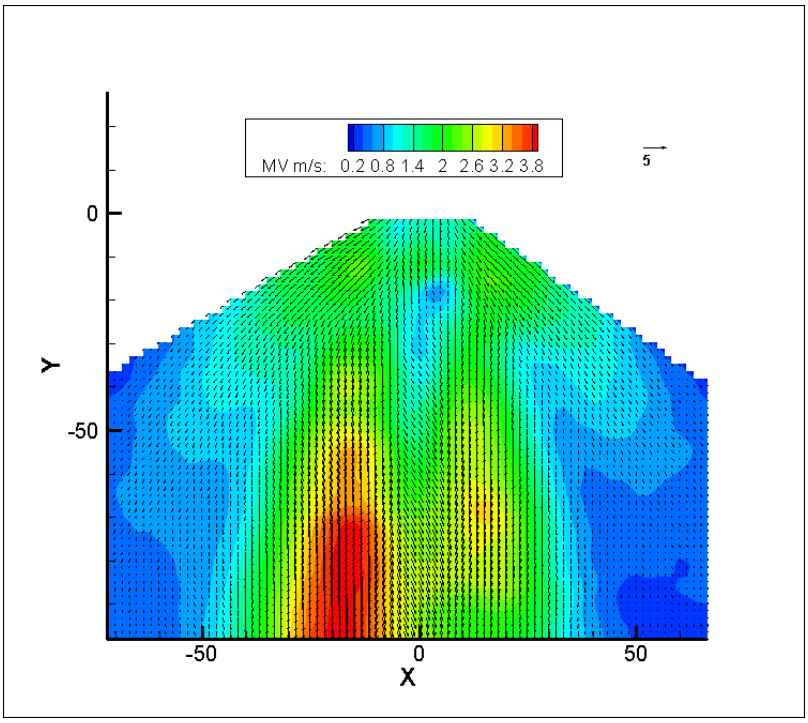

Figure 4.14 Average Velocity Profile for Fuel Substitute Flow of 2.57×10^{-3} kg/s and Air Flow of 4.93×10^{-3} kg/s

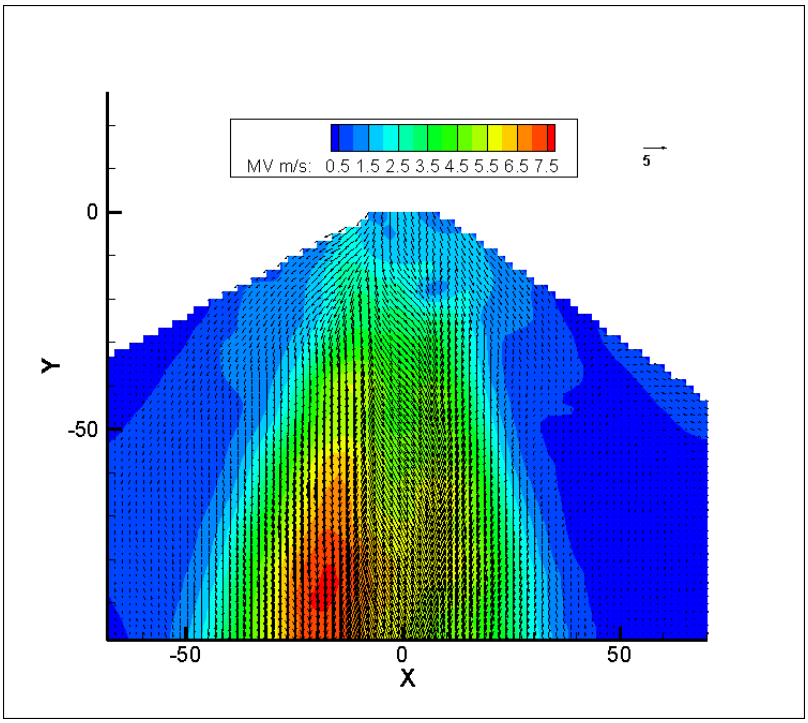

Figure 4.15 Average Velocity Profile for Fuel Substitute Flow of 2.57×10^{-3} kg/s and Air Flow of 7.40×10^{-3} kg/s

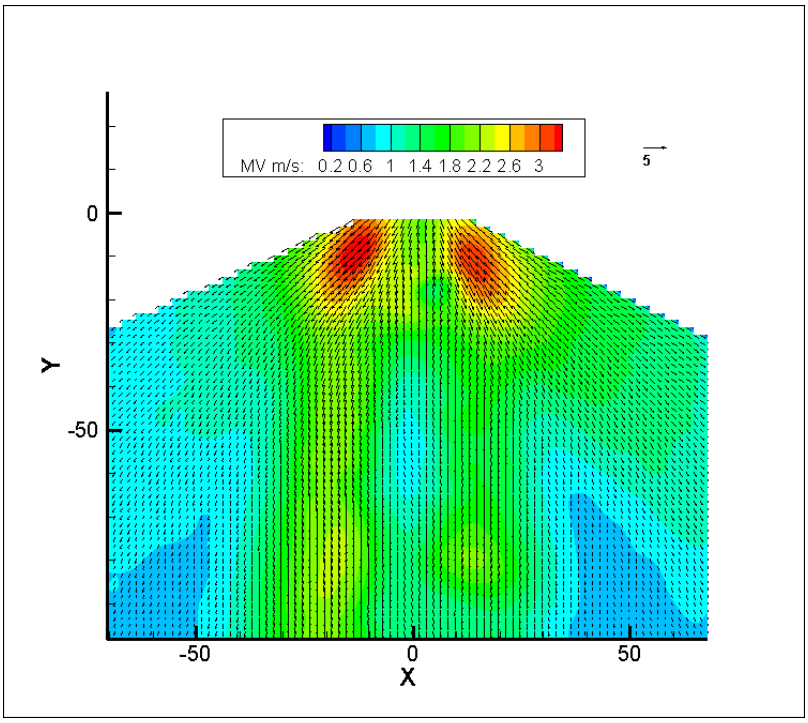

Figure 4.16 Average Velocity Profile for Fuel Substitute Flow of 5.13×10^{-3} kg/s and Air Flow of 2.47×10^{-3} kg/s

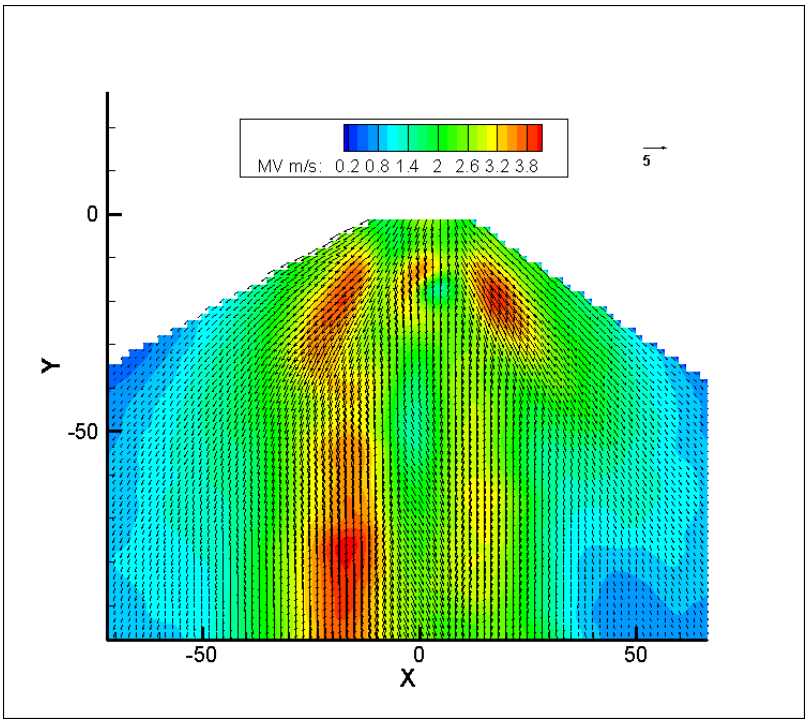

Figure 4.17 Average Velocity Profile for Fuel Substitute Flow of 5.13×10^{-3} kg/s and Air Flow of 4.93×10^{-3} kg/s

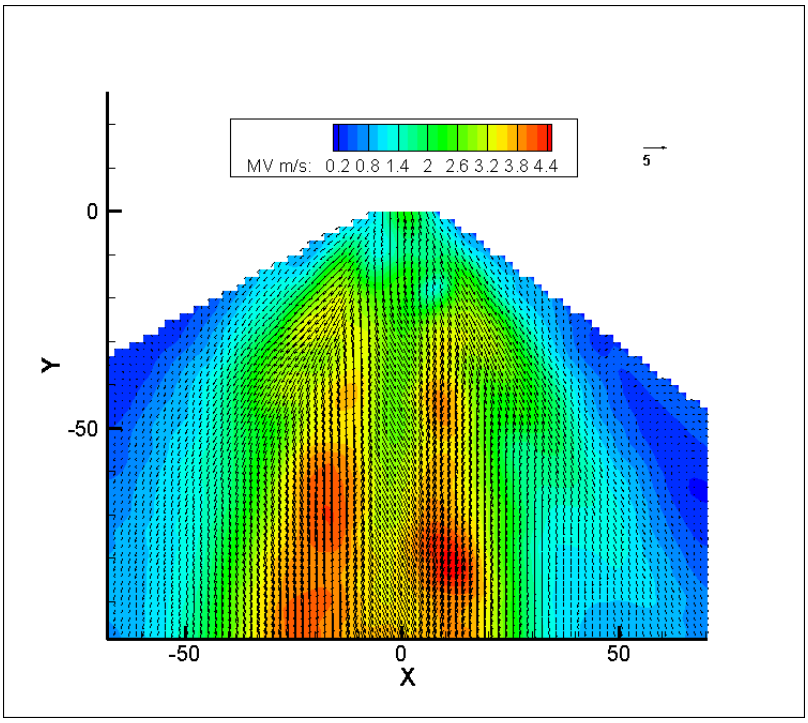

Figure 4.18 Average Velocity Profile for Fuel Substitute Flow of 5.13×10^{-3} kg/s and Air Flow of 7.40×10^{-3} kg/s

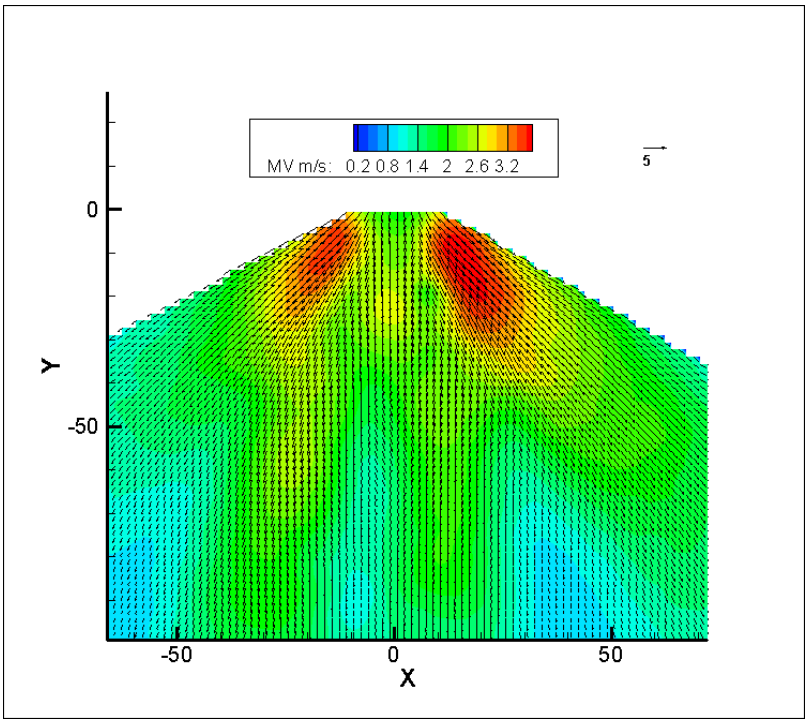

Figure 4.19 Average Velocity Profile for Fuel Substitute Flow of 7.70×10^{-3} kg/s and Air Flow of 2.47×10^{-3} kg/s

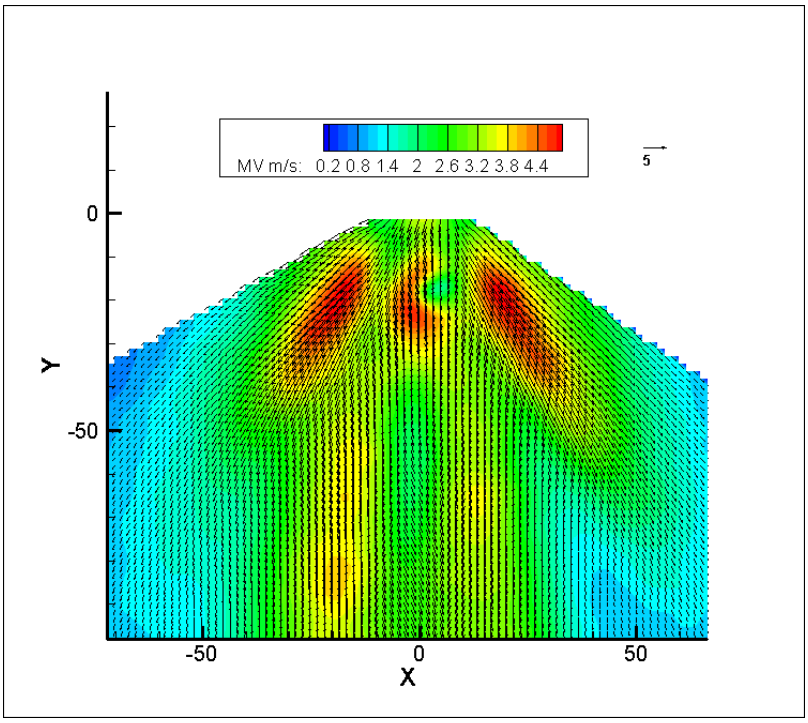

Figure 4.20 Average Velocity Profile for Fuel Substitute Flow of 7.70×10^{-3} kg/s and Air Flow of 4.93×10^{-3} kg/s

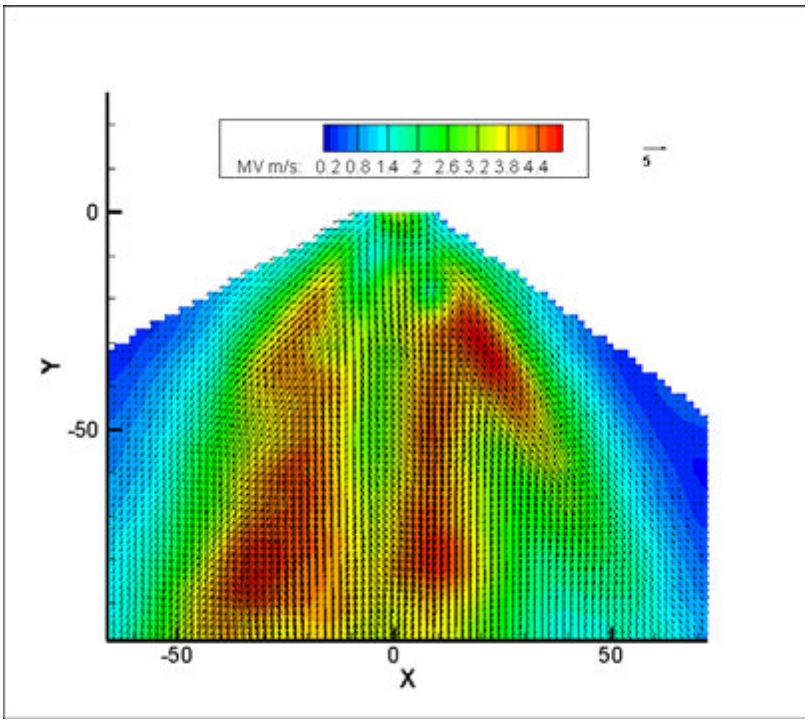

Figure 4.21 Average Velocity Profile for Fuel Substitute Flow of 7.70×10^{-3} kg/s and Air Flow of 7.40×10^{-3} kg/s

CHAPTER 5. STEREOSCOPIC PIV RESULTS

The results for the stereoscopic PIV measurements are reported in this chapter. These results include both the 3D velocity vector fields and a 2D velocity field projection onto the xy plane. All measurements are of the fuel substitute and air experiment. In all of the 3D plots, the velocity vectors are represented by the arrows and the contours are the magnitude of velocity. In the 2D projection plots, the vectors are the u and v velocity component projected onto the xy plane and the contours are the w component of velocity. All of the axes are shown in millimeters and the velocities are meters per second. The scales are not necessarily the same for all plots. The velocity averages are computed with more than one thousand image pairs.

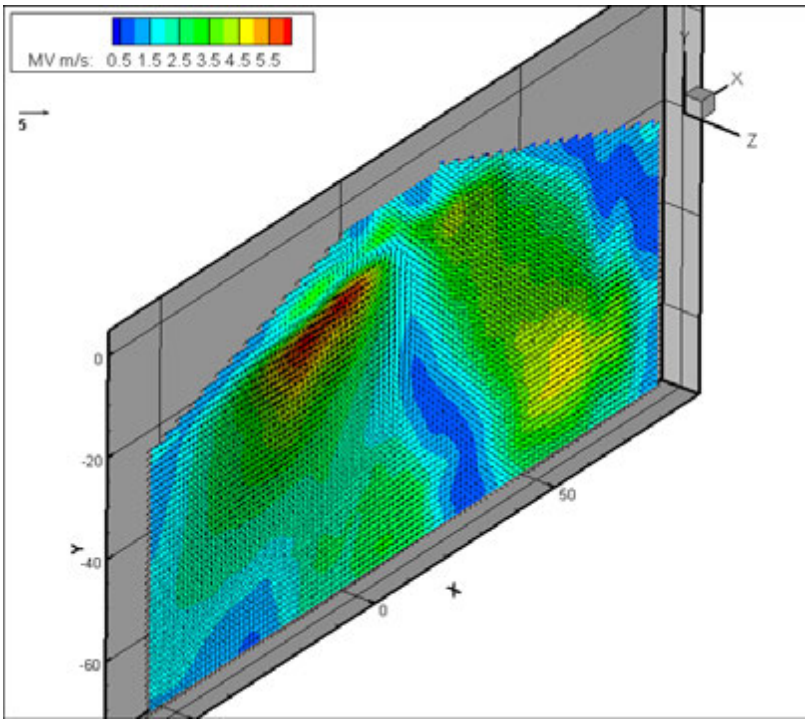

Figure 5.1 3D Average Velocity Profile for Fuel Substitute Mass Flow Rate of 2.57×10^{-3} kg/s and Air Mass Flow Rate of 2.47×10^{-3} kg/s

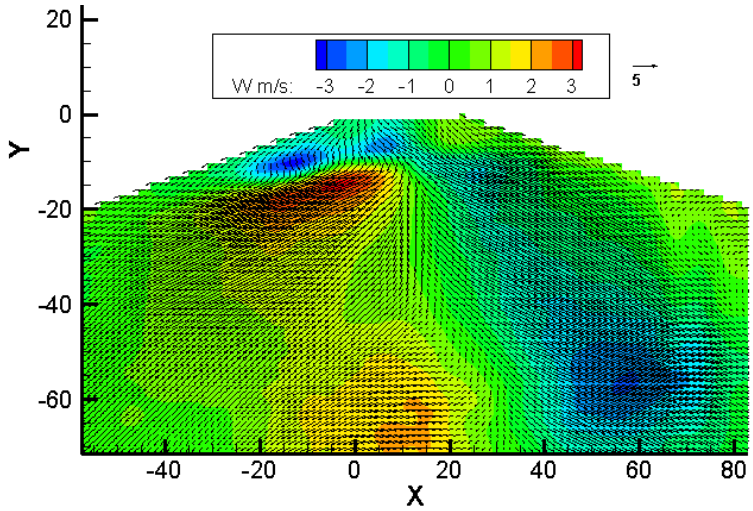

Figure 5.2 2D Average Velocity Projection for Fuel Substitute Mass Flow Rate of 2.57×10^{-3} kg/s and Air Mass Flow Rate of 2.47×10^{-3} kg/s

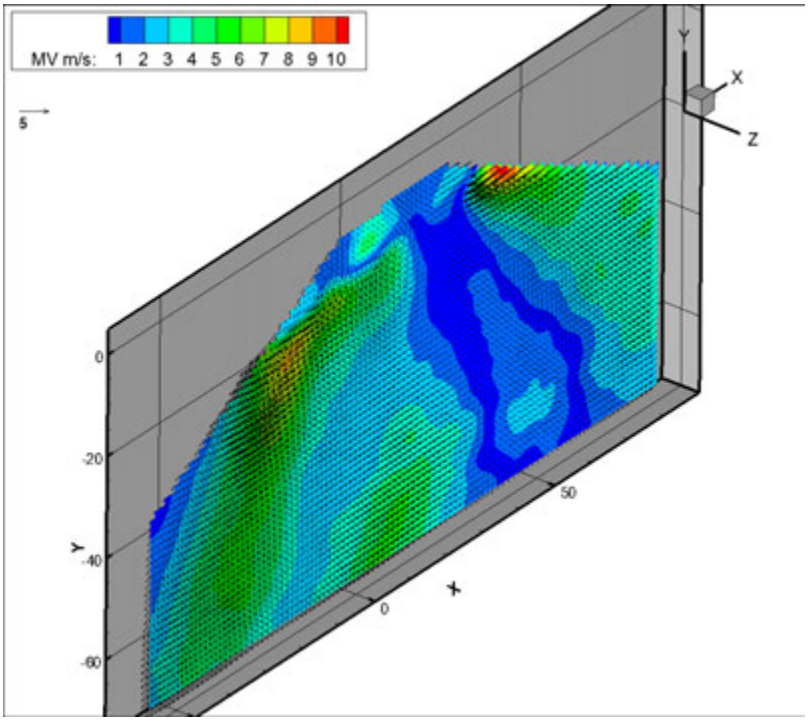

Figure 5.3 3D Average Velocity Profile for Fuel Substitute Mass Flow Rate of 2.57×10^{-3} kg/s and Air Mass Flow Rate of 4.93×10^{-3} kg/s

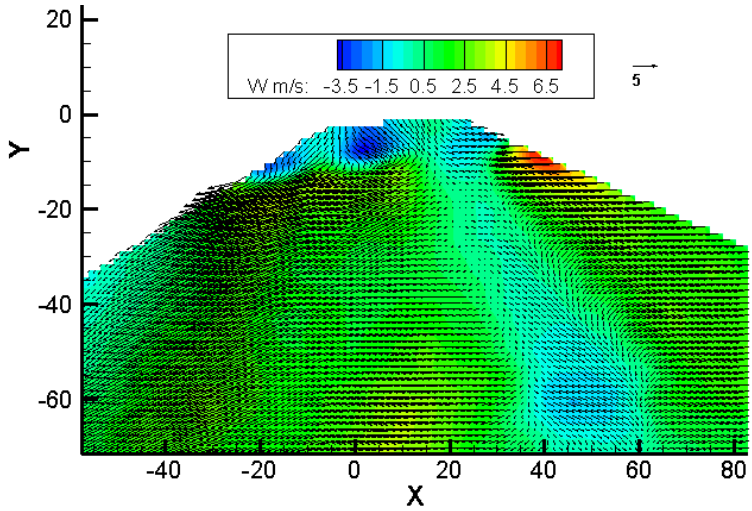

Figure 5.4 2D Average Velocity Projection for Fuel Substitute Mass Flow Rate of 2.57×10^{-3} kg/s and Air Mass Flow Rate of 4.93×10^{-3} kg/s

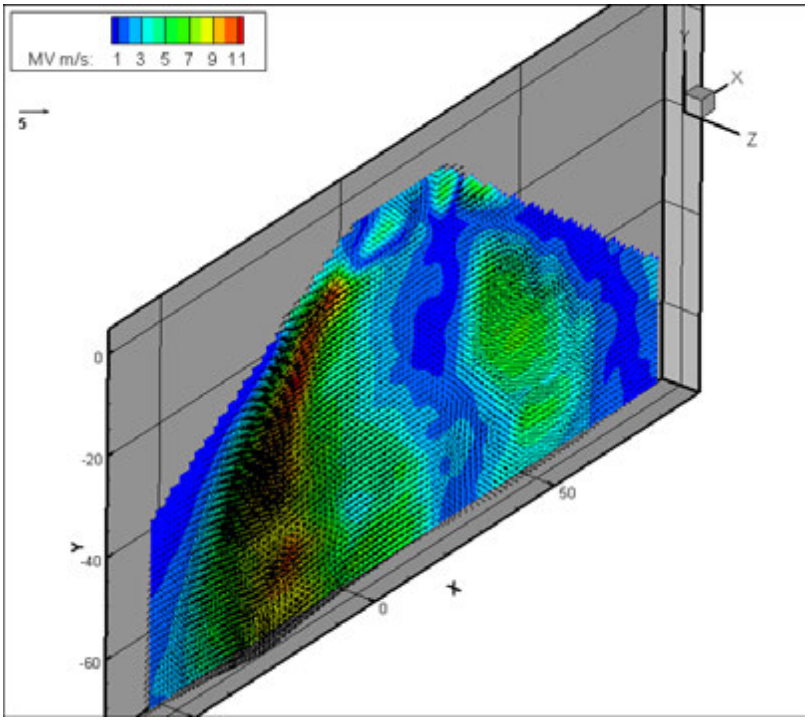

Figure 5.5 3D Average Velocity Profile for Fuel Substitute Mass Flow Rate of 2.57×10^{-3} kg/s and Air Mass Flow Rate of 7.40×10^{-3} kg/s

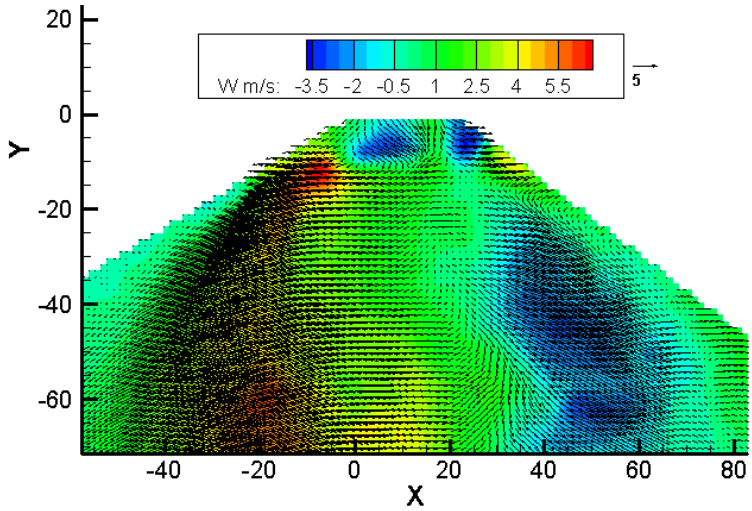

Figure 5.6 2D Average Velocity Projection for Fuel Substitute Mass Flow Rate of 2.57×10^{-3} kg/s and Air Mass Flow Rate of 7.40×10^{-3} kg/s

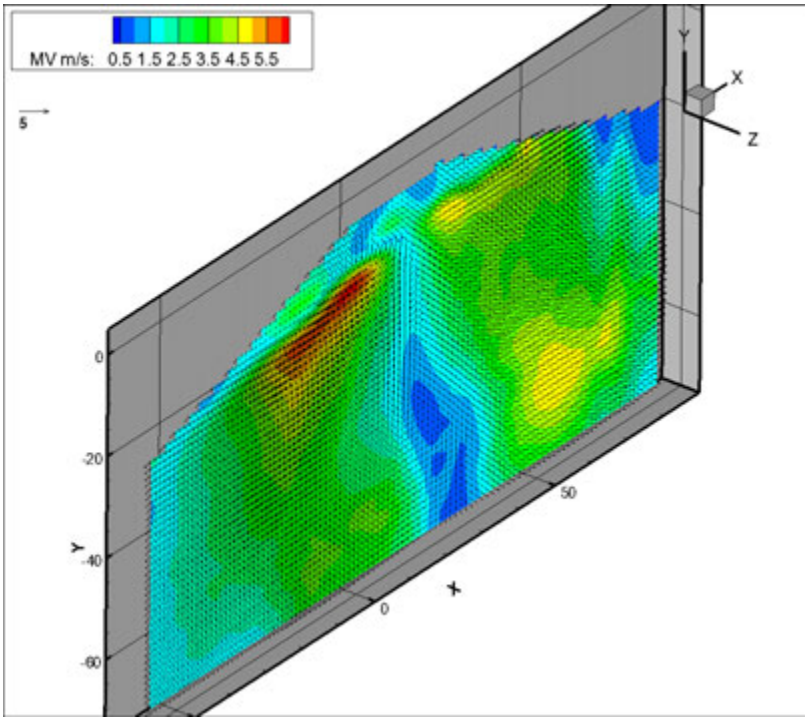

Figure 5.7 3D Average Velocity Profile for Fuel Substitute Mass Flow Rate of 5.13×10^{-3} kg/s and Air Mass Flow Rate of 2.47×10^{-3} kg/s

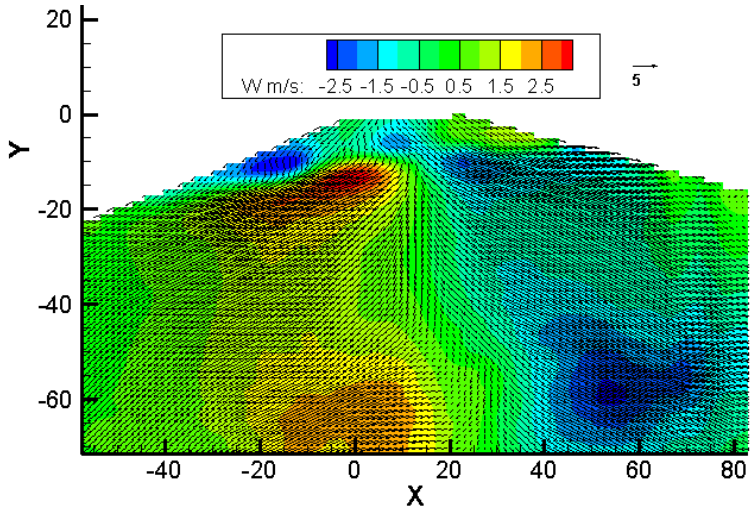

Figure 5.8 2D Average Velocity Projection for Fuel Substitute Mass Flow Rate of 5.13×10^{-3} kg/s and Air Mass Flow Rate of 2.47×10^{-3} kg/s

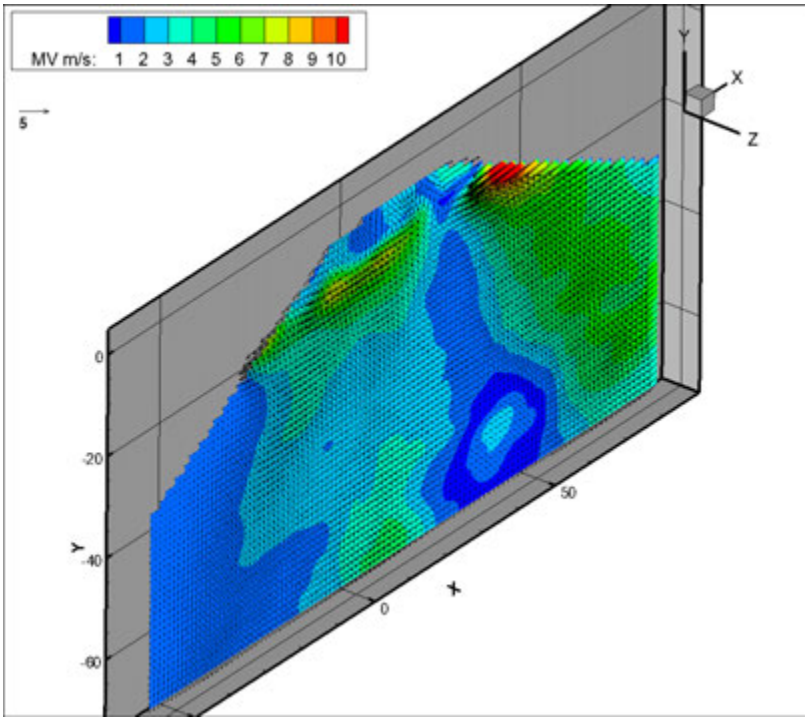

Figure 5.9 3D Average Velocity Profile for Fuel Substitute Mass Flow Rate of 5.13×10^{-3} kg/s and Air Mass Flow Rate of 4.93×10^{-3} kg/s

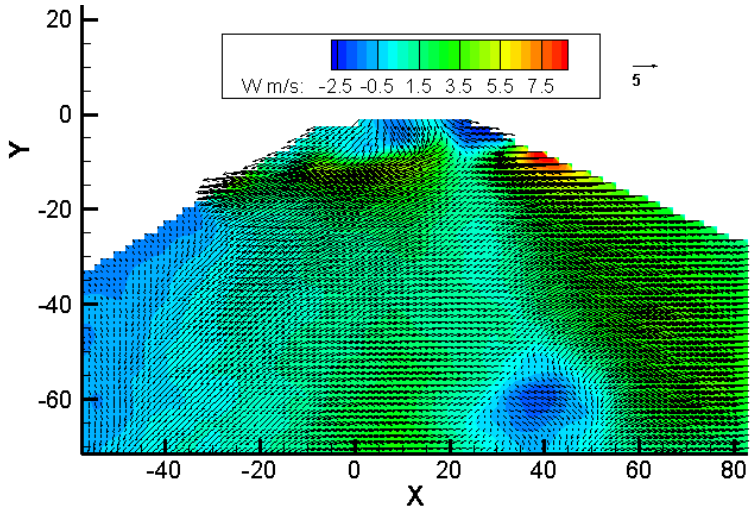

Figure 5.10 2D Average Velocity Projection for Fuel Substitute Mass Flow Rate of 5.13×10^{-3} kg/s and Air Mass Flow Rate of 4.93×10^{-3} kg/s

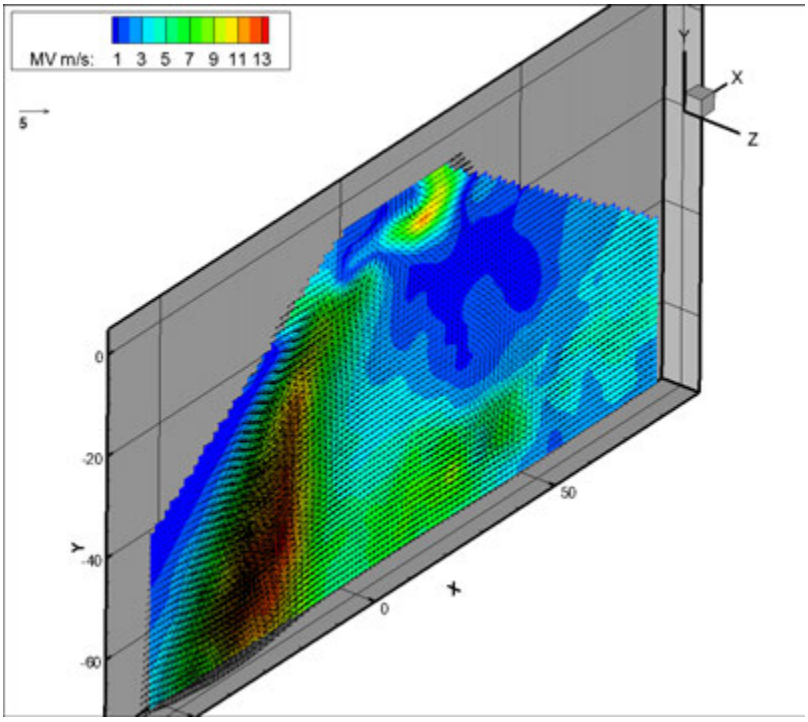

Figure 5.11 3D Average Velocity Profile for Fuel Substitute Mass Flow Rate of 5.13×10^{-3} kg/s and Air Mass Flow Rate of 7.40×10^{-3} kg/s

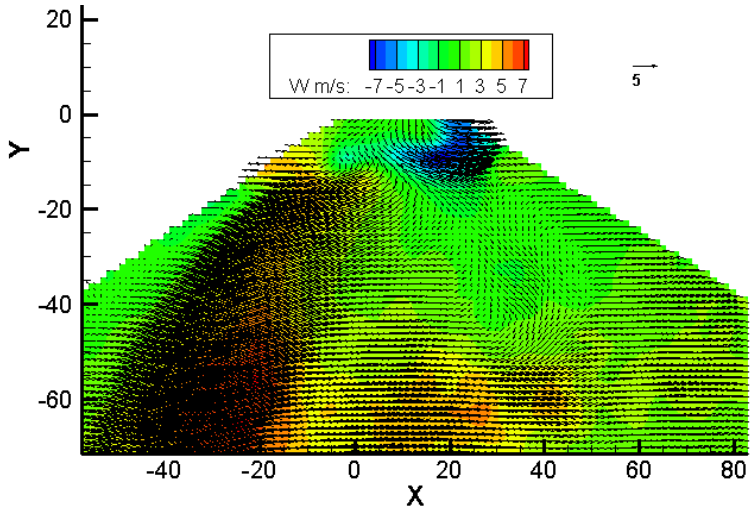

Figure 5.12 2D Average Velocity Projection for Fuel Substitute Mass Flow Rate of 5.13×10^{-3} kg/s and Air Mass Flow Rate of 7.40×10^{-3} kg/s

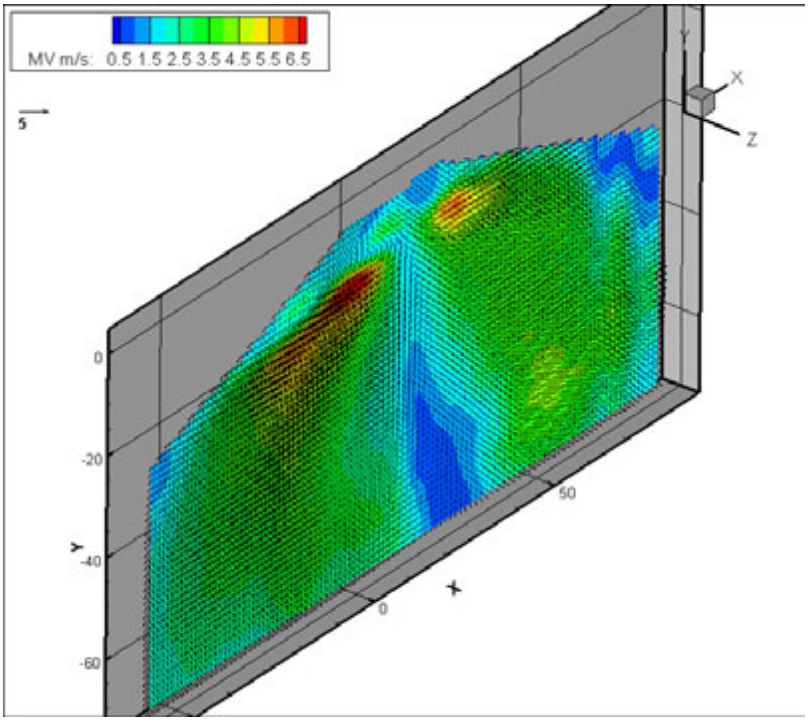

Figure 5.13 3D Average Velocity Profile for Fuel Substitute Mass Flow Rate of 7.70×10^{-3} kg/s and Air Mass Flow Rate of 2.47×10^{-3} kg/s

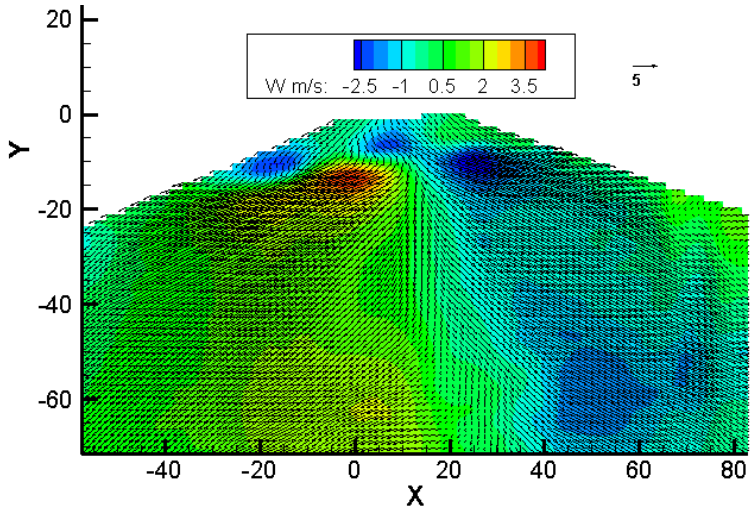

Figure 5.14 2D Average Velocity Projection for Fuel Substitute Mass Flow Rate of 7.70×10^{-3} kg/s and Air Mass Flow Rate of 2.47×10^{-3} kg/s

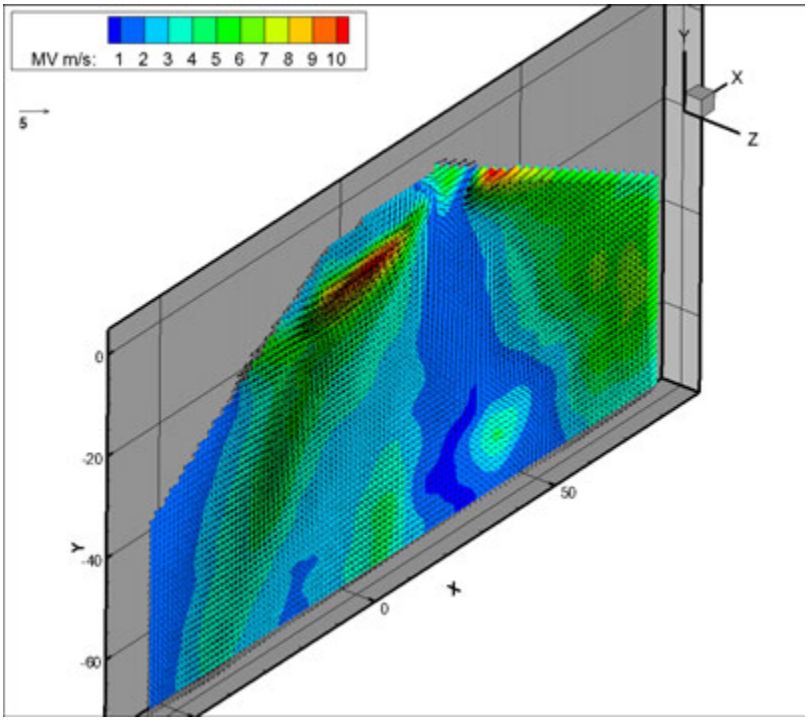

Figure 5.15 3D Average Velocity Profile for Fuel Substitute Mass Flow Rate of 7.70×10^{-3} kg/s and Air Mass Flow Rate of 4.93×10^{-3} kg/s

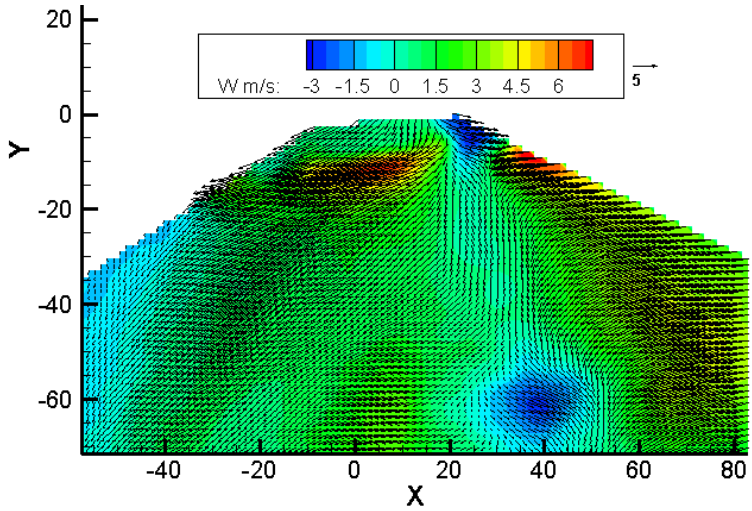

Figure 5.16 2D Average Velocity Projection for Fuel Substitute Mass Flow Rate of 7.70×10^{-3} kg/s and Air Mass Flow Rate of 4.93×10^{-3} kg/s

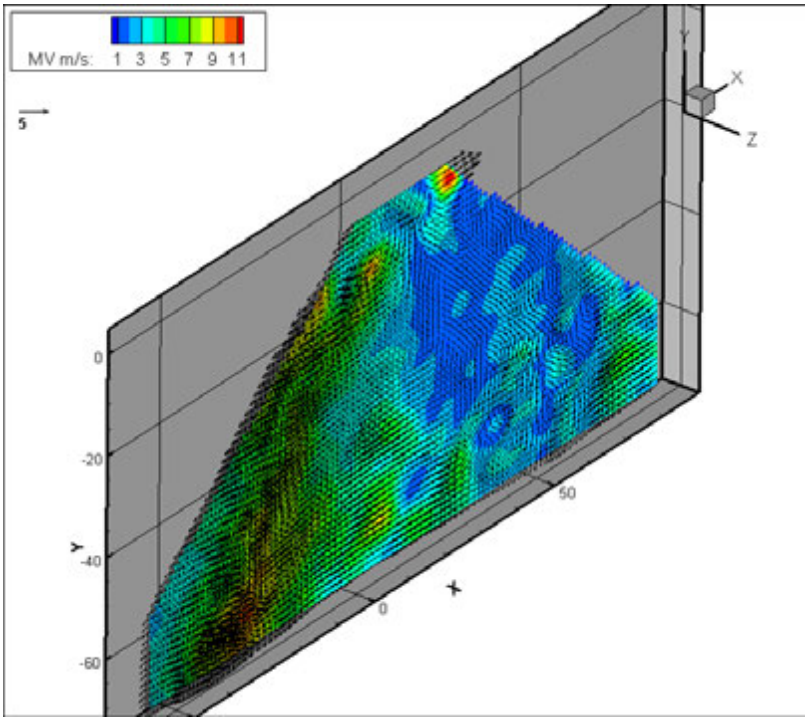

Figure 5.17 3D Average Velocity Profile for Fuel Substitute Mass Flow Rate of 7.70×10^{-3} kg/s and Air Mass Flow Rate of 7.40×10^{-3} kg/s

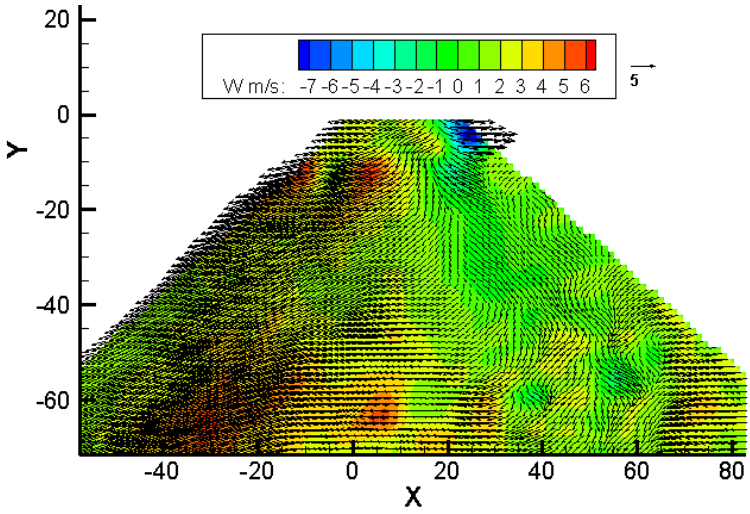

Figure 5.18 2D Average Velocity Projection for Fuel Substitute Mass Flow Rate of 7.70×10^{-3} kg/s and Air Mass Flow Rate of 7.40×10^{-3} kg/s

Figures 5.1 – 5.18 show the results for the stereoscopic PIV measurements. The odd numbered figures show the 3D velocity vectors and the even numbered figures show the 2D velocity vector projections. These results are significantly different as compared to the 2D PIV results. The general shape of the profile is closer to the expected shape for this type of nozzle. There are two areas of high velocity flow at the edge of the spray flow. In the middle, the velocity reduces greatly. This is noted in the 3D plots. However, there is an anomaly in these plots; the flow is not symmetric. The flow on the left side of the images has a higher velocity than on the right side of the images. This may be a result of the testing setup or measurement error, not a phenomenon of the flow itself. Looking at the 2D velocity projections, the u and v components of velocity behave as expected. These components are going diagonally away from the nozzle exit. The w component of velocity is interesting. In many of the plots, for example see Figure 5.8, there are pockets of high out of plane velocity flow which is not a continuous area of high velocity flow at the edge of the spray, as noted in the u and v components. Rather the w component displays distinct pairs of opposite high velocity regions. It appears as if the flow has taken a double helix pattern as it swirls about its axis. It is unclear what the cause of this result is; however, one explanation is that it resulted from a processing vortex core. Another observation is that the maximum w component of velocity is relatively large, over half of the

maximum total velocity.

A note on the results reported in this chapter: the error of the measurements increases as the flow rates increase, especially in the gas flow rate. Because of the testing setup, the image quality deteriorated as the flow rates increased, thus leading to more measurement error. This makes it difficult to see if there are any trends in the flow as the parameters change. Unlike the 2D PIV measurements of the fuel substitute and air, no major changes in the structure of the flow was noted as the flow rates increased. This difference is a subject for future research.

CHAPTER 6. VELOCITY PROFILE COMPARISONS

This chapter contains velocity profiles taken at different distances from the nozzle and compares them to the different experiments. The first section compares the 2D PIV water and air, the 2D PIV fuel substitute and air, and the SPIV tests. The second section compares the LDV results from Goodrich Engine Components and PIV. The water flow rates are always greater than the fuel substitute because of the miscalculation discussed in Section 3.6. Also the physical parameters are different for the fuel substitute than water. Table 6.1 gives a brief list of some of the physical parameters for these two fluids. A more complete list of the physical parameters for the fuel substitute is located in Appendix C. This gives different values of ALR for the water and air versus the fuel substitute and air as can be seen in Tables 3.1 and 3.2. This is deemed acceptable because of the small size of the variation and the little change in the flow between different ALR's for water. Also, the range of ALR values tested for water covers the range of ALR values tested for the fuel substitute.

	Water	Fuel Substitute
Specific Gravity	1.00	0.774
Kinematic Viscosity	1.139 centistrokes	1.220 centistrokes
Boiling Point	100°C	159°C

Table 6.1 Physical Parameters for the Fuel Substitute and Water at 60° F

6.1 Velocity Profile Comparisons

Figures 6.1 – 6.9 show the velocity profiles of the different tests for the conditions outlined in Table 3.2. In these figures, the first column is the u component of velocity, the second

column is the v component, and the third column is the w component. For the w component of velocity, only the results from the SPIV are shown as the others are zero by definition. The top row is a profile taken at one nozzle diameter away from the nozzle exit. The middle row is two nozzle diameters downstream and the bottom row is three nozzle diameters downstream. The nozzle diameter is 14.6 mm. All x axes are radial position measured in mm and all y axes are the velocity components measured in m/s.

In these figures, the velocity profiles vary greatly. It is clear that the type of liquid used makes a major difference, because the water and air profiles deviate from the fuel substitute and air profiles for both the 2D PIV and the SPIV. Although the 2D fuel substitute and the SPIV are closer in appearance, there are still variations in these profiles. Of the velocity components, the one that is in the most agreement is the u or radial component. These profiles are generally of the same shape, and the difference among the different tests is the magnitude of the velocity component. At the air mass flow rate of 2.47×10^{-3} kg/s, the SPIV results have the largest velocity; however, in the other cases the water has the largest velocity. The profile's shape was symmetric with one side of the central axis having negative velocities and the other side having positive velocities of equal size. This is expected. Nevertheless, some SPIV results deviate away from this symmetry. Also, the u component is the largest of the three components. The w component usually is similar to the u component. This is to be expected in an axis symmetric flow. The axial velocity, or v component, is interesting.

The water and air profiles are vastly different than the fuel substitute and air. In the water profiles the magnitude of the v component is larger than in the fuel substitute. With the water, the maximum velocity occurs on the central axis. With the fuel substitute, the maximum axial velocity occurs on either side, but just off, of the central axis. The velocity usually decreases significantly on the central axis. Although the 2D PIV and SPIV profiles for the fuel substitute are similar for the axial velocity, the two profiles are by no means the same. The profiles vary on the location of the peak velocity or sometimes the magnitude of the whole profile. The variations are greater for the larger flow rates. It should be noted that as with the Hadef, R. and Lenze, B. (2005) paper, all three of the velocity components are of the same order of magnitude.

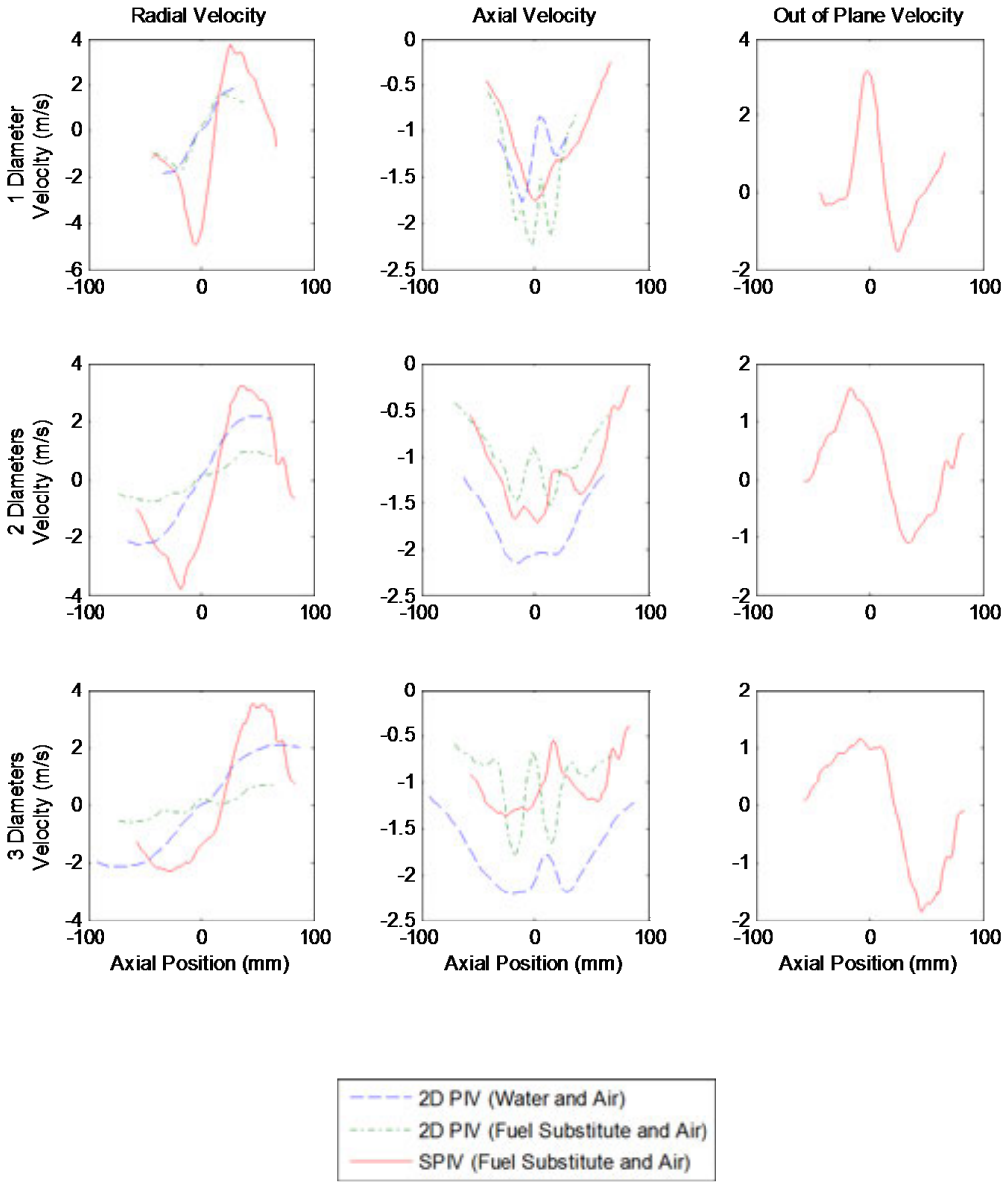

Figure 6.1 Velocity Component Profiles for Water Flow Rate of 3.33×10^{-3} kg/s, Fuel Substitute Flow Rate of 2.57×10^{-3} kg/s, and Air Flow Rate of 2.47×10^{-3} kg/s.

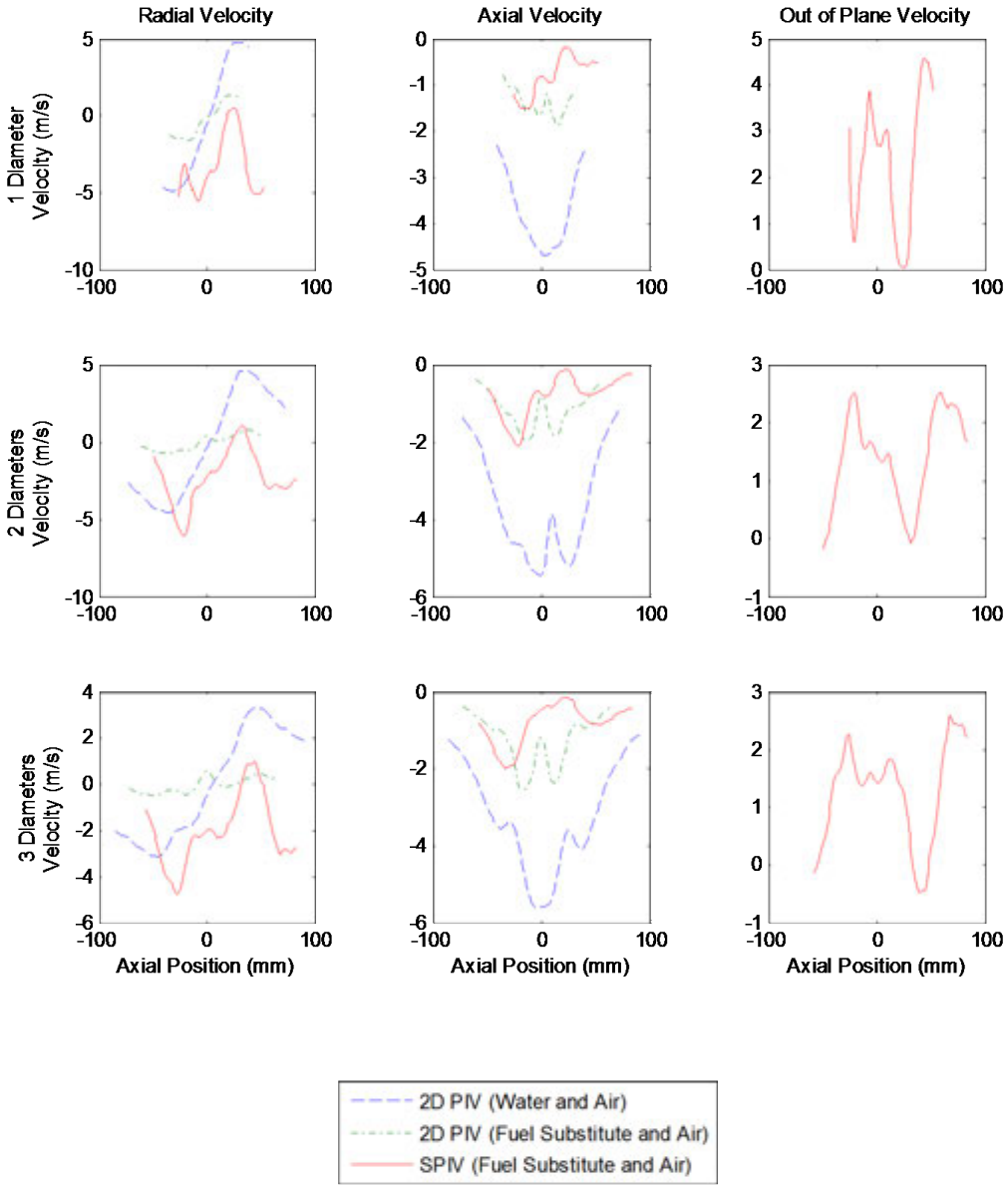

Figure 6.2 Velocity Component Profiles for Water Flow Rate of 3.33×10^{-3} kg/s, Fuel Substitute Flow Rate of 2.57×10^{-3} kg/s, and Air Flow Rate of 4.93×10^{-3} kg/s.

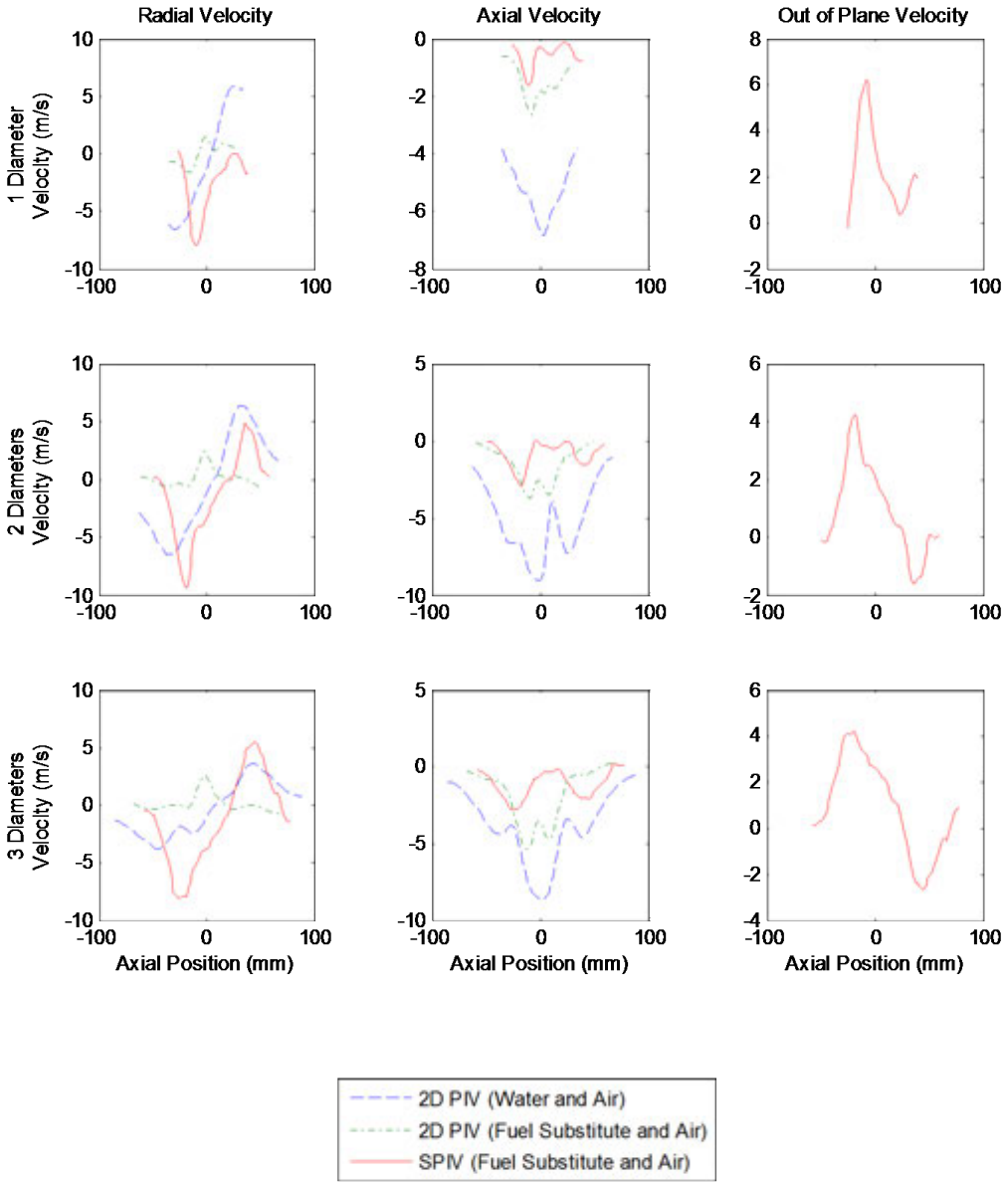

Figure 6.3 Velocity Component Profiles for Water Flow Rate of 3.33×10^{-3} kg/s, Fuel Substitute Flow Rate of 2.57×10^{-3} kg/s, and Air Flow Rate of 7.40×10^{-3} kg/s.

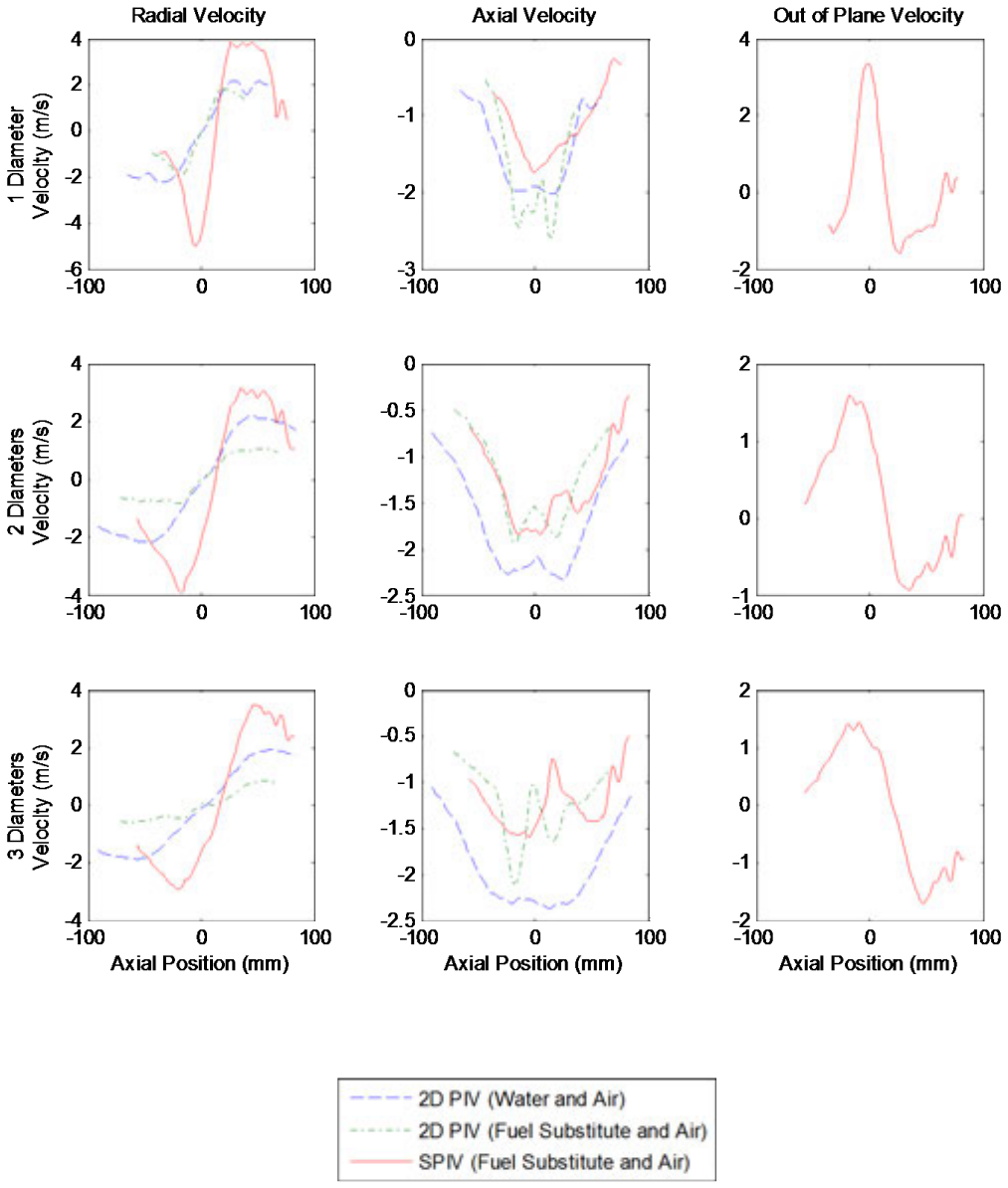

Figure 6.4 Velocity Component Profiles for Water Flow Rate of 6.66×10^{-3} kg/s, Fuel Substitute Flow Rate of 5.13×10^{-3} kg/s, and Air Flow Rate of 2.47×10^{-3} kg/s.

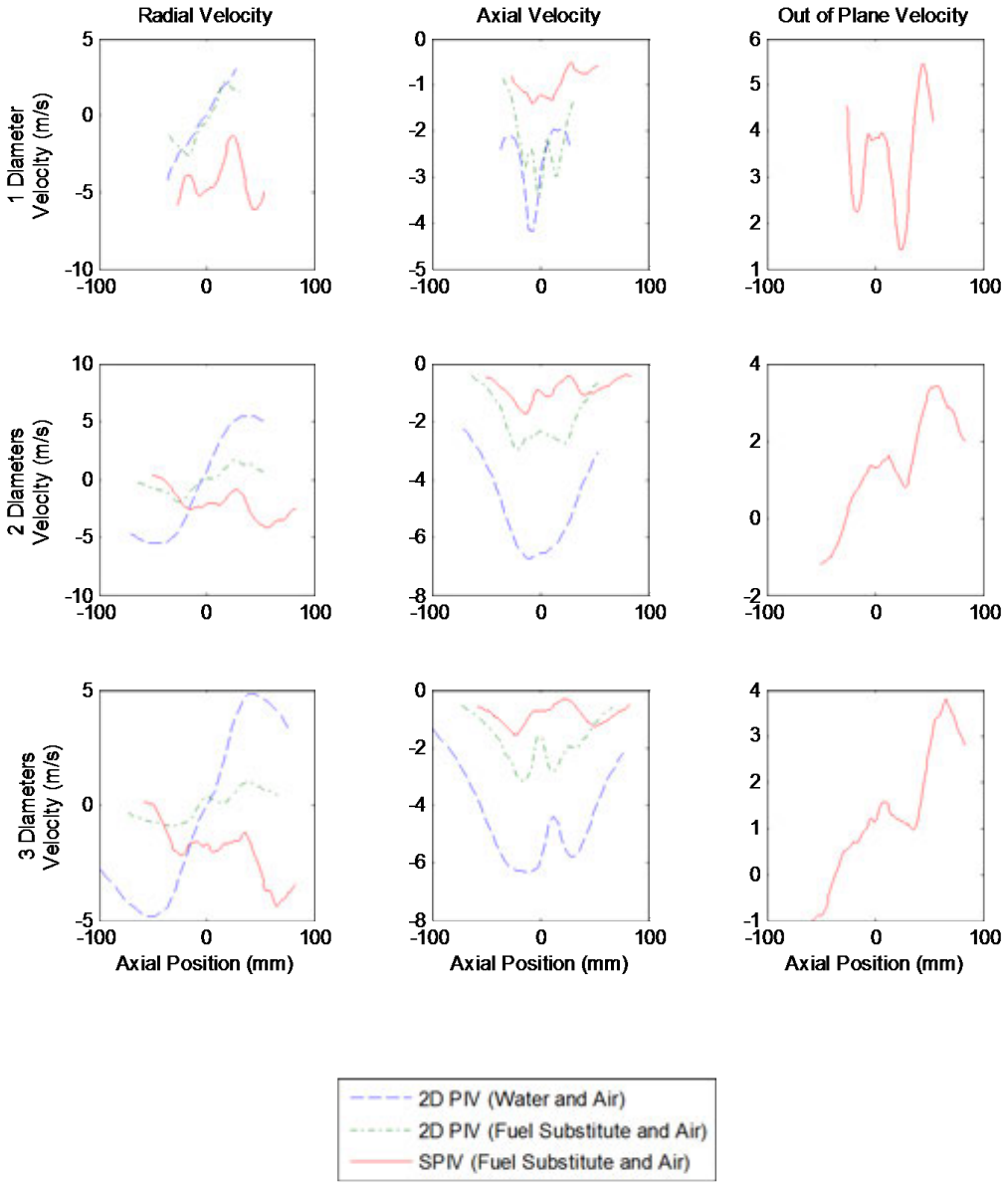

Figure 6.5 Velocity Component Profiles for Water Flow Rate of 6.66×10^{-3} kg/s, Fuel Substitute Flow Rate of 5.13×10^{-3} kg/s, and Air Flow Rate of 4.93×10^{-3} kg/s.

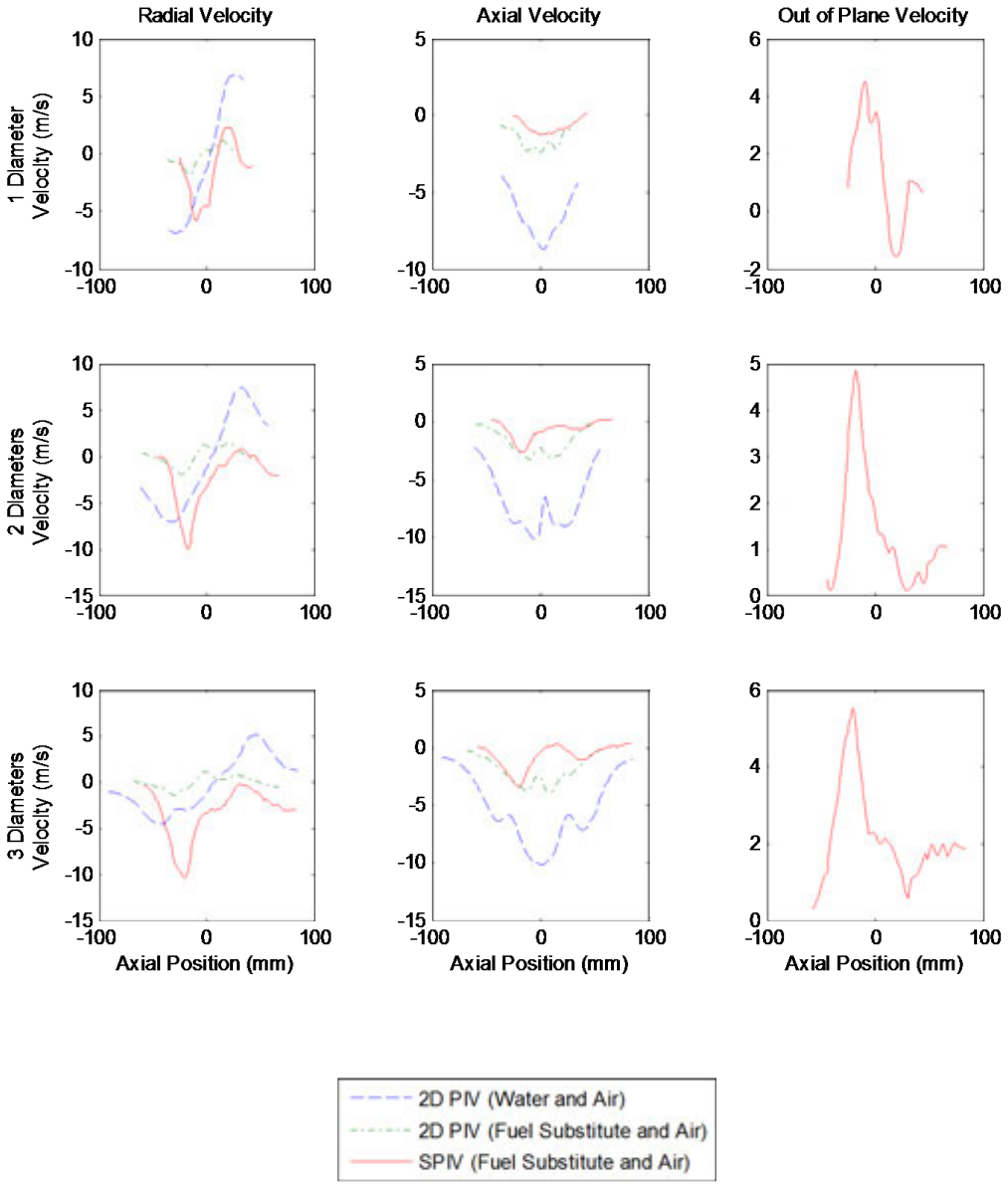

Figure 6.6 Velocity Component Profiles for Water Flow Rate of 6.66×10^{-3} kg/s, Fuel Substitute Flow Rate of 5.13×10^{-3} kg/s, and Air Flow Rate of 7.40×10^{-3} kg/s.

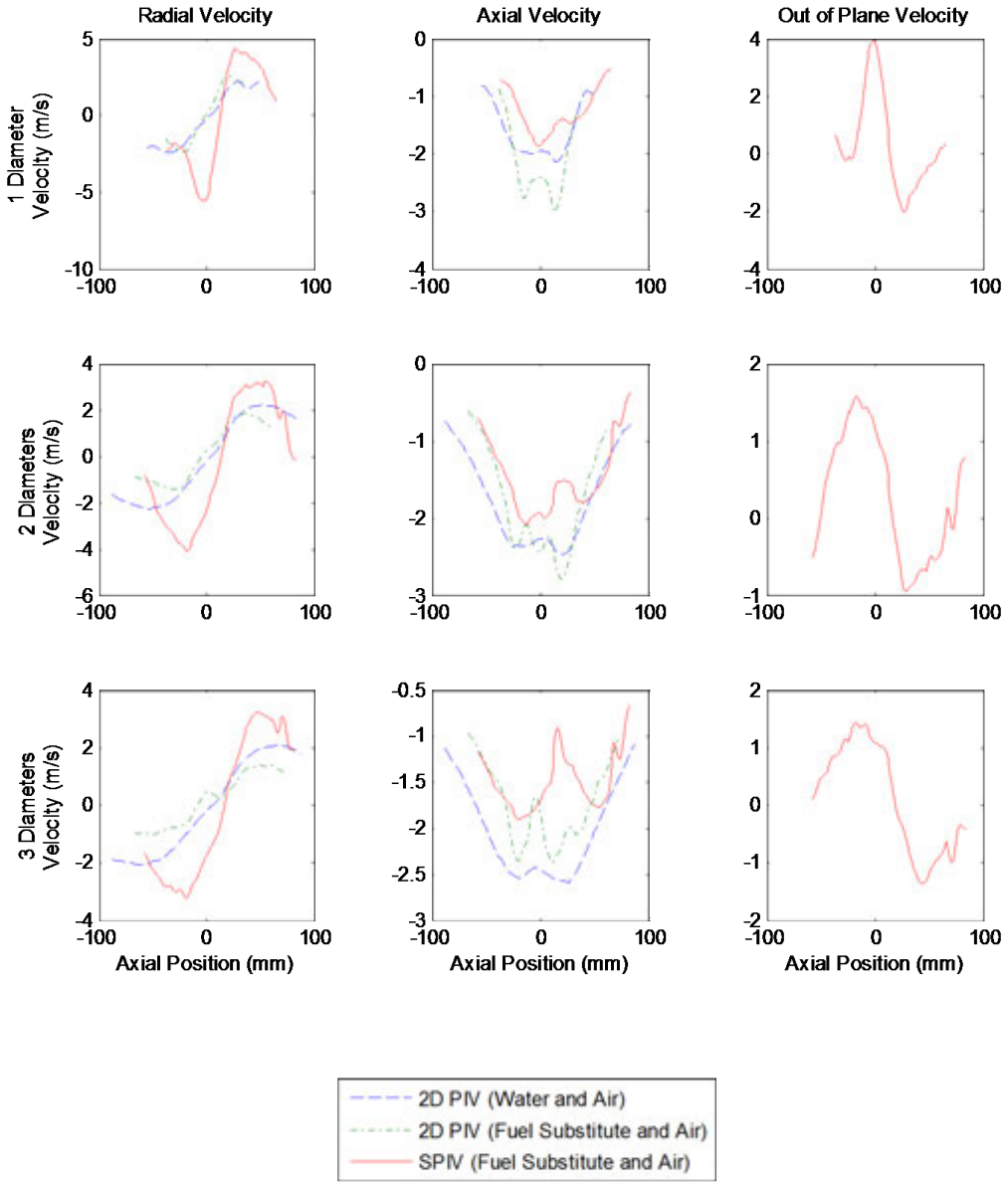

Figure 6.7 Velocity Component Profiles for Water Flow Rate of 9.99×10^{-3} kg/s, Fuel Substitute Flow Rate of 7.70×10^{-3} kg/s, and Air Flow Rate of 2.47×10^{-3} kg/s.

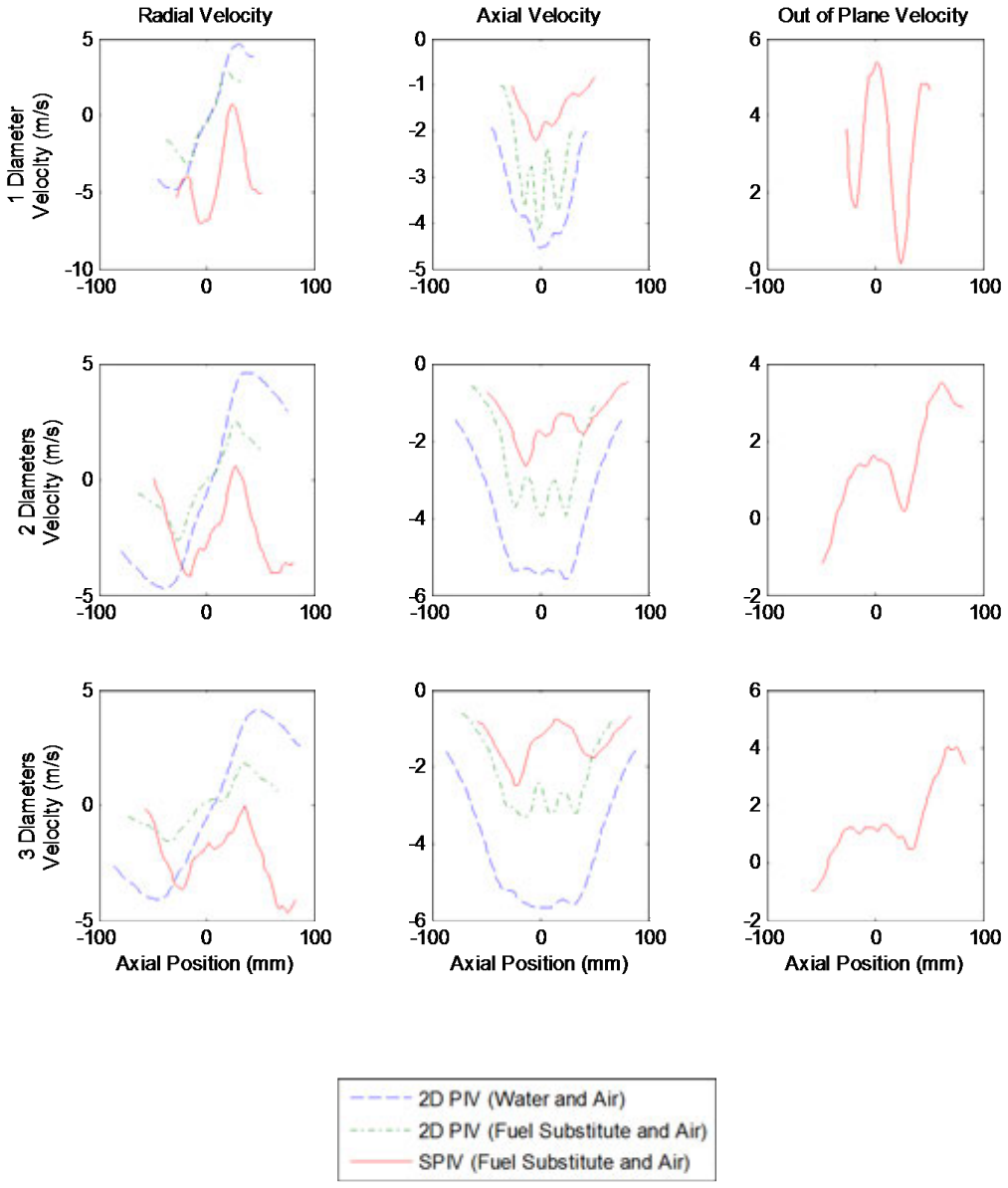

Figure 6.8 Velocity Component Profiles for Water Flow Rate of 9.99×10^{-3} kg/s, Fuel Substitute Flow Rate of 7.70×10^{-3} kg/s, and Air Flow Rate of 4.93×10^{-3} kg/s.

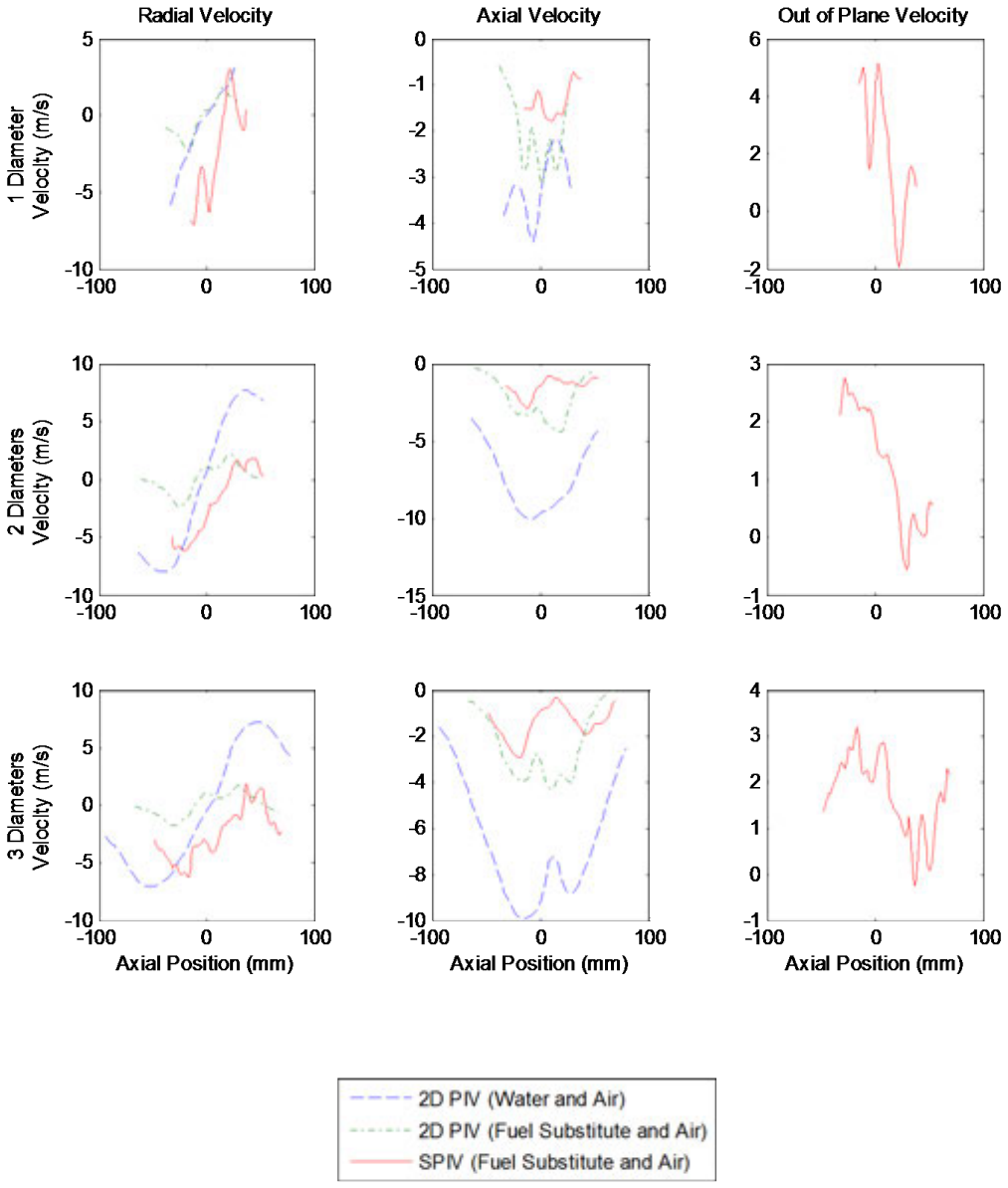

Figure 6.9 Velocity Component Profiles for Water Flow Rate of 9.99×10^{-3} kg/s, Fuel Substitute Flow Rate of 7.70×10^{-3} kg/s, and Air Flow Rate of 7.40×10^{-3} kg/s.

6.2 Comparison Between PIV and LDV

Goodrich Engine Components conducted LDV measurements of the spray flow under two flow conditions. These conditions are described in Section 3.6. Figures 6.10 – 6.13 show the comparison of the LDV to the PIV measurements. The velocity component in the radial direction, the u component, for the first control case (liquid flow rate of 2.52×10^{-3} kg/s and air flow rate of 3.46×10^{-3} kg/s) is shown in Figure 6.10. Figure 6.11 shows the axial velocity component, the v component, for the same flow conditions. Figures 6.12 and 6.13 show the radial and axial velocity components for the second control case (liquid flow rate of 7.36×10^{-3} kg/s and air flow rate of 6.93×10^{-3} kg/s). In both control cases, the liquid used for both the LDV measurements and the SPIV measurements is the fuel substitute. The liquids used for the 2D PIV measurements are both water and the fuel substitute. The velocity profiles are taken at one inch below the nozzle exit in all cases. The total flow vector fields are in Appendix B. As seen in Figures 6.10 and 6.12 the radial velocity components compare reasonably well. The water is of the correct magnitude and a similar shape, and the fuel substitute matches the shape, but has a much smaller magnitude. In Figure 6.12, the SPIV result matches the LDV result very well except that the peak velocities of the SPIV are smaller. In contrast the SPIV results in Figure 6.10, the peak velocities are higher than the LDV measurements. Figures 6.11 and 6.13 show that the axial velocity component profiles do not agree. Both the shape and the magnitude of the water PIV measurements do not match the LDV measurements. The shape of the velocity profile for water is a single hump profile with the maximum velocity on the central axis. However, the velocity profile for the LDV measurements is a double hump profile with the maximum velocity near, but not on, the central axis. Instead the velocity drops significantly at the central axis. Another difference between the water PIV and the LDV, is that the maximum velocity magnitude is much lower near the central axis for the water than it is for the LDV. The only place where the water PIV and the LDV axial velocity component profiles match is far from the central axis. Both profiles trend to the same profile in the far field. They match in both magnitude and shape. The axial velocity component profiles for the fuel substitute 2D PIV and the LDV agree better than the water PIV. The fuel substitute's double hump profile

resembles the shape of the LDV profile only on a smaller scale. The major difference is that the fuel substitute's 2D PIV profile is of a smaller magnitude than the LDV profile. The SPIV axial velocity results are comparable to the 2D PIV fuel substitute results both in shape and magnitude. However in the shape, the peaks and valleys of the SPIV are much more muted as compared to the 2D PIV of the fuel substitute. Also the SPIV results seem to be skewed in the positive x direction. Once again there seems to be a major difference between the behaviors of water in this atomizer verses the fuel substitute. It is also apparent that the velocity of the spray is under predicted by the PIV technique as compared to the LDV technique, especially near the central axis. Because this is consistent for all cases, a fundamental difference in the ability of PIV and LDV to measure these types of flows is suggested. It is recommended that further work be done to confirm and quantify these differences.

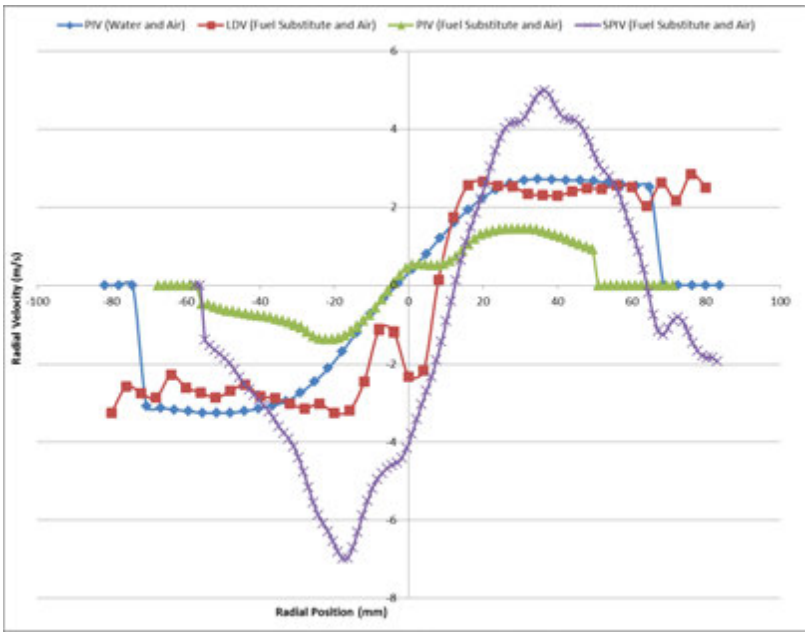

Figure 6.10 Comparison of Radial Velocity for LDV and PIV Measurements for Liquid Flow of 2.52×10^{-3} kg/s and Air Flow of 3.46×10^{-3} kg/s

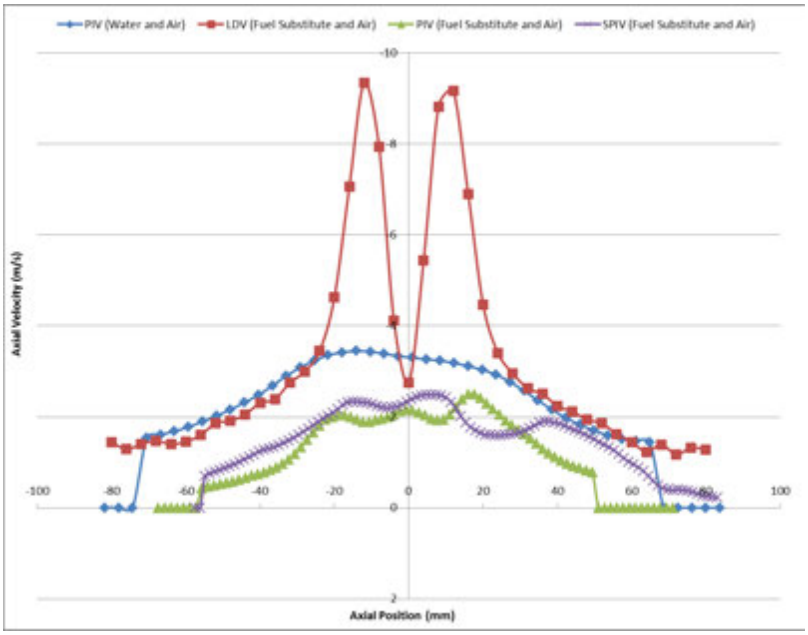

Figure 6.11 Comparison of Axial Velocity for LDV and PIV Measurements for Liquid Flow of 2.52×10^{-3} kg/s and Air Flow of 3.46×10^{-3} kg/s

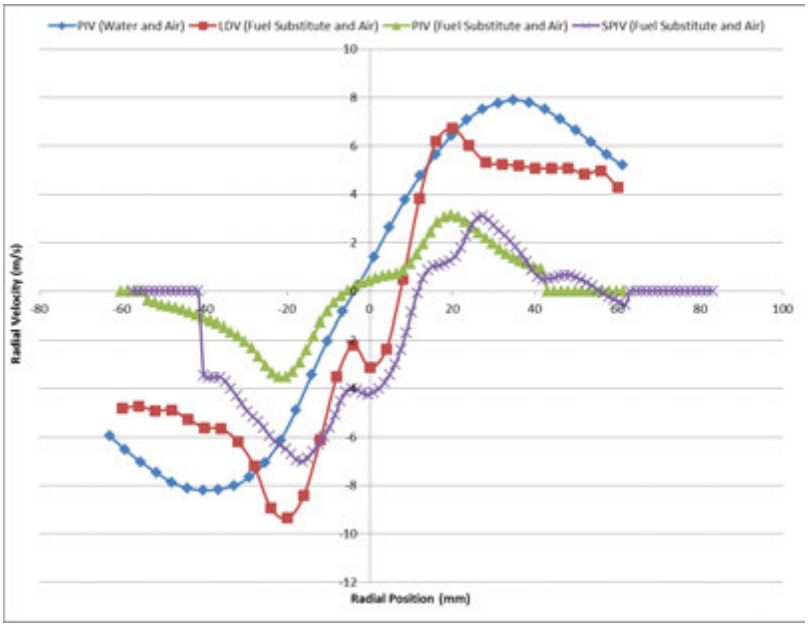

Figure 6.12 Comparison of Radial Velocity for LDV and PIV Measurements for Liquid Flow of 7.36×10^{-3} kg/s and Air Flow of 6.93×10^{-3} kg/s

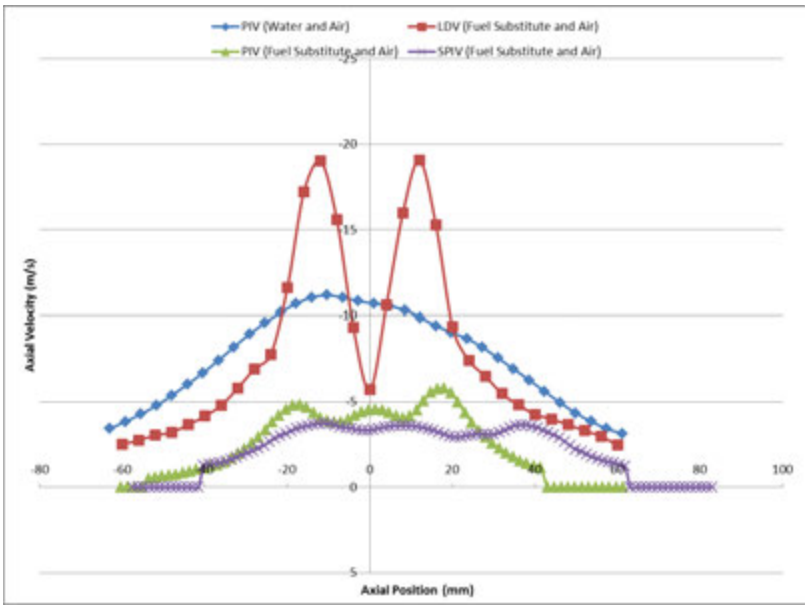

Figure 6.13 Comparison of Axial Velocity for LDV and PIV Measurements for Liquid Flow of 7.36×10^{-3} kg/s and Air Flow of 6.93×10^{-3} kg/s

6.3 Error Discussion

There are many sources of error in these experiments and reasons why the profiles do not agree for the LDV and all of the different PIV cases. One possible source of error could come from light scattering and whole cone illumination. This spray is predominately a hollow cone spray which means that there should be very few particles in the center of the flow when it is imaged on the central plane. However, when the light sheet passes through the left side of the flow, the light scatters everywhere. This causes two things to happen. First, the scattered light will illuminate the front and back portions of the flow, causing droplets to appear in the "center" of the flow. Second, the light sheet starts to expand. The expansion of the light sheet causes more of the cone to be illuminated but with less intensity on the right side of the flow. These two effects are offset by the imaging system. The camera and lens have a distinct and very small depth of focus. Therefore, images outside of this imaging volume will not be captured. They will appear as background noise that is filtered out during the PIV vector construction. In this study, the trade off relationship between the scattered light illumination and the depth of focus is not investigated and is left for future work. It is assumed that the

depth of focus greatly limited the light that appeared from extraneous sources. This is shown in Figure 6.14. This figure shows one of the raw images collected during the fuel substitute and air experiment. The image has two dense regions of droplets at the side of the spray and very few droplets in the center of the spray.

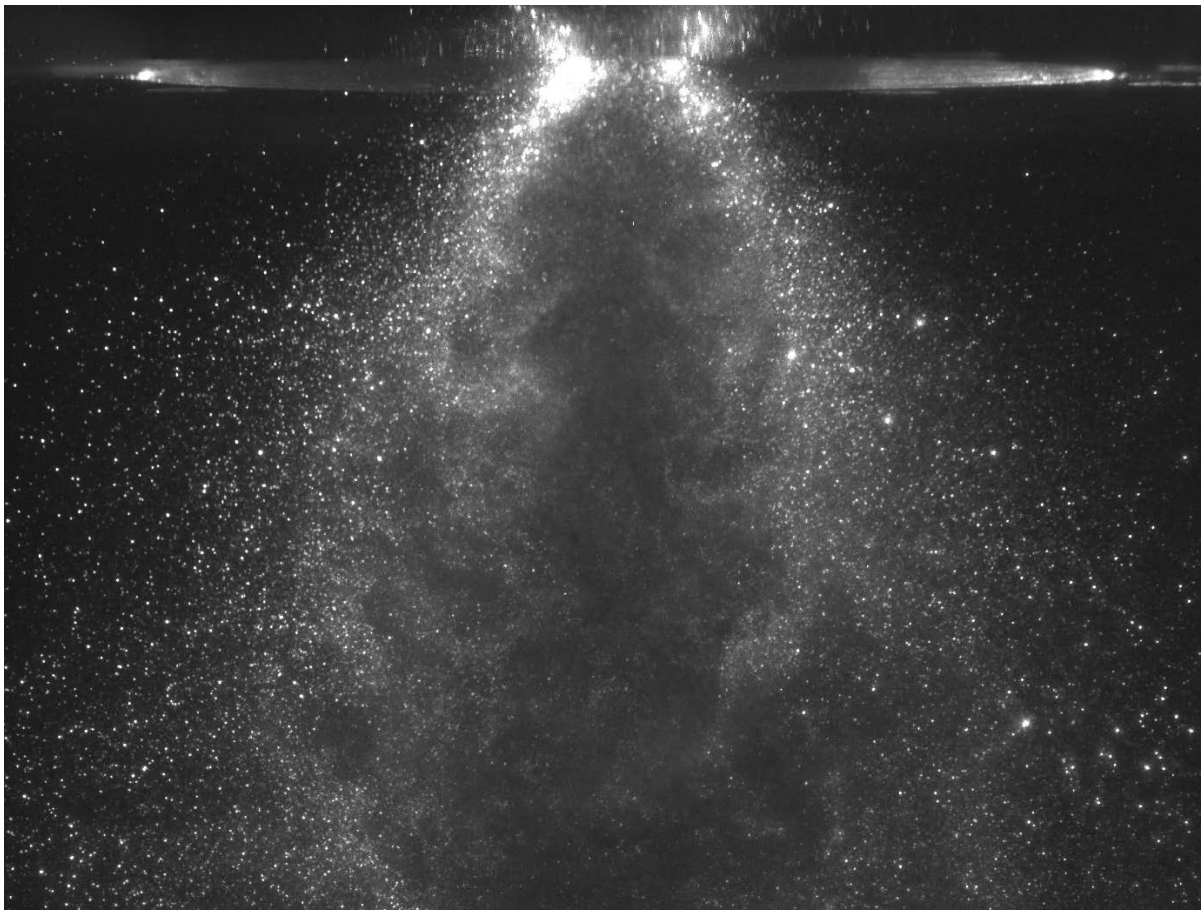

Figure 6.14 Raw Image for Fuel Substitute Flow of 5.13×10^{-3} kg/s and Air Flow of 4.93×10^{-3} kg/s.

Another reason why the PIV and LDV measurements might not line up well is that there are underlining fundamental differences between these two measurement techniques. One difference that becomes important in spray flow is the particle size. In well designed wind tunnel experiments, the seed particle size is uniform across the entire test section. However in spray flow, there are particles of many different sizes located throughout the flow. This is an important distinction because LDV and PIV are biased to different sized particles. LDV has a

small measurement volume and cannot measure any particles that are larger than the volume. LDV has biased measurements toward the velocity of the smallest particles within that volume. This is opposite in behavior than noted in PIV. In PIV the measurement volume is large. This volume fits most large droplets; however depending on the image resolution, some of the smallest droplets might not be recorded. When the PIV correlation algorithm is processed on the image, the velocity vectors are biased towards the velocity of the droplets with the strongest return in the interrogation window, a combination of the largest and most numerous droplets. In addition, after the velocity vectors are calculated, they are run through a smoothing algorithm in the post-processing code. This would produce a smoother profile as compared to the LDV results. Therefore, LDV velocity is biased towards the velocity of the smallest droplets, while PIV measurements are biased towards the velocity of the larger droplets. In a paper by Ghaemi, S. et al. (2008), it is found that the velocity of droplets of different sizes have vastly different velocity. This is expected and consistent with the findings of this investigation. Smaller droplets have a larger surface area to volume ratio. Therefore, they are affected by the air more than larger droplets because they have less inertia and relatively more force acting on them. It is clear the air mass flow rate is the driving force of the flow velocity, thus it is safe to assume that the smaller droplets will have greater velocity than the larger droplets. This helps to explain why the velocity measured by PIV is lower than the velocity measured by LDV. The effect is diminished the further you move away from the nozzle exit, as the droplets size distribution becomes more uniform. This is noted in Figures 6.10 – 6.13, as the velocity profiles are a closer match in the far field.

CHAPTER 7. CONCLUSION

The velocity profiles for spray produced from an air-blast atomizer were measured by a standard 2D PIV technique and a SPIV technique. These velocity profiles are for water and air, air only, and fuel substitute and air at several different flow input conditions using the 2D PIV technique. For fuel substitute and air, a variety of flow input conditions were used for the SPIV technique. The results of the water and air, and the fuel substitute and air PIV and SPIV measurements were compared to LDV measurements made by Goodrich Engine Components. In the 2D PIV measurements, it was found that the results depend heavily on the type of liquid in the spray. The water and air results produced a tri-lobed spray pattern that varied little with changing ALR. The air only measurements revealed a bi-lobed pattern with a strong CTRZ. The fuel substitute and air 2D PIV measurement results were a combination of the previous two results, varying from a bi-lobed pattern at high ALR to a tri-lobed pattern at low ALR. This suggested that there is a transition ALR present for the fuel substitute that is not present for water in the range of ALR's tested. This transition point was not seen in the SPIV fuel substitute and air results. In the SPIV results, the shape of the velocity magnitude showed two high velocity regions that were located on the side of the flow with relatively low velocity in the center. From the out of plane component of velocity, an apparent double helix shape of high velocity was noted. When compared to LDV measurements, the velocity profiles of the PIV measurements of water and air do not have the same shape, but do have similar magnitude. The PIV measurements of the fuel substitute and air have a similar shape to the LDV measurements, but a smaller magnitude. The SPIV results were close to the LDV measurements and to the 2D PIV fuel substitute results. It appeared that PIV measurements were able to successfully measure the spray flow; however, it seemed to consistently under estimate the velocity of the spray as compared to LDV and expected values. There were

asymmetric regions persistent throughout the flow. This asymmetry could come from the test setup and measurement errors. Using PIV to measure spray flow works well, although care needs to be taken in designing the experiment as the results are sensitive. It was clear from this investigation that the physical properties of the type of liquid used are a major factor for producing the spray flow characteristics. This should be of major consideration when designing an experiment or reading literature on spray flows. Using a single liquid, the ALR is a major controlling parameter that can control the spray flow characteristics; however, the extent of its effect varies.

There are many experiments and investigations that could be done as a follow up to this work. First, the findings of this work should be verified by repeating the results. The anomalies in the air only and the SPIV results should be investigated. Another experiment could look into what exactly is the transition ALR present in the 2D PIV fuel substitute results and why this occurs. That study could be followed up with why a transition is not seen in the water results. An investigation into the effects of light sheet scattering and whole cone illumination could be performed. This PIV measurement technique could also be extended to include temperature measurements. The liquid is already seeded with Rhodamine B; therefore the phosphorescent decay rate can be measured to calculate the temperature of the liquid. Both the temperature and velocity would then be simultaneously measured. One could also include a different fluorescent tracer for the air flow. It would then be theoretically possible to simultaneously measure both the liquid and gas flow's temperature and velocity.

APPENDIX A. CALCULATIONS

Each fluid flow rate is recorded in different units; however, they can all be converted into a common SI mass flow rate unit of kg/s. This is demonstrated in the flowing sections.

Air Mass Flow Rate

The air mass flow rate is recorded in standard liters per minute. In order to convert this to an SI mass flow rate unit, multiply the value by the density of air at the standard condition as seen in Equation A.1.

$$\dot{m}\left[\frac{kg}{s}\right] = \frac{P_{std}\,[Pa]}{R_{air}\left[\frac{J}{kg \cdot K}\right] T_{std}\,[K]} \dot{V}\,[SLPM]\,\frac{1\,[min]}{60\,[s]}\,\frac{1\,[m^3]}{1000\,[L]} \tag{A.1}$$

$$\text{Where:} \quad P_{std} = 14.6959\,[PSI] \quad R_{air} = 287\left[\frac{J}{kg \cdot K}\right] \quad T_{std} = 25\,[^{\circ}C]$$

Water Mass Flow Rate

The mass flow rate of the water is measured as a volumetric flow rate in liters per minute. It is assumed that the density of water remains constant; therefore, the volumetric flow rate can be converted to a mass flow rate by multiplying it by the density as in Equation A.2.

$$\dot{m}\left[\frac{kg}{s}\right] = \rho_{water}\left[\frac{kg}{m^3}\right] \times \dot{V}\left[\frac{L}{min}\right]\,\frac{1\,[min]}{60\,[s]}\,\frac{1\,[m^3]}{1000\,[L]} \tag{A.2}$$

$$\text{Where:} \quad \rho_{water} = 998\left[\frac{kg}{m^3}\right]$$

Fuel Substitute Mass Flow Rate

The fuel substitute mass flow rate is directly measured in pounds per hour. This is converted into kilograms per second in Equation A.3.

$$\dot{m}\left[\frac{kg}{s}\right] = \dot{m}\left[\frac{lb}{hr}\right]\frac{1\,[hr]}{3600\,[s]}\frac{1\,[kg]}{2.205\,[lb]} \tag{A.3}$$

LDV Comparison

The LDV measurements made by Goodrich Engine Components for the mass flow rates of the fuel substitute and air are reported in pounds per hour. These rates can be converted into the SI units of kilograms per second by using Equation A.3.

APPENDIX B. ADDITIONAL RESULTS

This appendix includes the remaining velocity vector fields and profiles not included in the main text. They are included here for fullness and completeness.

Water and Air 2D PIV Results

Figures B.1 – B.16 show the remaining average velocity fields for the standard 2D PIV water and air experiment.

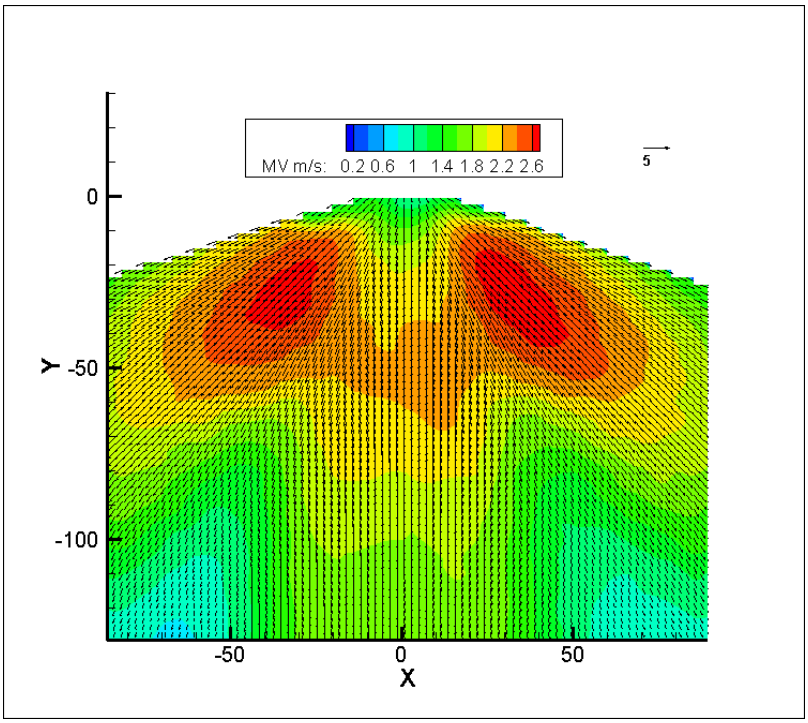

Figure B.1 Average Velocity Profile for Water Flow of 5.00×10^{-3} kg/s and Air Flow of 2.47×10^{-3} kg/s

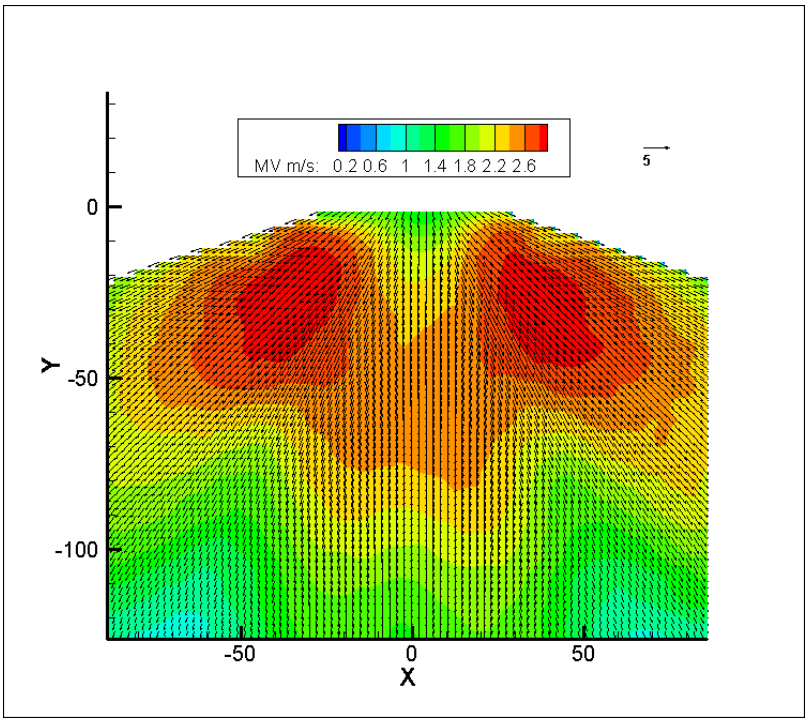

Figure B.2 Average Velocity Profile for Water Flow of 8.33×10^{-3} kg/s and Air Flow of 2.47×10^{-3} kg/s

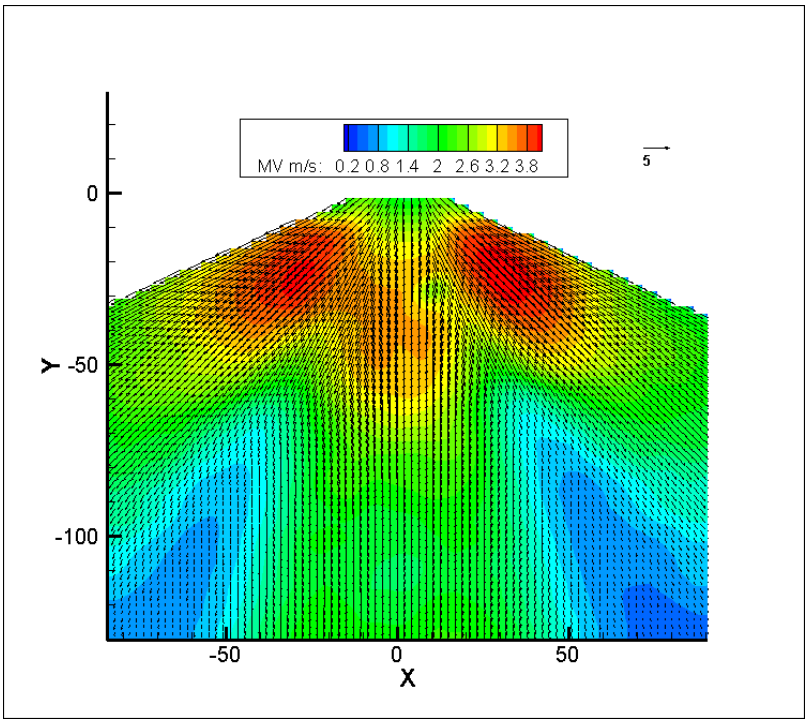

Figure B.3 Average Velocity Profile for Water Flow of 3.33×10^{-3} kg/s and Air Flow of 3.70×10^{-3} kg/s

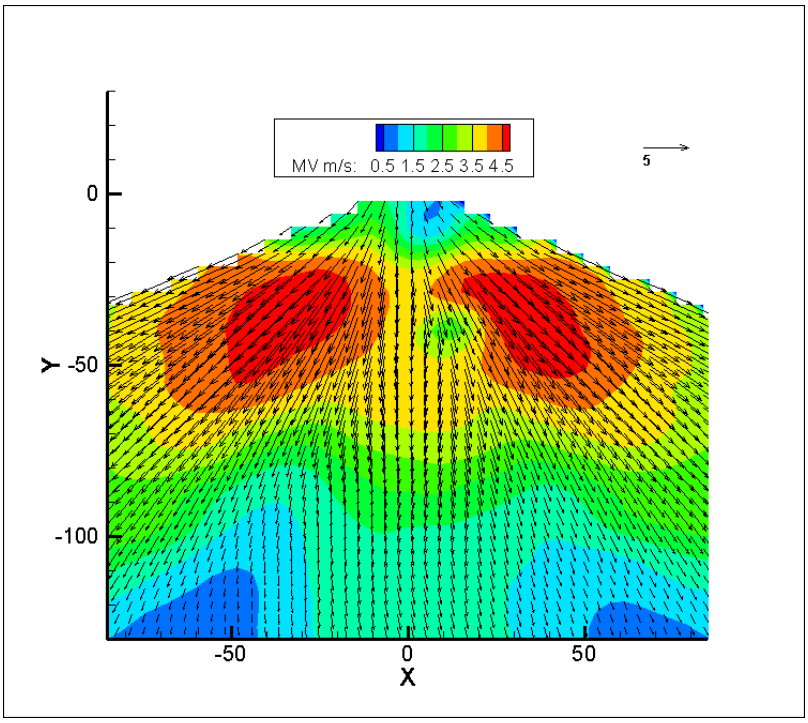

Figure B.4 Average Velocity Profile for Water Flow of 5.00×10^{-3} kg/s and Air Flow of 3.70×10^{-3} kg/s

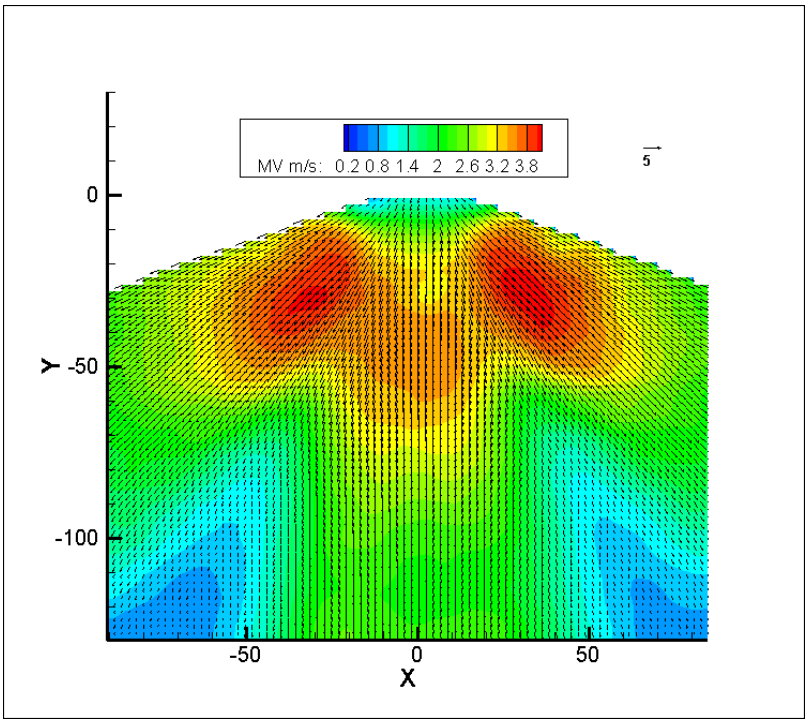

Figure B.5 Average Velocity Profile for Water Flow of 6.66×10^{-3} kg/s and Air Flow of 3.70×10^{-3} kg/s

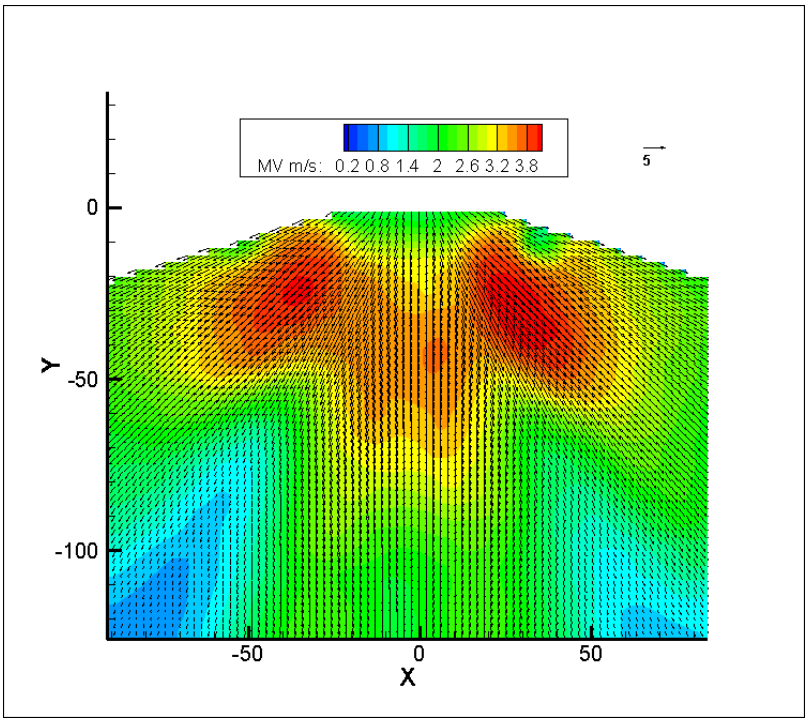

Figure B.6 Average Velocity Profile for Water Flow of 8.33×10^{-3} kg/s and Air Flow of 3.70×10^{-3} kg/s

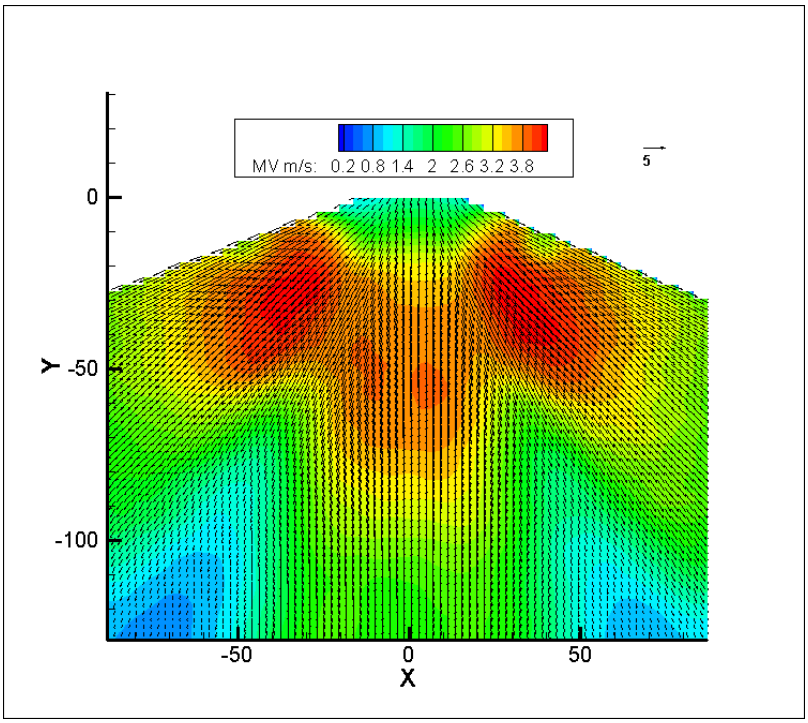

Figure B.7 Average Velocity Profile for Water Flow of 9.99×10^{-3} kg/s and Air Flow of 3.70×10^{-3} kg/s

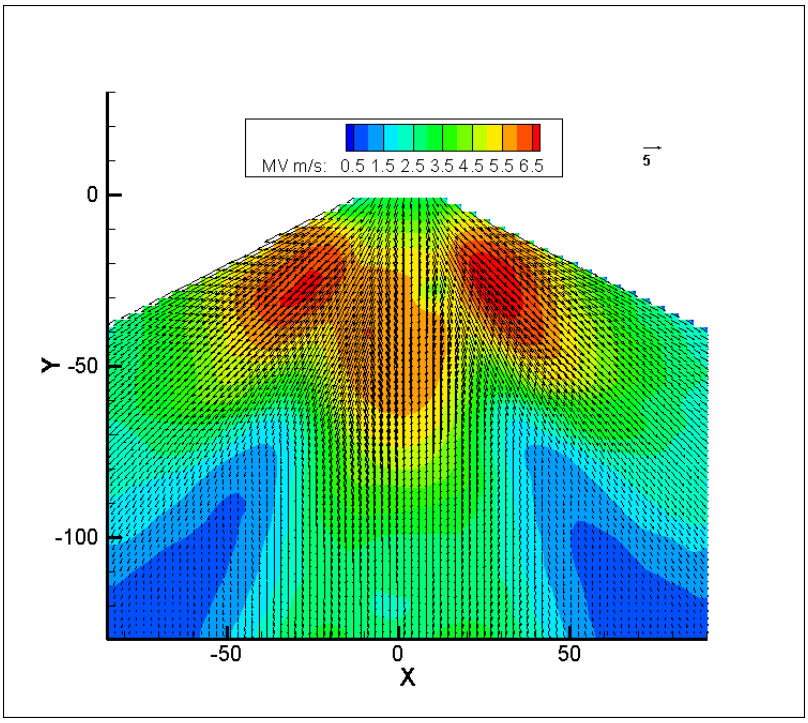

Figure B.8 Average Velocity Profile for Water Flow of 5.00×10^{-3} kg/s and Air Flow of 4.93×10^{-3} kg/s

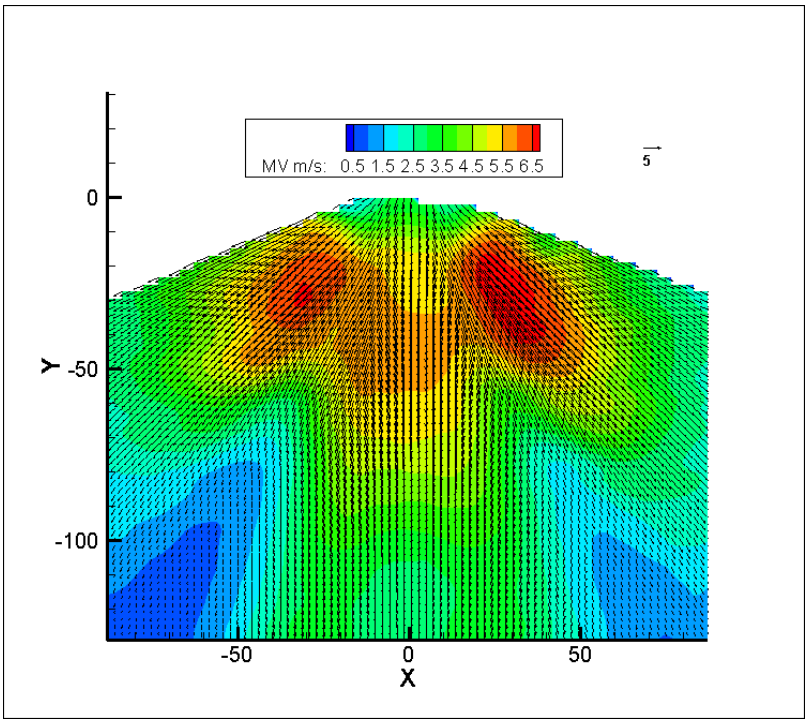

Figure B.9 Average Velocity Profile for Water Flow of 8.33×10^{-3} kg/s and Air Flow of 4.93×10^{-3} kg/s

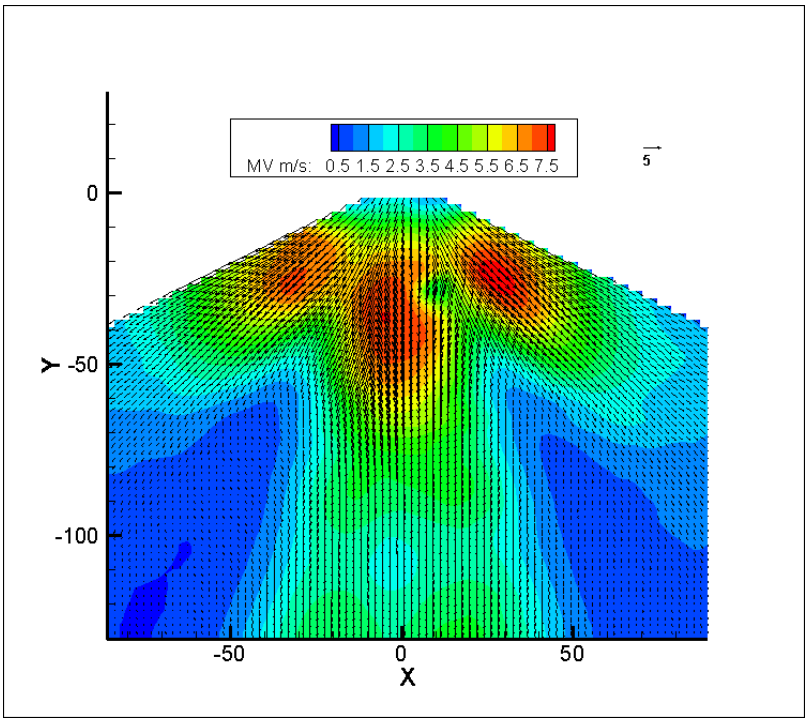

Figure B.10 Average Velocity Profile for Water Flow of 3.33×10^{-3} kg/s and Air Flow of 6.17×10^{-3} kg/s

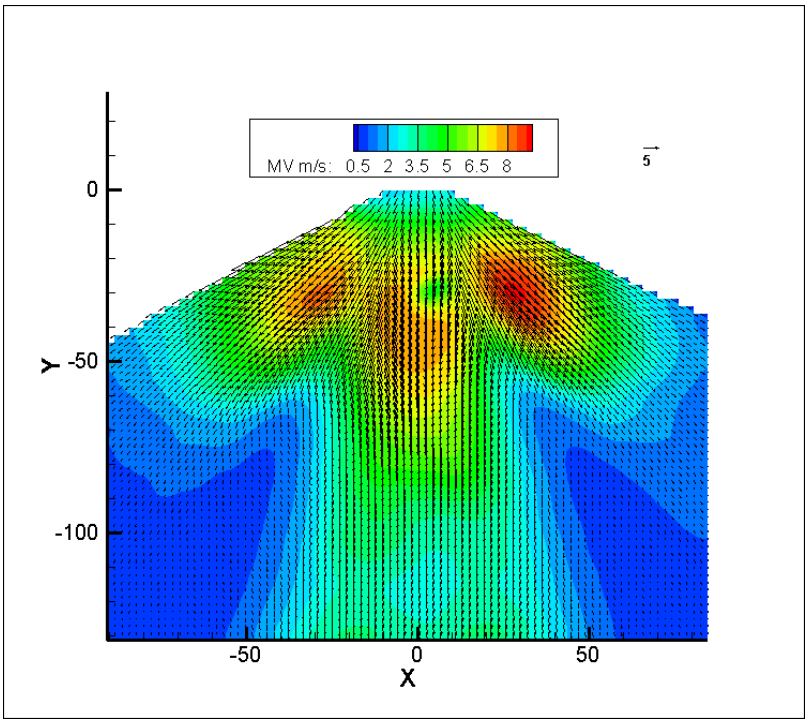

Figure B.11 Average Velocity Profile for Water Flow of 5.00×10^{-3} kg/s and Air Flow of 6.17×10^{-3} kg/s

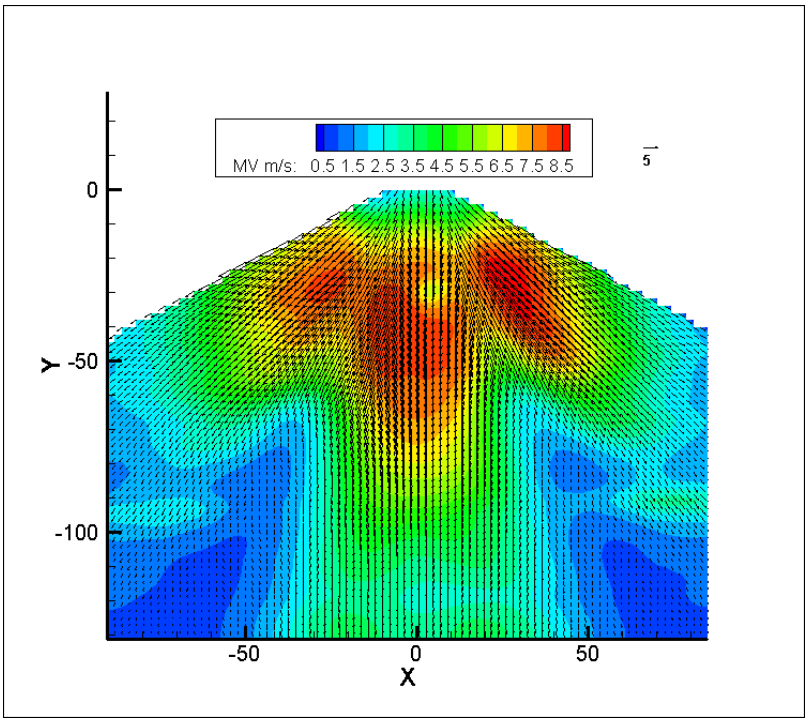

Figure B.12 Average Velocity Profile for Water Flow of 6.66×10^{-3} kg/s and Air Flow of 6.17×10^{-3} kg/s

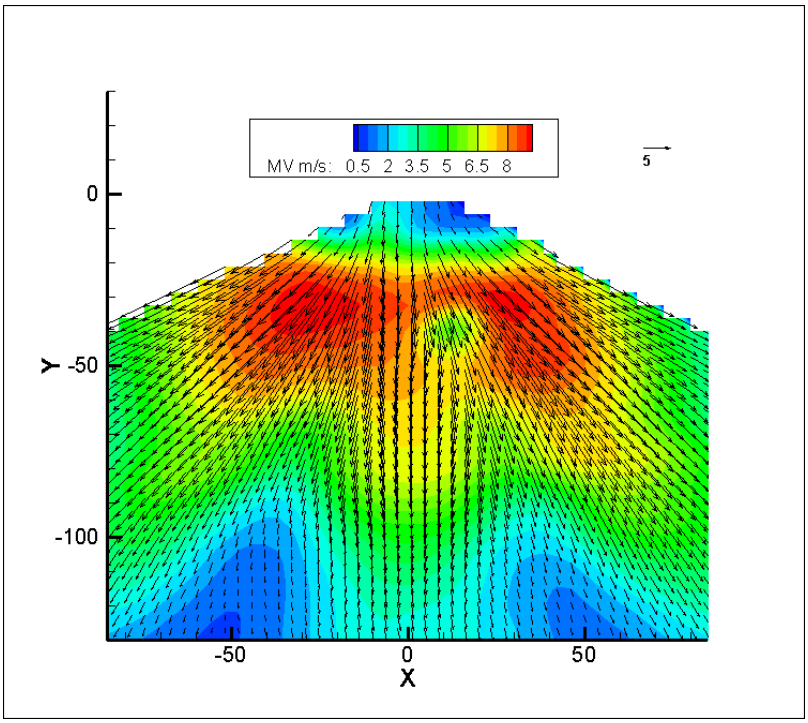

Figure B.13 Average Velocity Profile for Water Flow of 8.33×10^{-3} kg/s and Air Flow of 6.17×10^{-3} kg/s

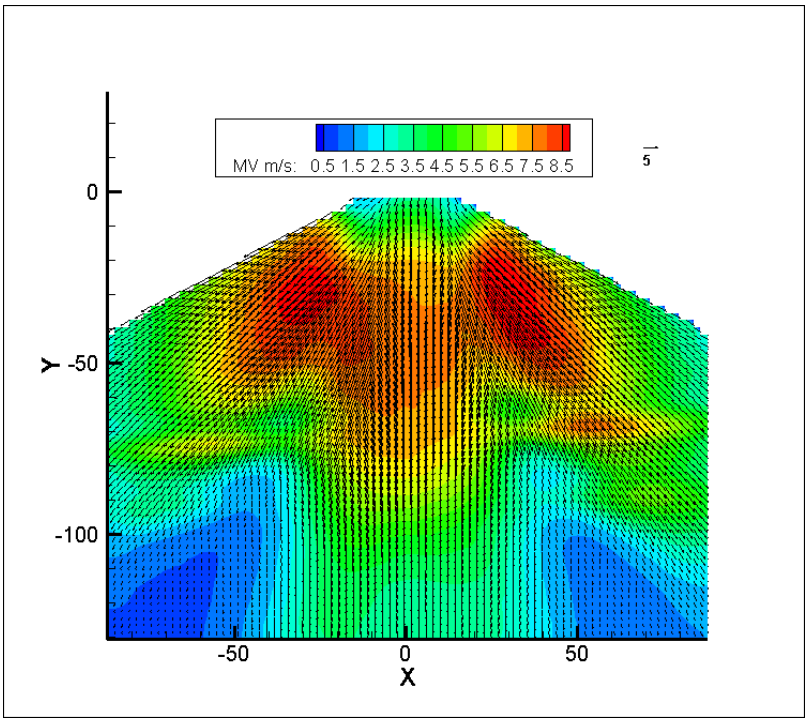

Figure B.14 Average Velocity Profile for Water Flow of 9.99×10^{-3} kg/s and Air Flow of 6.17×10^{-3} kg/s

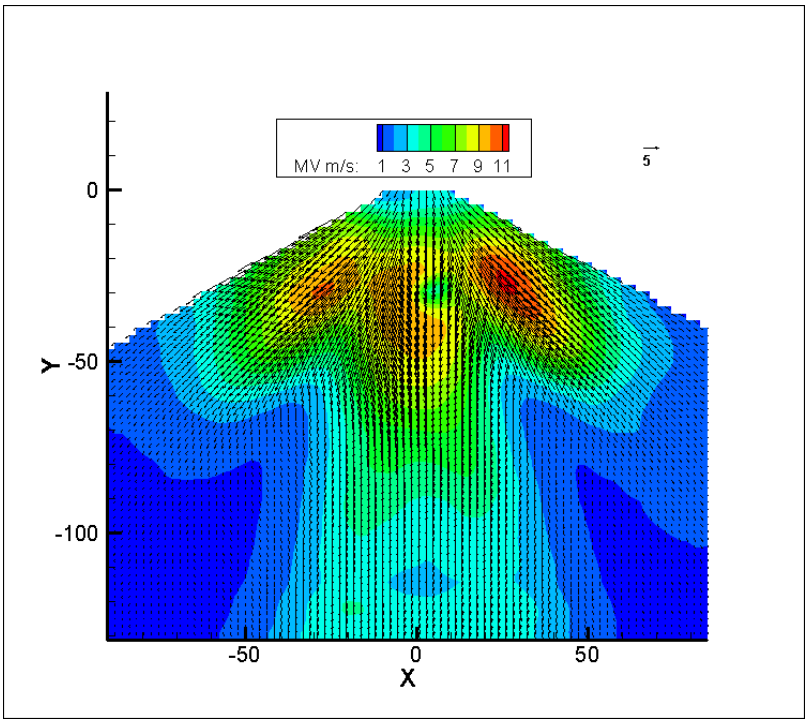

Figure B.15 Average Velocity Profile for Water Flow of 5.00×10^{-3} kg/s and Air Flow of 7.40×10^{-3} kg/s

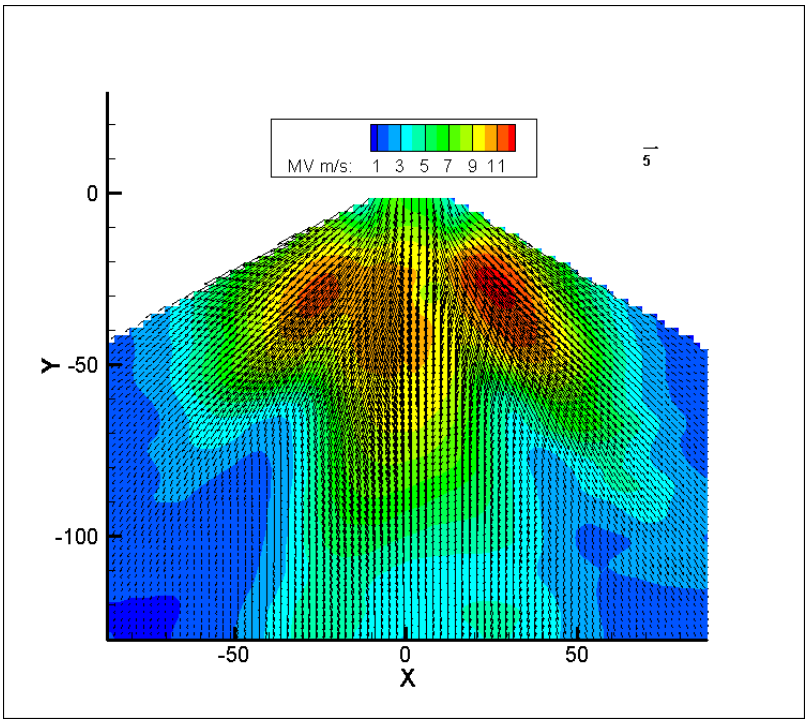

Figure B.16 Average Velocity Profile for Water Flow of 8.33×10^{-3} kg/s and Air Flow of 7.40×10^{-3} kg/s

Water and Air Velocity Profiles

Figures B.17 – B.21 show the remaining velocity profiles at one, two, and three diameters for water and air. They are plotted with one air mass flow per figure.

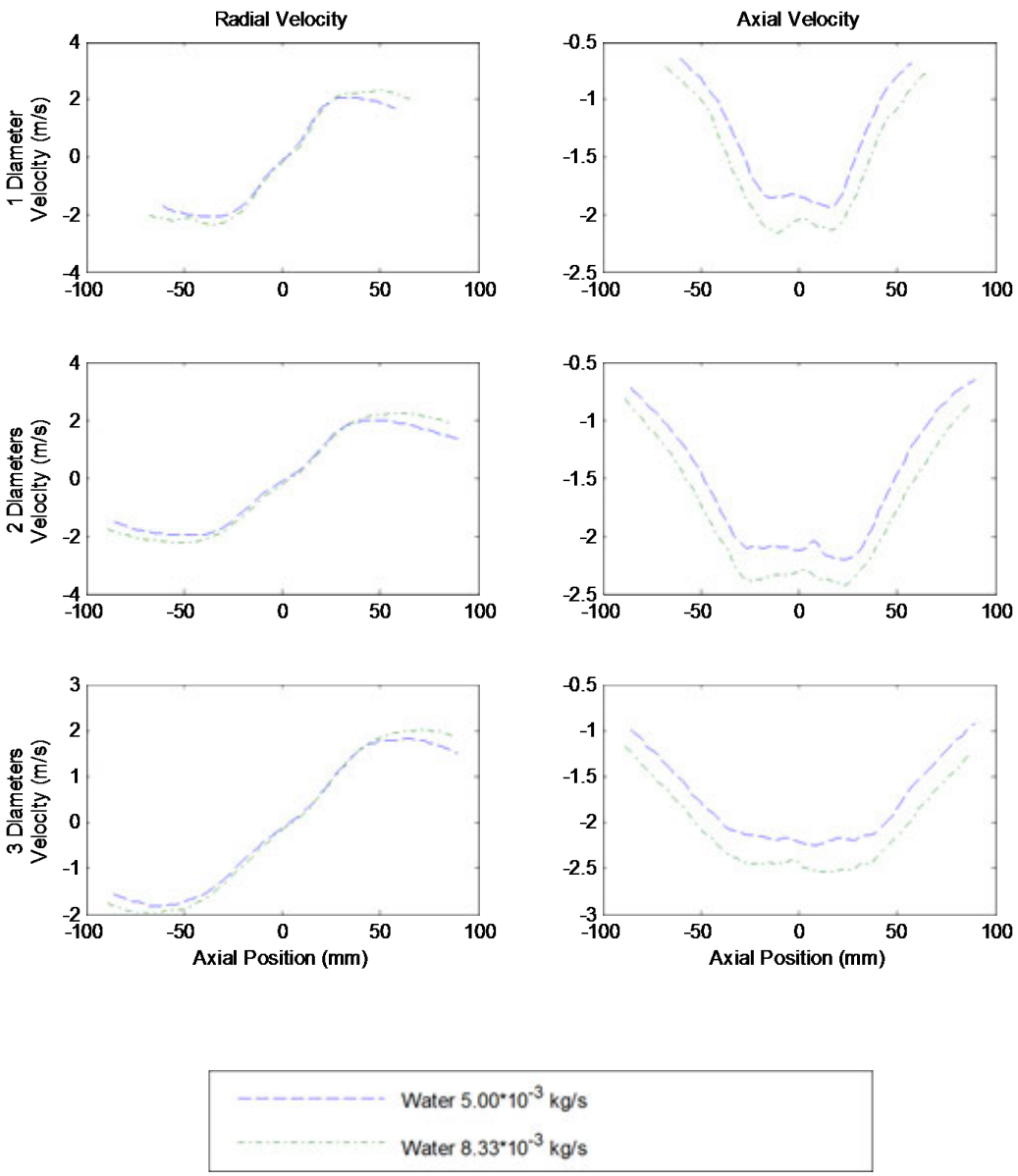

Figure B.17 Average Velocity Profiles for Water Flow Rates of 5.00×10^{-3} kg/s and 8.33×10^{-3} kg/s and Air Flow of 2.47×10^{-3} kg/s

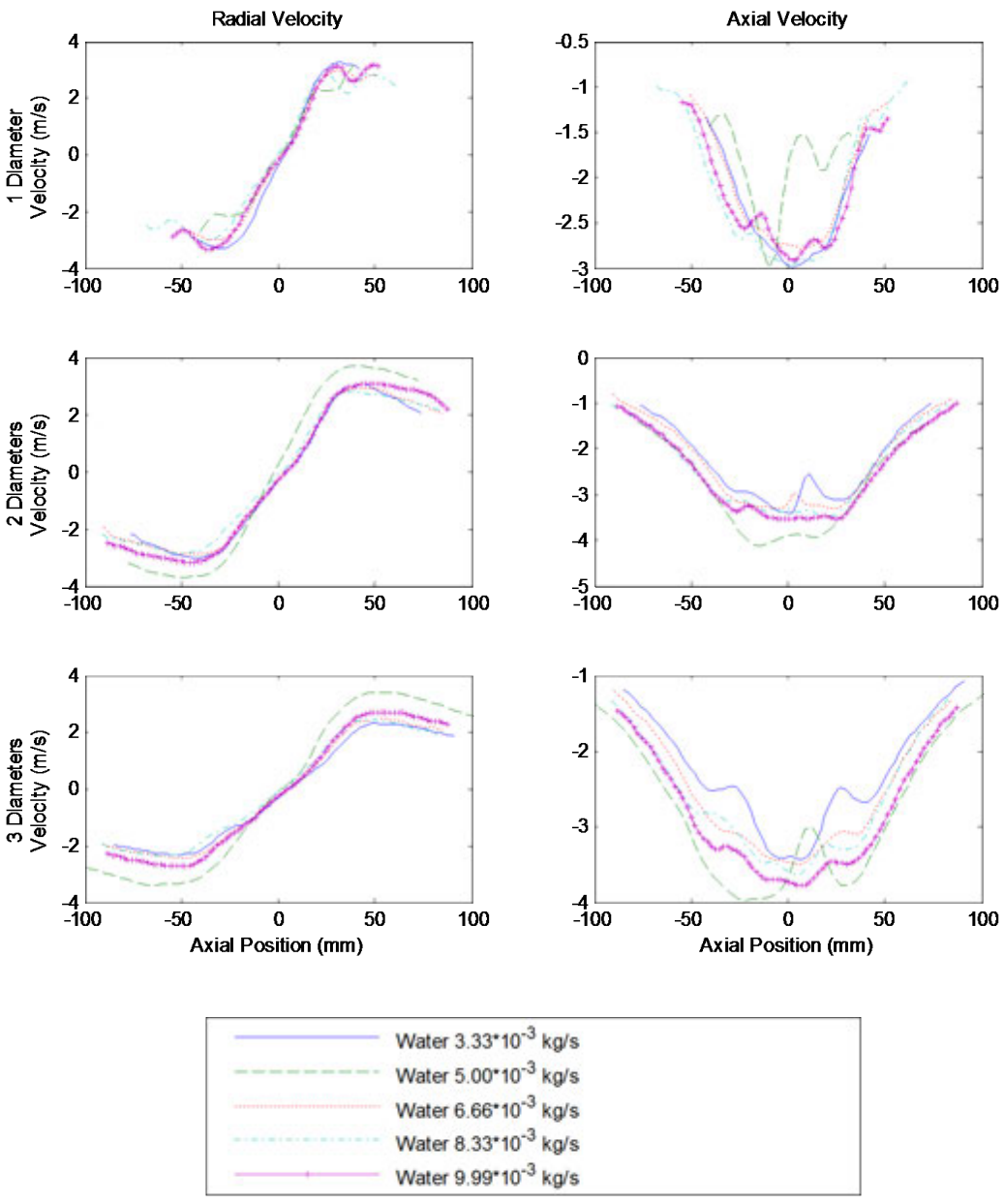

Figure B.18 Average Velocity Profiles for Water Flow Rates of 3.33×10^{-3}, 5.00×10^{-3}, 6.66×10^{-3}, 8.33×10^{-3}, and 9.99×10^{-3} kg/s and Air Flow of 3.70×10^{-3} kg/s

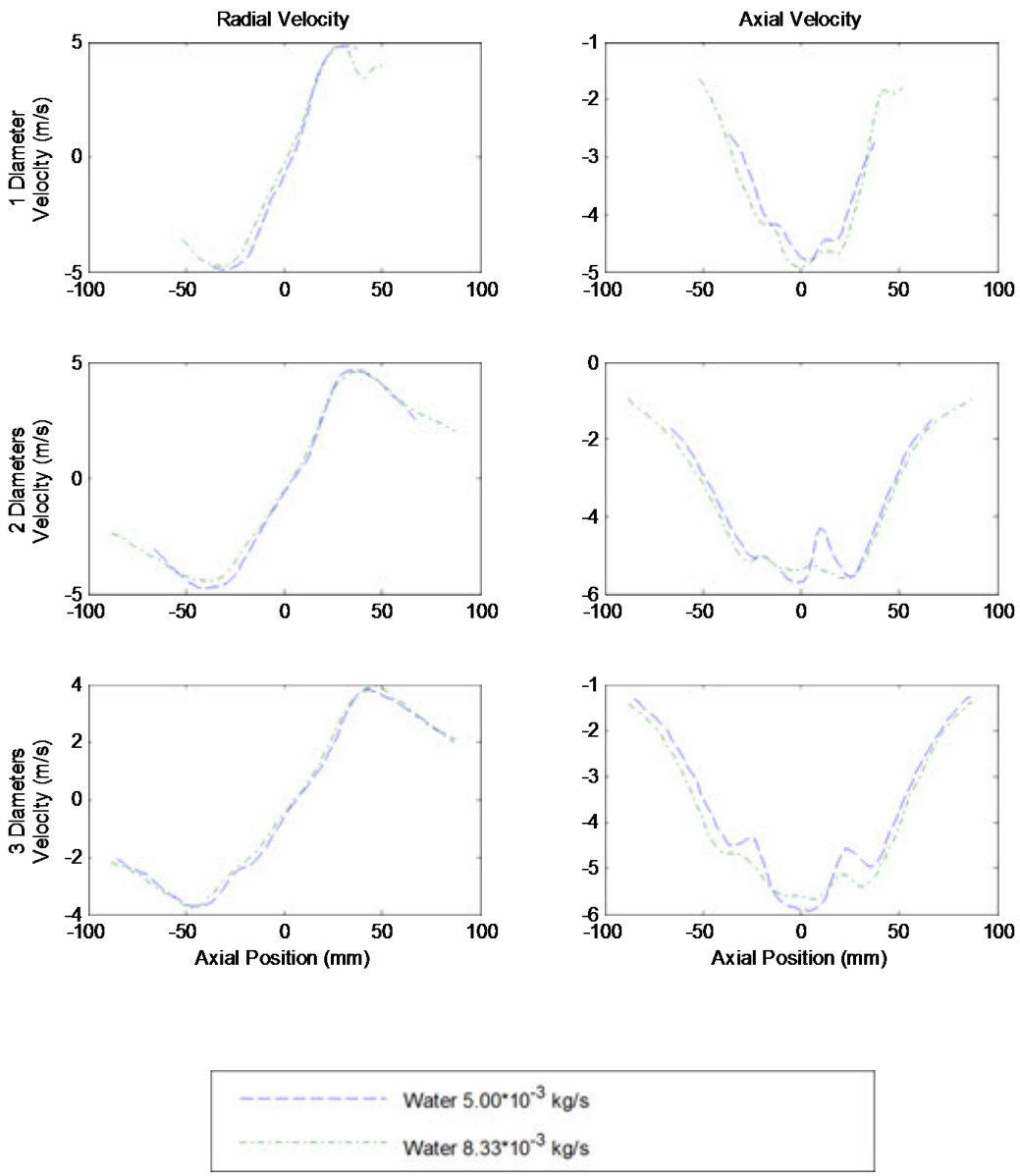

Figure B.19 Average Velocity Profiles for Water Flow Rates of 5.00×10^{-3} kg/s and 8.33×10^{-3} kg/s and Air Flow of 4.93×10^{-3} kg/s

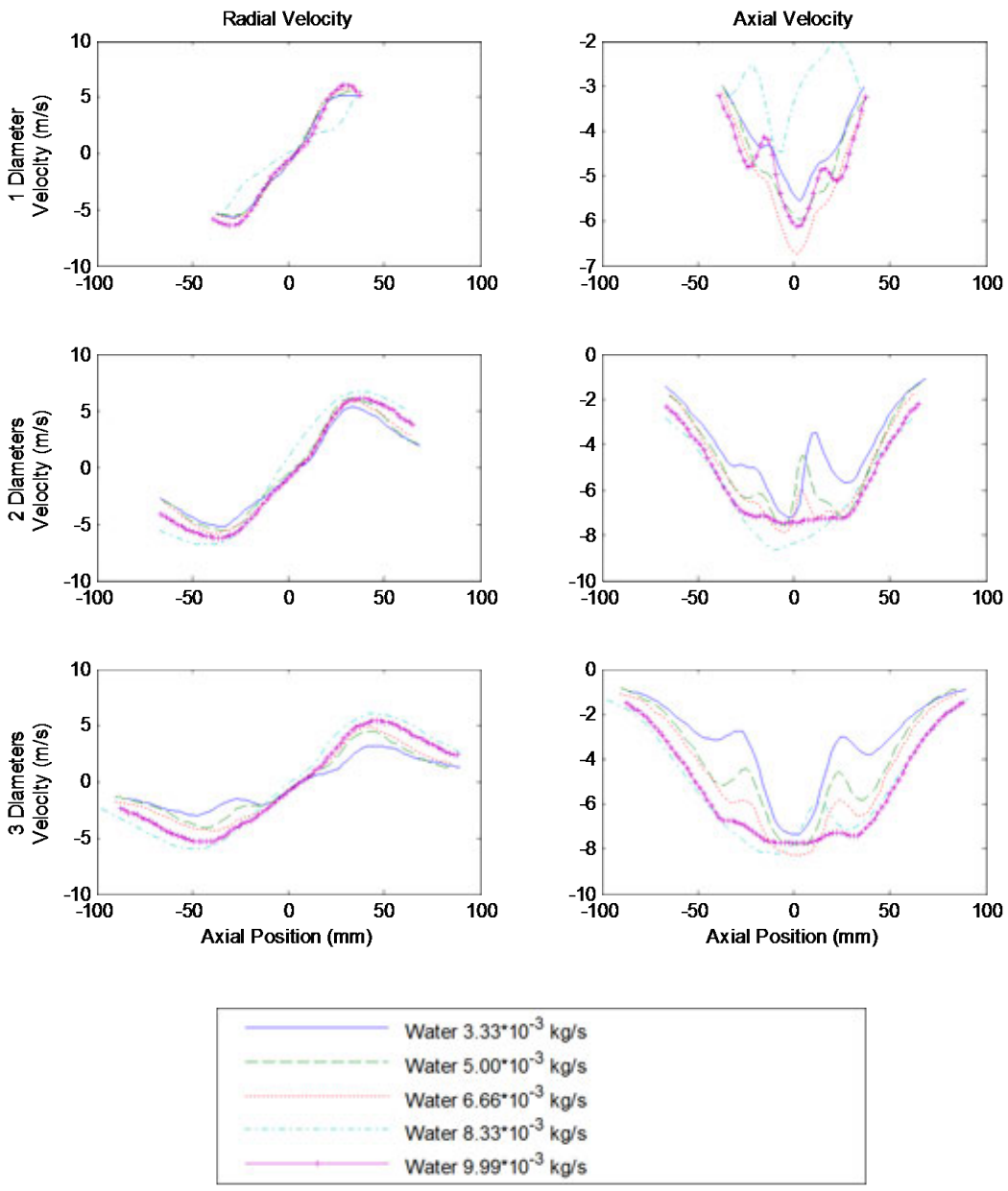

Figure B.20 Average Velocity Profiles for Water Flow Rates of 3.33×10^{-3}, 5.00×10^{-3}, 6.66×10^{-3}, 8.33×10^{-3}, and 9.99×10^{-3} kg/s and Air Flow of 6.17×10^{-3} kg/s

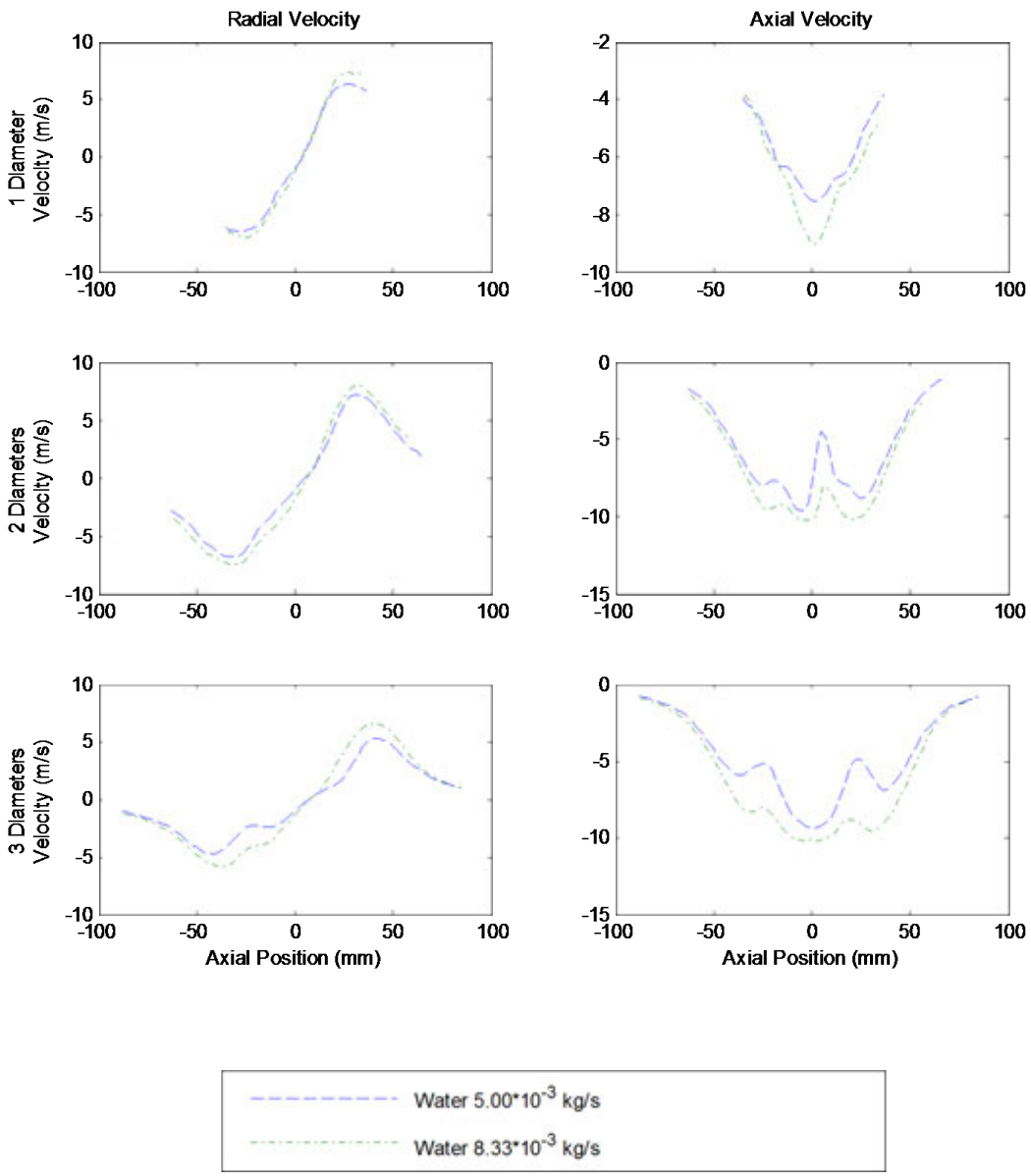

Figure B.21 Average Velocity Profiles for Water Flow Rates of 5.00×10^{-3} kg/s and 8.33×10^{-3} kg/s and Air Flow of 7.40×10^{-3} kg/s

Control Experiment Velocity Field Results

Figures B.22 – B.25 show the low flow rate, liquid flow rate of 2.52×10^{-3} kg/s and air flow rate of 3.46×10^{-3} kg/s, control experiment velocity field results. Figures B.26 – B.29 show the high flow rate (liquid flow rate of 7.36×10^{-3} kg/s and air flow rate of 6.93×10^{-3} kg/s) control experiment velocity field results.

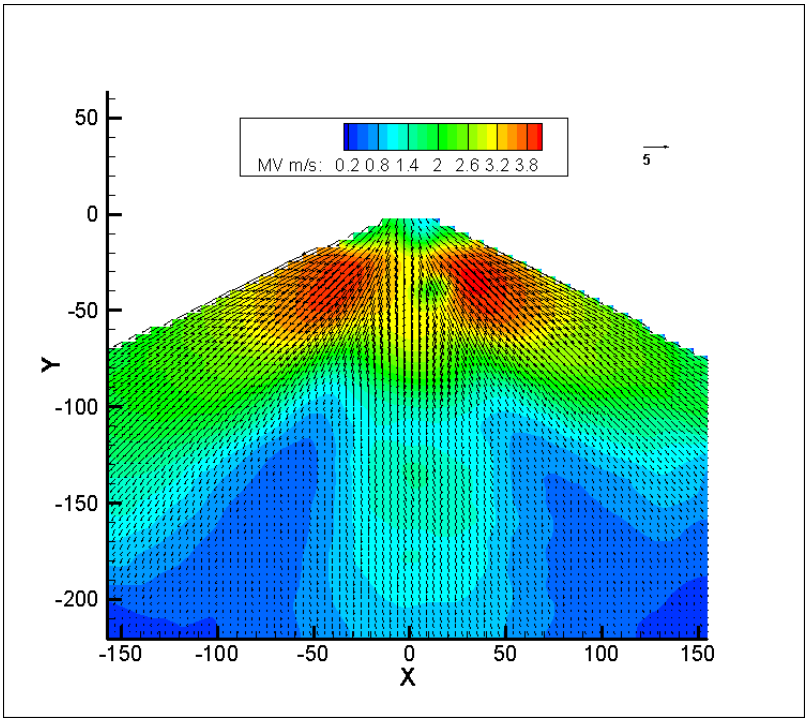

Figure B.22 Average Velocity Profile for Water Flow of 3.33×10^{-3} kg/s and Air Flow of 3.22×10^{-3} kg/s

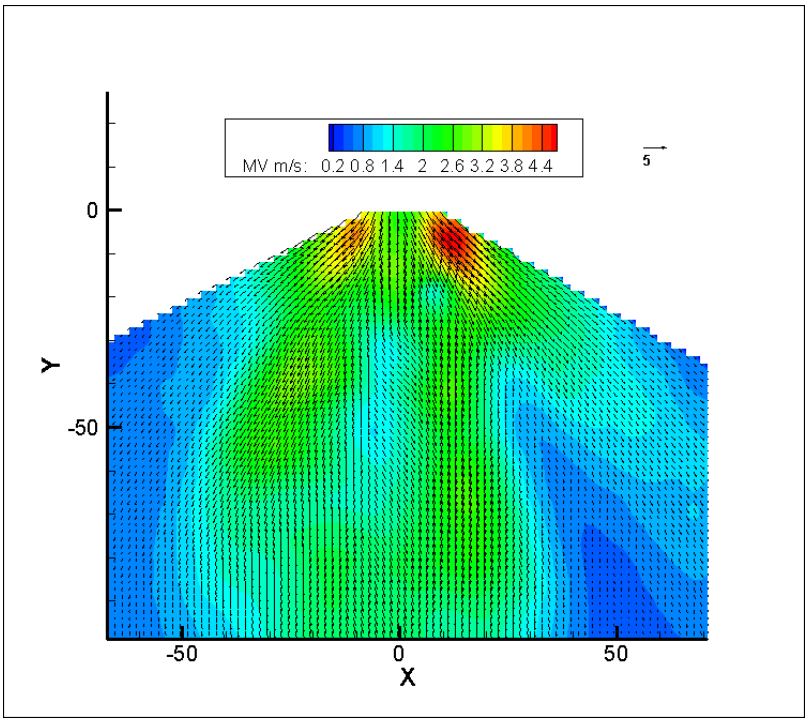

Figure B.23 Average Velocity Profile for Fuel Substitute Flow of 2.52×10^{-3} kg/s and Air Flow of 3.22×10^{-3} kg/s

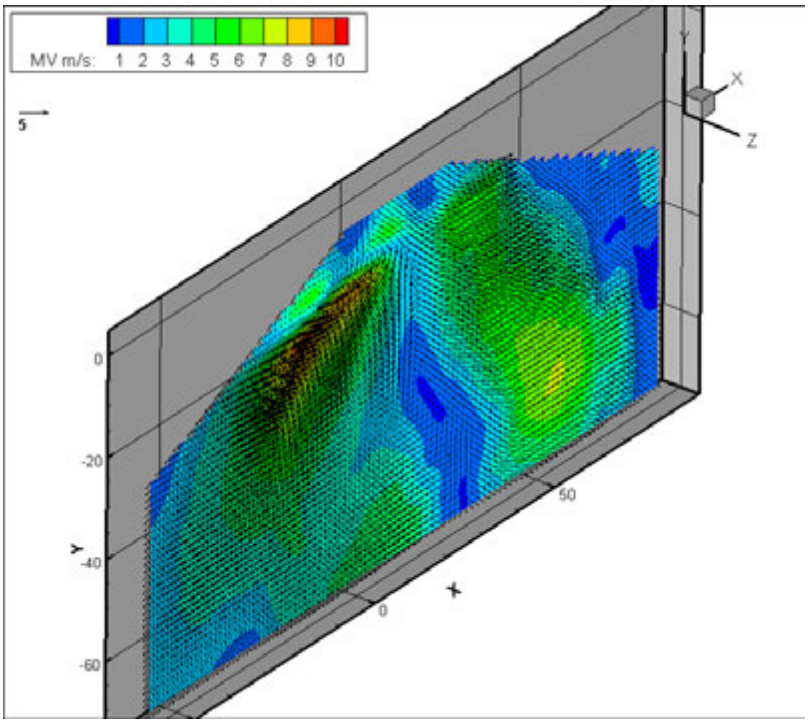

Figure B.24 3D Average Velocity Profile for Fuel Substitute Mass Flow Rate of 2.52×10^{-3} kg/s and Air Mass Flow Rate of 3.46×10^{-3} kg/s

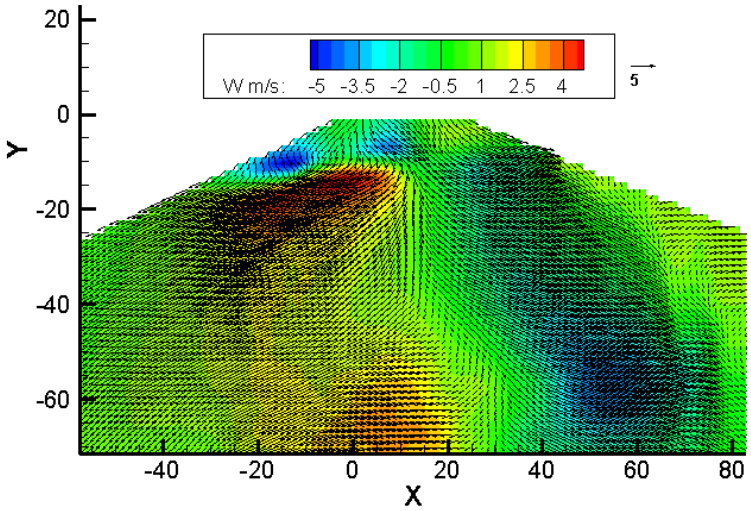

Figure B.25 2D Average Velocity Projection for Fuel Substitute Mass Flow Rate of 2.52×10^{-3} kg/s and Air Mass Flow Rate of 3.46×10^{-3} kg/s

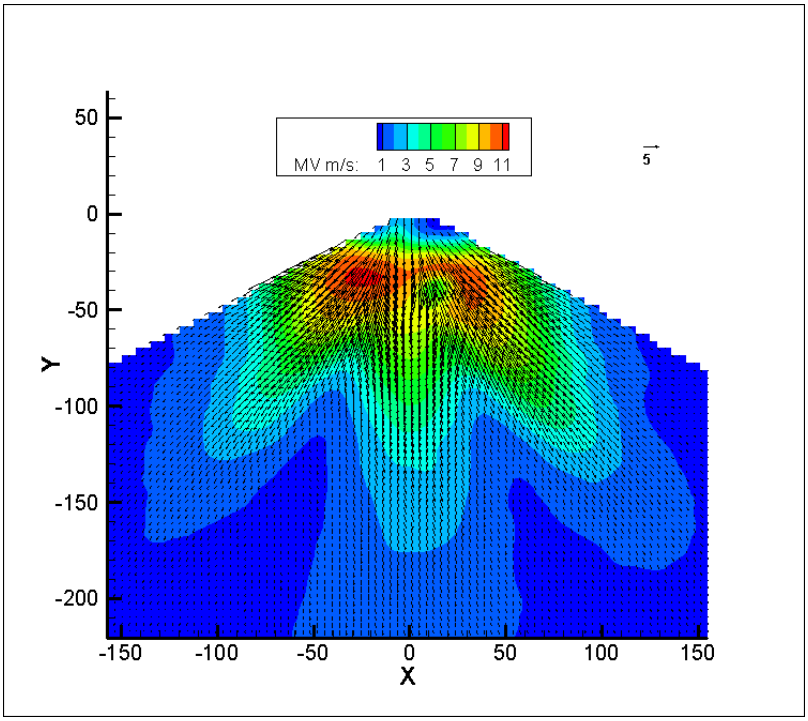

Figure B.26 Average Velocity Profile for Water Flow of 9.48×10^{-3} kg/s and Air Flow of 6.69×10^{-3} kg/s

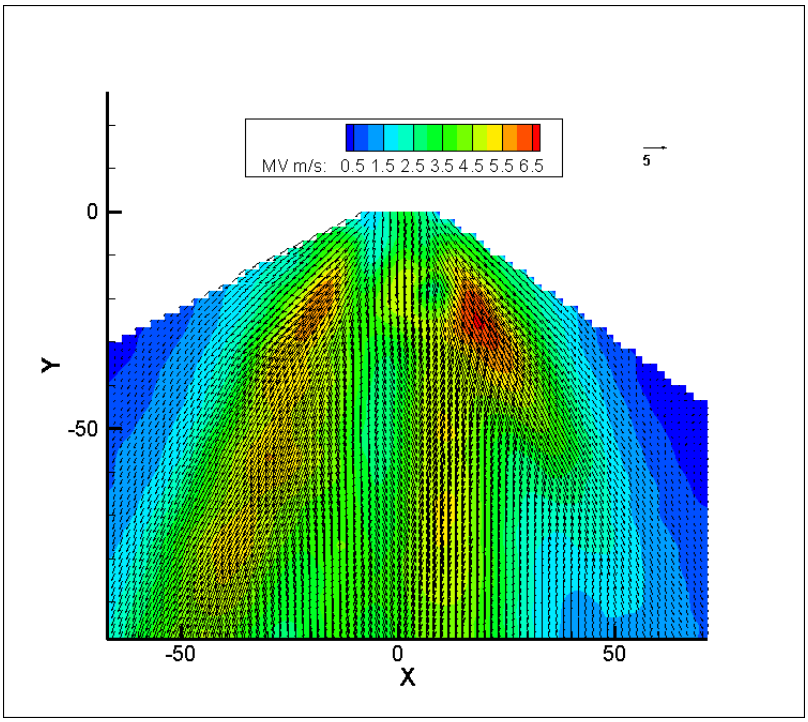

Figure B.27 Average Velocity Profile for Fuel Substitute Flow of 7.36×10^{-3} kg/s and Air Flow of 6.69×10^{-3} kg/s

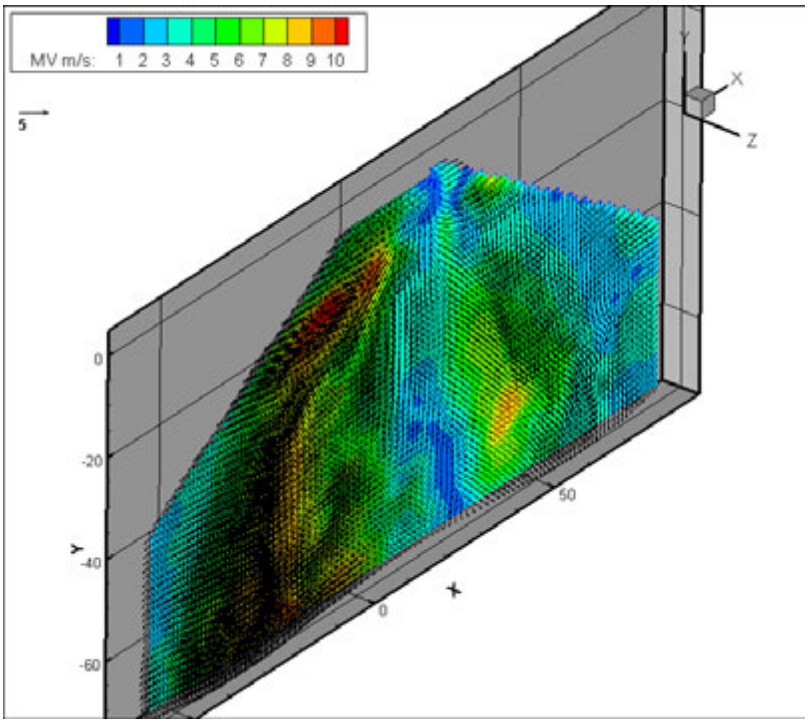

Figure B.28 3D Average Velocity Profile for Fuel Substitute Mass Flow Rate of 7.36×10^{-3} kg/s and Air Mass Flow Rate of 6.93×10^{-3} kg/s

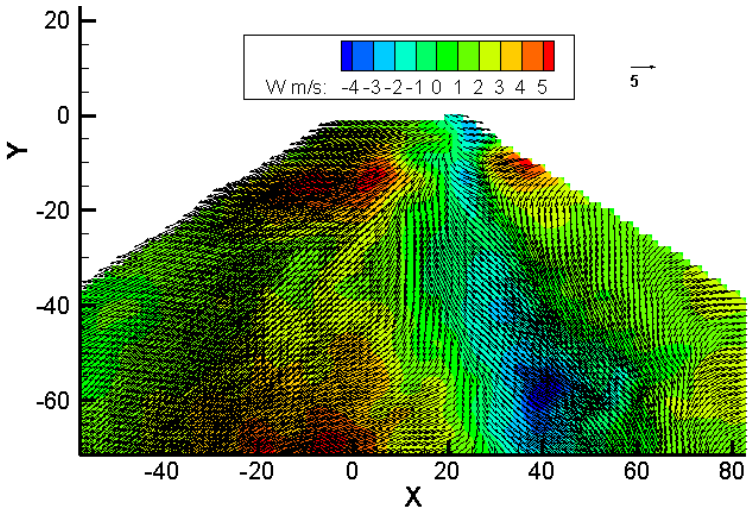

Figure B.29 2D Average Velocity Projection for Fuel Substitute Mass Flow Rate of 7.36×10^{-3} kg/s and Air Mass Flow Rate of 6.93×10^{-3} kg/s

APPENDIX C. FUEL SUBSTITUTE TECHNICAL SPECIFICATIONS

This appendix includes technical specifications on the fuel substitute used in the experiments. The first document is the Material Safety Data Sheet (MSDS). The second document is the military specification document (Mil-Spec).

MSDS

ACTIO MSDS ID: 545649

View Section : 1 2 3 4 5 6 7 8 9 10 11 12 13 14 15 16

SECTION 1: CHEMICAL PRODUCT and COMPANY IDENTIFICATION (N/A)

Product Name: **Mil PRF-7024 Type II**

Distributor Name: Barton Solvents, Inc.

Distributor Address: P.O. Box 221
1920 NE Broadway
Des Moines, IA 50306-0221

Distributor Telephone: (515) 265-7998

CHEMTREC Numbers:

For emergencies in the US, call CHEMTREC: 800-424-9300

Revision Date: 1/5/2010
Supersedes: 7/26/05
Supersedes: 6/4/03
Supersedes: 1/8/02
Supersedes: 7/23/01
Supersedes: 2/10/98
Supersedes: No Previous Validation.
Version: 1

Manufacturer Name: Barton Solvents, Inc.

Responsible name: Barton Solvents, Inc.

Hazardous Material Information System (U.S.A.):
Caution: HMIS® ratings are based on a 0-4 rating scale, with 0 representing minimal hazards or risks, and 4 representing significant hazards or risks Although HMIS® ratings are not required on MSDSs under 29 CFR 1910.1200, the preparer may choose to provide them. HMIS® ratings are to be used with a fully implemented HMIS® program. HMIS® is a registered mark of the National Paint & Coatings Association (NPCA). HMIS® materials may be purchased exclusively from J.J. Keller (800) 327-6868.

The customer is responsible for determining the PPE code for this material.

NFPA

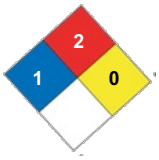

HMIS

HEALTH	1
FIRE	2
REACTIVITY	0
PPE	

Product Codes: 02016000

To Top of page

SECTION 2 : COMPOSITION, INFORMATION ON INGREDIENTS : (N/A)

Ingredient Name	CAS#	Ingredient Percent
Medium Aliphatic Solvent Naphtha (M)	64742-88-7	> 9% by Weight

EC Index Number: 1

There are no additional ingredients present which, within the current knowledge of the supplier and in the concentrations applicable, are classified as hazardous to health or the environment and hence require reporting in this section.

To Top of page

SECTION 3 : HAZARDS IDENTIFICATION : (N/A)

Emergency Overview: Caution!
FLAMMABLE LIQUID AND VAPOR.
VAPOR MAY CAUSE FLASH FIRE.
Keep away from heat, sparks and flame. Keep container closed. Use only with adequate ventilation.

Physical State: Liquid.

Odor: Hydrocarbon.

OSHA/HCS status: This material is considered hazardous by the OSHA Hazard Communication Standard (29 CFR 1910.1200).

Medium Aliphatic Solvent Naphtha (M) :

Route of Exposure: Inhalation.

Potential Health Effects:

Eye Contact: Acute: This product may irritate eyes upon contact.

Skin Contact: Acute: This product may irritate skin upon contact.

Inhalation: Acute: Inhalation of the spray or mist may produce severe irritation of respiratory tract, characterized by coughing, choking, or shortness of breath.

MSDS

Ingestion:	Acute: Aspiration hazard if swallowed. Can enter lungs and cause damage. Harmful if swallowed.
Chronic Health Effects:	Contains material that may cause target organ damage, based on animal data.
Carcinogenicity:	No known significant effects or critical hazards.
Teratogens Information:	No known significant effects or critical hazards.
Mutagens Information:	No known significant effects or critical hazards.
Target Organs:	Contains material which may cause damage to the following organs: brain, skin, central nervous system (CNS).
Aggravation of Pre-Existing Conditions:	Repeated or prolonged exposure is not known to aggravate any medical condition. Developmental effects: No known significant effects or critical hazards. Fertility effects: No known significant effects or critical hazards. See toxicological Information (section 11)

To Top of page

SECTION 4 : FIRST AID MEASURES : (N/A)

Eye Contact:	In case of contact, immediately flush eyes with plenty of water for at least 15 minutes. Get medical attention if irritation occurs.
Skin Contact:	In case of contact, immediately flush skin with plenty of water. Remove contaminated clothing and shoes. Wash clothing before reuse. Clean shoes thoroughly before reuse. Get medical attention.
Inhalation:	If inhaled, remove to fresh air. If breathing is difficult, give oxygen. If not breathing, give artificial respiration. Get medical attention.
Ingestion:	Do not induce vomiting unless directed to do so by medical personnel. Never give anything by mouth to an unconscious person. If vomiting occurs, the head should be kept low so that vomit does not enter the lungs. Get medical attention immediately.
Note to Physicians:	No specific treatment. Treat symptomatically. Contact poison treatment specialist immediately if large quantities have been ingested or inhaled. Protection of first-aiders: No action shall be taken involving any personal risk or without suitable training. It may be dangerous to the person providing aid to give mouth-to-mouth resuscitation.

To Top of page

SECTION 5 : FIRE FIGHTING MEASURES : (N/A)

Fire:	Flammability of the product: Flammable liquid and vapor. Vapor may cause flash fire. Vapors may accumulate in low or confined areas or travel a considerable distance to a source of ignition and flash back. Runoff to sewer may create fire or explosion hazard. Flammable limits: Greatest known range: Lower: 1 % Upper: 7% (Solvent Naphtha (Petroleum), Medium Aliphatic)
Flash Point:	37.8 deg C (100 deg F)
Flash Point Method:	Open cup: (Tagliabue.). Not available.
Extinguishing Media:	Use dry chemical, CO2 water spray (fog) or foam.
Unsuitable Media:	Do not use water jet.
Hazardous Combustion Byproducts:	No specific data.
Fire Fighting Equipment:	Special protective equipment for fire-fighters: Fire-fighters should wear appropriate protective equipment and self-contained breathing apparatus (SCBA) with a full face-piece operated in positive pressure mode.

To Top of page

SECTION 6 : ACCIDENTAL RELEASE MEASURES : (N/A)

Personal Precautions:	Immediately contact emergency personnel. Eliminate all ignition sources. Keep unnecessary personnel away. Use suitable protective equipment (section 8). Do not touch or walk through spilled material.
Environmental Precautions:	Avoid dispersal of spilled material and runoff and contact with soil, waterways, drains and sewers.
Large Spill:	If emergency personnel are unavailable, contain spilled material. For small spills, add absorbent (soil may be used in the absence of other suitable materials) and use a non-sparking or explosion-proof means to transfer material to a sealed, appropriate container for disposal. For large spills, dike spilled material or otherwise contain it to ensure runoff does not reach a waterway. Place spilled material in an appropriate container for disposal.
Small Spill:	Stop leak if without risk. Move containers from spill area. Dilute with water and mop up if water-soluble or absorb with an inert dry material and place in an appropriate waste disposal container. Use spark-proof tools and explosion-proof equipment. Dispose of via a licensed waste disposal contractor.

To Top of page

SECTION 7 : HANDLING and STORAGE : (N/A)

Handling:	Keep container closed. Use only with adequate ventilation. Keep away from heat, sparks and flame. To avoid fire or explosion, dissipate static electricity during transfer by grounding and bonding containers and equipment before transferring material. Use explosion-proof electrical (ventilating, lighting and material handling) equipment.
Storage:	Store in a segregated and approved area. Keep container in a cool, well-ventilated area. Keep container tightly closed and sealed until ready for use. Avoid all possible sources of ignition (spark or flame).
Hygiene Practices:	Wash hands, forearms and face thoroughly after handling chemical products, before eating, smoking and using the lavatory and at the end of the working period. Appropriate techniques should be used to remove potentially contaminated clothing. Wash contaminated clothing before reusing. Ensure that eyewash stations and safety showers are close to the workstation location.

To Top of page

SECTION 8 : EXPOSURE CONTROLS, PERSONAL PROTECTION : (N/A)

Engineering Controls:	Use only with adequate ventilation. Use process enclosures, local exhaust ventilation or other engineering controls to keep worker exposure to airborne contaminants below any recommended or statutory limits. The engineering controls also need to keep gas, vapor or dust concentrations below any lower explosive limits. Use explosion-proof ventilation equipment.
Skin Protection Description:	Personal protective equipment for the body should be selected based on the task being performed and the risks involved and should be approved by a specialist before handling this product.
Hand Protection Description:	Chemical-resistant, impervious gloves complying with an approved standard should be worn at all times when handling chemical products if a risk assessment indicates this is necessary.
Eye/Face Protection:	Safety eyewear complying with an approved standard should be used when a risk assessment indicates this is necessary to avoid exposure to liquid splashes, mists or dusts.
Respiratory Protection:	Use a properly fitted, air-purifying or air-fed respirator complying with an approved standard if a risk assessment indicates this is necessary. Respirator selection must be based on known or anticipated exposure levels, the hazards of the product and the safe working limits of the selected respirator. Recommended monitoring procedures: If this product contains ingredients with exposure limits, personal, workplace atmosphere or biological monitoring may be required to determine the effectiveness of the ventilation or other control measures and/or the necessity to use respiratory protective equipment. Hygiene measures: Wash hands, forearms and face thoroughly after handling chemical products, before eating, smoking and using the lavatory and at the end of the working period. Appropriate techniques should be used to remove potentially contaminated clothing. Wash contaminated clothing before reusing. Ensure that eyewash stations and safety showers are close to the workstation location. Environmental exposure controls: Emissions from ventilation or work process equipment should be checked to ensure they comply with the requirements of environmental protection legislation. In some cases, fume scrubbers, filters or engineering modifications to the process equipment will be necessary to reduce emissions to acceptable levels.

To Top of page

SECTION 9 : PHYSICAL and CHEMICAL PROPERTIES : (N/A)

Color:	Clear
Odor:	Hydrocarbon. Not applicable.
Physical State:	Liquid.
Vapor Density:	Highest known value: 4.7 (Air = 1) (Solvent Naphtha (Petroleum), Medium Aliphatic)
Flash Point:	37.8 deg C (100 deg F)
Flash Point Method:	Open cup: (Tagliabue.). Not available.
Boiling Point:	Condensation point: Lowest known value: 159 deg C (318.2 deg F). (Solvent Naphtha (Petroleum), Medium Aliphatic) Not available.
Solubility:	Soluble in the following materials: acetone. Insoluble in the following materials: cold water.
Density:	Relative: 0.774 @ 60 deg F (Water = 1) Not available.
Evaporation Point:	0.27 (Solvent Naphtha (Petroleum), Medium Aliphatic) compared with Butyl acetate.
Percent Volatile:	100% (v/v)
Volatile Organic Compound Content:	100 (%) Flammable limits: Greatest known range: Lower: 1 % Upper: 7% (Solvent Naphtha (Petroleum), Medium Aliphatic) Dispersion properties: Not dispersible in the following materials: cold water, hot water. See solubility in the following materials: acetone.

MSDS

To Top of page

SECTION 10 : STABILITY and REACTIVITY : (N/A)

Chemical Stability:	The product is stable.
Conditions to Avoid:	Avoid all possible sources of ignition (spark or flame). Do not pressurize, cut, weld, braze, solder, drill, grind or expose containers to heat or sources of ignition.
Incompatibilities with Other Materials:	Materials to avoid: Reactive or incompatible with the following materials: oxidizing materials
Hazardous Polymerization:	Will not occur.
Hazardous Decomposition Products:	Under normal conditions of storage and use, hazardous decomposition products should not be produced.

To Top of page

SECTION 11 : TOXICOLOGICAL INFORMATION : (N/A)

Medium Aliphatic Solvent Naphtha (M) :

Acute Health Effects:	Conclusion/Summary: Not available.
Chronic Effects:	Conclusion/Summary: Not available.
Carcinogenicity:	Conclusion/Summary: Not available.
Mutagenicity:	Conclusion/Summary: Not available.
Teratogenicity:	Conclusion/Summary: Not available.
Reproductive Toxicity:	Conclusion/Summary: Not available.

To Top of page

SECTION 12 : ECOLOGICAL INFORMATION : (N/A)

Environmental Fate:	Environmental effects: No known significant effects or critical hazards.
Biodegradation:	Conclusion/Summary: Not available.
Effect of Material On Aquatic Life:	Aquatic ecotoxicity: Conclusion/Summary: Not available.

To Top of page

SECTION 13 : DISPOSAL CONSIDERATIONS : (N/A)

Waste Disposal:	The generation of waste should be avoided or minimized wherever possible. Avoid dispersal of spilled material and runoff and contact with soil, waterways, drains and sewers. Disposal of this product, solutions and any by-products should at all times comply with the requirements of environmental protection and waste disposal legislation and any regional local authority requirements. Disposal should be in accordance with applicable regional, national and local laws and regulations. Refer to Section 7: HANDLING AND STORAGE and Section 8: EXPOSURE CONTROLS/PERSONAL PROTECTION for additional handling information and protection of employees.

To Top of page

SECTION 14 : TRANSPORT INFORMATION : (N/A)

DOT Shipping Name:	Petroleum distillates n.o.s. Combustible Liquid
DOT UN Number:	UN1268
DOT Hazard Class:	Combustible liquid
DOT Packing Group:	III*
Comments:	PG*: Packing group

To Top of page

SECTION 15 : REGULATORY INFORMATION : (N/A)

Medium Aliphatic Solvent Naphtha (M) :

TSCA 8(b): Inventory Status:	U.S. Federal regulations: All components are listed or exempted. United States inventory (TSCA 8b): All components are listed or exempted.
Section 302:	SARA 302 extremely hazardous substances: No products were found. SARA 302 emergency planning and notification: No products were found. SARA 302 hazardous chemicals: No products were found.
Section 304:	SARA 304 extremely hazardous substances: No products were found. SARA 304 emergency planning and notification: No products were found. SARA 304 hazardous chemicals: No products were found.
Section 312 Hazard Category:	SARA 311/312 extremely hazardous substances: No products were found. SARA 311/312 hazardous chemicals: No products were found. SARA 311/312 MSDS distribution - chemical inventory - hazard identification: MIL PRF- 7024E TYPE II:

MSDS

Acute:	Yes
Chronic:	Yes
Fire:	Yes
Section 112(r): Clean Air Act	Clean Air Act (CAA) 112 accidental release prevention: No products were found. Clean Air Act (CAA) 112 regulated flammable substances: No products were found. Clean Air Act (CAA) 112 regulated toxic substances: No products were found.
Section 116.4 part 117: Clean Water Act	Clean Water Act (CWA) 307: No products were found. Clean Water Act (CWA) 311: No products were found.
OSHA 29 CFR 1200:	This material is considered hazardous by the OSHA Hazard Communication Standard (29 CFR 1910.1200).
HCS Classification:	Combustible liquid Target organ effects

To Top of page

SECTION 16 : ADDITIONAL INFORMATION : (N/A)

HMIS:	
Health Hazard:	1
Fire Hazard:	2
Reactivity:	0
NFPA:	
Health:	1
Fire Hazard:	2
Reactivity:	0
Label Text:	Label Requirements: FLAMMABLE LIQUID AND VAPOR. VAPOR MAY CAUSE FLASH FIRE.
MSDS Revision Date:	1/5/2010 Supersedes: 7/26/05 Supersedes: 6/4/03 Supersedes: 1/8/02 Supersedes: 7/23/01 Supersedes: 2/10/98 Supersedes: No Previous Validation. Version: 1 No Indicates information that has changed from previously issued version.
MSDS Author:	Responsible name: Barton Solvents, Inc.

Disclaimer:

Notice to reader:
To the best of our knowledge, the information contained herein is accurate. However, neither the above- named supplier, nor any of its subsidiaries, assumes any liability whatsoever for the accuracy or completeness of the information contained herein.
Final determination of suitability of any material is the sole responsibility of the user. All materials may present unknown hazards and should be used with caution. Although certain hazards are described herein, we cannot guarantee that these are the only hazards that exist.

Hazardous Material Information System (U.S.A.):
Caution: HMIS® ratings are based on a 0-4 rating scale, with 0 representing minimal hazards or risks, and 4 representing significant hazards or risks Although HMIS® ratings are not required on MSDSs under 29 CFR 1910.1200, the preparer may choose to provide them. HMIS® ratings are to be used with a fully implemented HMIS® program. HMIS® is a registered mark of the National Paint & Coatings Association (NPCA). HMIS® materials may be purchased exclusively from J.J. Keller (800) 327-6868.

The customer is responsible for determining the PPE code for this material.

Other special considerations:
02-10-98 Corrected UN ##; 0723-01 Name Change; 01-08-02 Corrected Contents; Change in name 06/04/03; Updated 07/26/2005; Specific gravity correction 1/5/10

To Top of page

INCH-POUND
MIL-PRF-7024E
1 Oct 1997
Superseding
MIL-C-7024D
30 August 1990

PERFORMANCE SPECIFICATION
CALIBRATING FLUIDS, AIRCRAFT FUEL SYSTEM COMPONENTS

This specification has been approved for all Departments and Agencies of the Department of Defense.

1. SCOPE

1.1 Scope. This specification covers the requirements for three types of calibrating fluid used in the calibration of aircraft fuel system components.

1.2 Classification. The fluids will be of the following types as specified (6.2):

Type I - Normal Heptane
Type II - Special Run Stoddard Solvent
Type III - High Flash Point Fluid

2. APPLICABLE DOCUMENTS.

2.1 General. The documents listed in this section are specified in sections 3 and 4 of this specification. This section does not include documents cited in other sections of this specification or those identified as recommended for additional information or as examples. While every effort has been made to ensure the completeness of this list, document users are cautioned that they must meet all the requirements of the specified documents cited in sections 3 and 4 of this specification, whether or not they are listed.

2.2 Government Documents.

2.2.1 Specifications, Standards, and Handbooks. The following specifications, standards, and handbooks form a part of this document to the extent specified herein. Unless otherwise specified, the issues of these documents are those listed in the issue of the Department of Defense Index of Specifications and Standards (DoDISS) and supplement thereto, cited in the solicitation (see 6.2).

SPECIFICATIONS

DEPARTMENT OF DEFENSE

MIL-I-25017 Inhibitor, Corrosion/Lubricity Improver, Fuel Soluble

AMSC N/A FSC 6850

2.3 Non-Government publications. The following documents form a part of this document to the extent specified herein. Unless otherwise specified, the issues of the documents which are DOD adopted are those listed in the issue of the DoDISS cited in the solicitation. Unless otherwise specified, the issues of documents not listed in the DoDISS are the issues of the non-Government documents which are current on the date of the solicitation.

American Society for Testing and Materials (ASTM)

ASTM D 56 - Test Method for Flash Point by Tag Closed Tester (DoD adopted)

ASTM D 86 - Method for Distillation of Petroleum Products (DoD adopted)

ASTM D 130 - Methods for Detection of Copper Corrosion from Petroleum Products by the Copper Strip Tarnish Test (DoD adopted)

ASTM D 156 - Test Method for Saybolt Color of Petroleum products (Saybolt Chronometer Method) (DoD adopted)

ASTM D 323 - Test Method for Vapor Pressure of Petroleum Products (Reid Method) (DoD adopted)

ASTM D 381 - Test Method for Existent Gum in Fuels by Jet Evaporation (DoD adopted)

ASTM D 445 - Test Method for Kinematic Viscosity of Transparent and Opaque Liquids (and the Calculation of Dynamic Viscosity) (DoD adopted)

ASTM D 873 - Test Method for Oxidation Stability of Aviation Fuel (Potential Residue Method) (DoD adopted)

ASTM D 1093 - Test Method for Acidity of Distillation Residues or Hydrocarbon Liquids (DoD adopted)

ASTM D 1298 - Test Method for Density, Relative Density, (Specific Gravity), or API Gravity of Crude Petroleum Petroleum Products by Hydrometer Method (DoD adopted)

ASTM D 1319 - Test Method for Hydrocarbon Types in Liquid Petroleum Products by Fluorescent Indicator Adsorption (DoD Adopted)

ASTM D 2276 - Test Method for Particulate Contaminant in Aviation Turbine Fuels (DoD adopted)

ASTM D 2386 - Test Method for Freezing Point of Aviation Fuels (DoD adopted)

ASTM D 3227 - Test Method for Mercaptan Sulfur in Gasoline, Kerosene, Aviation Turbine, and Distillate Fuels (Potentiometric Method) (DoD adopted)

ASTM D 3242 - Test Method for Total Acidity in Aviation Turbine Fuel (DoD adopted)

ASTM D 3606 - Test Method for Determination of Benzene and Toluene in Finished Motor and Aviation Gasoline by Gas Chromatography

ASTM D 4052 - Test Method for Density and Relative Density of Liquids by Digital Density Meter (DoD adopted)

ASTM D 4057 - Practice for Manual Sampling of Petroleum and Petroleum Products (DoD adopted)

ASTM D 4952 - Test Method for Quantitative Analysis for Active Sulfur Species in Fuels and Solvents (Doctor Test)

ASTM D 5972 - Test Method for Freezing Point of Aviation Fuels (Automatic Phase Transition Method)

ASTM E 29 - Recommended Practice for Indicating Which Places of Figures are to be Considered Significant in Specified Limiting Values (DoD adopted)

(Application for copies of ASTM documents should be addressed to the American Society for Testing and Materials, 100 Barr Harbor Drive, West Conshohocken, PA 19428-2959).

(Non-Government standards and other publications are normally available from the organizations that prepare or distribute the documents. These documents also may be available in or through libraries or other informational services.)

2.4 Order of precedence. In the event of a conflict between the text of this document and the references cited herein, the text of this document takes precedence. Nothing in this document, however, supersedes applicable laws and regulations unless a specific exemption has been obtained.

Mil-Spec

TABLE I. Chemical and Physical Requirements and Test Methods.

REQUIREMENTS	Type I	Type II	Type III	ASTM Test Method
Specific Gravity, 15.6°C/15.6°C (60°F/60°F)	0.699 ±0.002	0.770 ±0.005	0.780 ±0.005	D 1298 D 4052
Color, Saybolt, Lighter Than	+25		+25	D 156
Viscosity, Centistokes at 0°C (32°F)	0.785 ±0.01			D 445
25°C (77°F)		1.17 ±0.05		
37.8°C (100°F)	0.54 ±0.01		2.47 ±0.10	
Vapor Pressure at 37.8°C (100°F), kPa (psi) Max	13.8 (2.0)			D 323
Existent Gum, mg/100ml Max	2.0	5.0		D 381 1/
Potential Gum, mg/100ml Max	5.0			D 873 2/
Distillation: Initial BP °C (°F) Min		149(300)	216(420)	D 86
Recovered 10% °C (°F)			3/	
Recovered 50% °C (°F)			221-232 (430-450)	
Recovered 90% °C (°F)			3/	

TABLE I. Chemical and Physical Requirements and Test Methods(cont).

Final Boiling Point °C (°F)		210 (410) Max	232-246 (450-475)	
Recovery, Percent Min		98.5		
Range, 5 to 95% points °C (°F)	1.7 (3) 4/			
Residue, Volume %, Max			1.5	
Loss, Volume %, Max			1.5	
Flash Point,°C(°F),Min		38 (100)	79 (175)	D 56
Aromatics, Vol %, Max		20.0		D 1319
Benzene, Vol %, Max	0.01	0.01	0.01	D 3606
Olefins, Vol %, Max		5.0		D 1319
Particulate Matter, mg/l, Max		2.0		D 2276
Mercaptan Sulfur, %Wt, Max or Doctor Test		0.001 Sweet		D 3227 D 4952
Copper Corrosion, Max	No. 1	No. 1	No. 1	D 130
Total Acid Number, mg/l, Max		0.015		D 3242
Freezing Point,°C(°F), Max			-54 (-65)	D 2386 D 5972
Acidity, Distillation Residue, Max			Neutral	D 1093

1/ Air Jet Method
2/ 5-Hour Aging Period
3/ To Be Reported-Not Limited
4/ Must Include Temperature of 98°C(208°F)

3. REQUIREMENTS

3.1 Materials. The fluids shall consist completely of hydrocarbon compounds, except as otherwise specified herein.

3.2 Chemical and Physical Requirements. The product shall conform to the requirements as specified in Table I. Requirements in Table I are absolute and not subject to correction for tolerance of test methods. The finished calibrating fluid shall be homogenous, visually free from water, sediment, or suspended matter and shall be clear and bright at the ambient temperature or at 21 degrees Centigrade (70 degrees Fahrenheit), whichever is higher.

3.3 Additives - Corrosion Inhibitor. If so specified by the procuring activity, a corrosion inhibitor conforming to MIL-I-25017 shall be blended into the calibration fluid by the contractor. The amount added shall be equal to or greater than the minimum effective concentration listed in the latest revision of QPL-25017. The supplier may add any one of the corrosion inhibitors listed on the latest revision of QPL-25017. The supplier shall maintain documentation that the corrosion inhibitor used is an approved QPL-25017 product.

3.4 Additives-Antioxidants. If so specified by the procuring activity, an anti-oxidant additive shall be blended into the type II calibrating fluid in total concentration not less than 4.2 pounds of inhibitor (not including weight of solvents) per 1000 barrels of fluid nor more than 8.4 pounds per 1000 barrels, in order to prevent the formation of gums and peroxides. The following additives or additive blends are approved for use:

a. 2,6-di-tert-butyl-4-methylphenol

b. 6-tert-butyl-2,4-dimethylphenol

c. 2,6-di-tert-butylphenol

d. 75 percent min 2,6-di-tert-butylphenol
25 percent max tert-butylphenols and tri-tert-butylphenols

e. 72 percent min 6-tert-butyl-2,4-dimethylphenol
28 percent max tert-butyl-methylphenols and tert-butyl-dimethylphenols

f. 55 percent min 6-tert-butyl-2,4-dimethylphenol
45 percent max mixture of tert-butylphenols and di-tert-butylphenols

g. 60 to 80 percent 2,6-dialkylphenols
20 to 40 percent mixture of 2,3,6-trialkylphenols and 2,4,6-trialkylphenols

h. 35 percent min 2,6-di-tert-butyl-4-methylphenol
65 percent max mixture of methyl-, ethyl-, and dimethyl-tert-butylphenols

i. 60 percent min 2,4-di-tert-butylphenol
40 percent max mixture of tert-butylphenols

j. 30 percent min mixture of 2,3,6-trimethylphenol and 2,4,6-trimethylphenol
70 percent max mixture of dimethylphenols

k. 65 percent min mixture of 2,4,5-triisopropylphenol and 2,4,6 triisopropylphenol
35 percent max mixture of other isopropylphenols and biphenols

l. 55 percent min butylated ethyl phenols
45 percent max butylated methyl and dimethyl phenols

3.5 Workmanship. The finished calibrating fluid shall be homogenous, visually free from undissolved water, sediment, or suspended matter and shall be clear and bright at the ambient temperature or at 21°C (70°F), whichever is higher.

3.6 Toxicity. The finished calibrating fluid shall have no adverse effect on the health of personnel when used for its intended purpose. The fluid shall contain no components which produce noxious vapors in such concentrations that would cause physical irritation to personnel during use or formulation under conditions of adequate ventilation. Percent composition of benzene shall be less than 0.01% of the total volume of the calibrating fluid due to benzene's toxic properties.

3.7 Limiting Values. The following applies to all specified limits in this performance specification: For the purposes of determining conformance with these requirements, an observed value or a calculated value shall be rounded off "to the nearest unit" in the last right-hand digit used in expressing the specification limit according to the rounding-off method of ASTM Practice E 29 for using Significant Digits in Test Data to Determine Conformance with Specifications.

4. VERIFICATION

4.1 Classification of Inspection. The inspections shall be classified as quality conformance inspections.

4.2 Quality Conformance Inspection. Inspections of individual lots shall serve as a basis for acceptance and shall consist of all the examinations and tests specified in section 3. Use the chemical and physical requirements and applicable test methods as specified in Table I for conformance testing.

4.3 Lot Definitions.

a. Bulk Lot of Material. An indefinite quantity of a homogeneous mixture of material contained in one isolated tank or kettle which is greater than 55 gallons in size, or a quantity manufactured by a single plant run through the same processing equipment during one continuous operation not exceeding a 24-hour period.

b. Packaged Lot of Material. A container lot of material shall be defined as an indefinite number of 55-gallon drums or smaller unit containers of identical size and type, filled with a homogeneous mixture of material manufactured by a single plant run through the same processing equipment during one continuous operation not exceeding a 24 hour period.

4.4 Sample. Each sample shall be of sufficient size to conduct all the quality conformance tests as specified herein. Unless otherwise specified, the quality conformance tests shall be performed on each required sample.

4.5 Sampling. Sampling shall be in accordance with ASTM D 4057.

4.5.1 Drums. The number of drums selected for sampling from each lot shall be according to Table II. The calibrating fluid from each container sampled shall constitute a separate sample.

TABLE II. Sampling for test.

Number of containers in lot	Number of containers to be sampled
2-25	2
26-150	3
151-1200	5
1201-7000	8

4.2.2.1.4 Portable tanks, cargo tanks, and tank cars. Each portable tank, cargo tank, or tank car shall constitute a lot. Unless otherwise specified, the sample shall be composited into one sample when one-third portions are withdrawn from the bottom, center, and top thirds of the tank.

4.2.2.1.5 Other containers. Unless otherwise specified, other containers of 100 gallons or less water capacity shall be sampled according to 4.2.2.1.3. Containers greater than 100 gallons water capacity shall be sampled according to 4.2.2.1.4.

4.6 Government Requested Sample. When requested, a 1-gallon sample shall be forwarded to the laboratory designated by the procuring activity for testing as specified herein.

4.7 Rejection. Failure of any calibrating fluid sample to conform to any of the specification requirements shall be cause for rejection of the lot represented.

5. PACKAGING

5.1 Packaging. For acquisition purposes, the packaging requirements shall be as specified in the contract or order (see 6.2). When actual packaging of materiel is to be performed by DoD personnel, they will contact the responsible packaging activity to ascertain requisite packaging requirements. Packaging requirements are maintained by the Inventory Control Point's packaging activity within the Military Department or Defense Agency, or within the Military Department's System Command. Packaging data retrieval is available from the managing Military Department's or Defense Agency's automated packaging files, CD-ROM products, or by contacting the responsible packaging activity.

6. NOTES

(This section contains information of a general or explanatory nature that may be helpful but is not mandatory.)

6.1 Intended Use. The fluids covered by this specification are intended for use in the calibration of aircraft fuel system components. Exercise caution to avoid prolonged contact with the skin and observe Occupational Safety and Health Administration (OSHA) guidelines.

Questions pertaining to the toxic effects should be referred to the appropriate departmental medical service.

6.2 Acquisition Requirements. Acquisition documents should specify the following:

a. Title, number, and date of this specification
b. Type
c. Issue of DoDISS to be cited in the solicitation, and if required, the specific issue of individual documents referenced (see 2.2.1 and 2.3)
d. Facility where Government requested test sample should be sent
e. Quantity required, and size and type of containers required
f. Packaging requirements (see 5.1)
g. Addition of corrosion inhibitor to the calibrating fluid
h. Addition of anti-oxidant additive to the calibrating fluid

6.3 Part or Identifying Number (PIN). The PIN number is created as shown below. It serves to identify a product during procurement and also in the Federal Supply System.

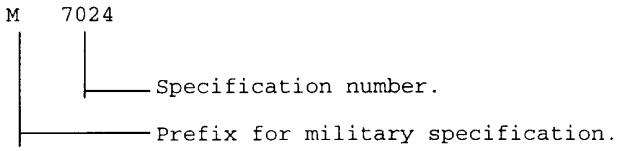

6.4 Changes from Previous Issue. Marginal notations are not used in this revision to identify changes with respect to the previous issue due to the extent of the changes.

6.5 Subject Term (key word) Listing.

High Flash Point
Corrosion Inhibitor
Antioxidant

Custodians:
Army - AV
Navy - AS
Air Force - 68

Review Activities:
Army - EA, MD
Air Force - 11
DLA - GS

Preparing activity:
Air Force - 68

(Project 6850-1205)

STANDARDIZATION DOCUMENT IMPROVEMENT PROPOSAL

INSTRUCTIONS

1. The preparing activity must complete blocks 1, 2, 3, and 8. In block 1, both the document number and revision letter should be given.
2. The submitter of this form must complete blocks 4, 5, 6, and 7.
3. The preparing activity must provide a reply within 30 days from receipt of the form.

NOTE: This form may not be used to request copies of documents, nor to request waivers, or clarification of requirements on current contracts. Comments submitted on this form do not constitute or imply authorization to waive any portion of the referenced document(s) or to amend contractual requirements.

I RECOMMEND A CHANGE:	1. DOCUMENT NUMBER MIL-PRF-7024E	2. DOCUMENT DATE (YYMMDD) 1 OCT 1997

3. DOCUMENT TITLE CALIBRATING FLUIDS, AIRCRAFT FUEL SYSTEM COMPONENTS

4. NATURE OF CHANGE *(Identify paragraph number and include proposed rewrite, if possible. Attach extra sheets as needed.)*

5. REASON FOR RECOMMENDATION

6. SUBMITTER

a. NAME *(Last, First, Middle Initial)*	b. ORGANIZATION	
c. ADDRESS *(Include Zip Code)*	d. TELEPHONE (Include Area Code) (1) Commercial (2) AUTOVON *(if applicable)*	7.DATE SUBMITTED (YYMMDD)

8. PREPARING ACTIVITY

a. NAME SA-ALC/SFSP	b. TELEPHONE *Include Area Code)* (1) Commercial (2) AUTOVON
c. ADDRESS *(Include Zip Code)* 1014 BILLY MITCHELL BLVD. STE. 1 KELLY AFB, TX 78241-5603	**IF YOU DO NOT RECEIVE A REPLY WITHIN 45 DAYS, CONTACT:** DEFENSE QUALITY AND STANDARDIZATION OFFICE 5203 Leesburg Pike, Suite 1403, Falls Church, VA 22401-3466 Telephone (703) 756-2340 AUTOVON 289-2340

DD Form 1426, OCT 89 *Previous editions are obsolete.* 198/290

BIBLIOGRAPHY

Batarseh, F. Z., Gnirß, M., Roisman, I. V., and Tropea, C. (2009). Fluctuations of a spray generated by an airblast atomizer. *Exp Fluids*, 46:1081–1091.

Charalampous, G. and Hardalupas, Y. (2011). Numerical evaluation of droplet sizing based on the ratio of fluorescent and scattered light intensities (lif/mie technique). *Applied Optics*, 50(9):1197–1209.

Charalampous, G., Hardalupas, Y., and Taylor, A. M. K. P. (2009). Novel technique for measurements fo continuous liquid jet core in an atomizer. *AIAA Journal*, 47(11):2605–2615.

Dankers, S., Gotthardt, M., Stengler, T., Ohmstede, G., and Hentschel, W. (2008). Two-phase piv: Fuel-spray interaction with surrounding air. *Topics Appl. Physics*, 112:333–343.

Davis, S. C., Diegel, S. W., and Boundy, R. G. (2011). Transportation energy data book. Technical Report 30, Oak Ridge National Laboratory, Oak Ridge, Tennessee 37831-6073.

Fan, H. T., Kuo, H., and Simmer, J. (2011). Measuring paint droplet size, velocity, and charge-to-mass ratio distribution for electrostatic rotary bell spray simulation. In *International Mechanical Engineering Congress & Exposition*, Denver, Colorado, USA.

Ghaemi, S., Rahimi, P., and Nobes, D. (2008). Measurement of droplet centricity and velocity in the spray field of an effervescent atomizer. In *14th Int Symp on Applications of Laser Techniques to Fluid Mechanics*, Lisbon, Portugal.

Gnirß, M. and Tropea, C. (2008). Simultaneous piv concentration measurements in a gas-turbine combustor model. *Exp Fluids*, 45:643–656.

Gui, L., Merzkirch, W., Strömungslehre, L., and Essen, U. (1996). Phase-separation of piv measurements in two-phase flow by applying a digital mask technique. *European Research Community on Flow Turbulence and Combustion*, 30:45–48.

Hadef, R. and Lenze, B. (2005). Measurements of droplets characteristics in a swirl-stabilized spray flame. *Experimental Thermal and Fluid Science*, 30:117–130.

Hu, H. and Jin, Z. (2010). An icing physics study by using lifetime-based molecular tagging thermometry technique. *International Journal of Multiphase Flow*, 36:672–681.

Hu, H., Jin, Z., Nocera, D., Lum, C., and Koochesfahani, M. M. (2010). Experimental invextigations of micro-scale flow and heat transfer phenomena by using molecular tagging techniques. *Measurement Science and Technology*, 21:085401,1–14.

Hu, H. and Koochesfahani, M. M. (2006a). Molecular tagging velocimetry and thermometry and its application to the wake of a heated circular cylinder. *Measurement Science and Technology*, 17:1269–1281.

Hu, H. and Koochesfahani, M. M. (2006b). A novel molecular tagging technique for simultaneous measuremetns of flow velocity and temperature fields. *Journal of Visualization*, 9(4):357.

Hu, H., Koochesfahani, M. M., and Lum, C. (2006). Molecular tagging thermometry with adjustable temperature sensitivity. *Experiments in Fluids*, 40:753–763.

Huang, D. and Hu, H. (2007). Molecular tagging thermometry for transient temperature mapping within a water droplet. *Optics Letters*, 32(24):3534–3536.

Huang, Y. and Yang, V. (2009). Dynamics and stability of lean-premixed swirl-stabilized combustion. *Progress in Energy and Combustion Science*, 35:293–364.

Ibrahim, A. A. and Jog, M. A. (2007). Nonlinear breakup model for a liquid sheet emanating from a pressure-swirl atomizer. *Journal of Engineering for Gas Turbines and Power*, 129:945–953.

Jiang, X., Siamas, G. A., Jagus, K., and Karayiannis, T. G. (2010). Physical modelling and advanced simulations of gas – liquid two-phase jet flows in atomization and sprays. *Progress in Energy and Combustion Science*, 36:131–167.

Karnawat, J. and Kushari, A. (2006). Controlled atomixation using a twin-fluid swirl atomizer. *Exp Fluids*, 41:649–663.

Lavieille, P., Lemoine, F., Lavergne, G., and Lebouché (2001). Evaporating and combusting droplet temperature measurements using two-color laser-induced fluorescence. *Experiments in Fluids*, 31:45–55.

Lawson, N. J. (2004). The application of laser measurement techniques to aerospace flows. In *Proceedings of the Institution of Mechanical Engineers, Part G: Journal of Aerospace Engineering*.

Li, T., Nishida, K., and Hiroyasu, H. (2011). Droplet size distribution and evaporation characteristics of fuel spray by a swirl type atomizer. *Fuel*, 90:2367–2376.

Midgley, K., Spencer, A., and McGuirk, J. (2005). Unsteady flow structures in radial swirler fed fuel injectors. *Journal of Engineering for Gas Turbines and Power*, 127:755–764.

Müller, S. H. R., Böhm, B., Gleißner, M., Grzeszik, R., Arndt, S., and Dreizler, A. (2009). Flow field measurements in an optically accessible, direct-injection spray-guided internal combustion engine using high-speed piv. *Exp Fluids*, 48:281–290.

Providakis, T., Scouflaire, P., Zimmer, L., and Ducruix, S. (2010). Time-resolved piv measurements applied to a non-reactive dodecane-air mixture in a two-staged multi-injection burner. In *15th Int Symp on Applications of Laser Techniques to Fluid Mechanics*, Lisbon, Portugal.

Rottenkolber, G., Gindele, J., Raposo, J., Dullenkopf, K., Hentschel, W., Wittig, S., Spicher, U., and Merzkirch, W. (2002). Spray analysis of a gasoline direct injector by means of two-phase piv. *Experiments in Fluids*, 32:710–721.

Saeki, S. and Hart, D. P. (2001). Investigation on yag(532) laser dyes for oil film thickness and temperature measurement. In *Proceedings of PSFVIP-3*, Maui, Hawaii, USA.

Sedarsky, D., Gord, J., Carter, C., Meyer, T., and Linne, M. (2009). Fast-framing ballistic imaging of velocity in an aerated spray. *Optics Letters*, 34(18):2748–2750.

Sivakumar, D. and Kulkarni, V. (2011). Regimes of spray formation in gas-centered swirl coaxial atomizers. *Exp Fluids*.

Spencer, A., McGuirk, J., and Midgley, K. (2008). Vortex breakdown in swirling fuel injector flows. *Journal of Engineering for Gas Turbines and Power*, 130:021503–1–021503–8.